Copper oxide-carbon catalysts for the oxidation of methylene blue

A dissertation submitted to the Faculty of Applied and Computer Sciences, Department of Chemistry, Vaal University of Technology, Vanderbijlpark, in fulfilment of the requirements for the degree of Magister Technologie

By

Anza Reliance Makamu

Supervisor: Dr EL Viljoen

Co-supervisor: Prof Ofomaja

Date:

DECLARATION

Prima Facie, I declare that this dissertation was composed by myself, that the work contained herein is my own except where explicitly stated otherwise in the text, and that this work has not been previously submitted for any other degree or professional qualification at another university.

……....

(Candidate's signature)

……..day of……

I DEDICATION

To my mom, Mufandilani Jane Makamu and my dad, Maluta Joel Makamu. You are dearly loved and I hope I’ve made you proud.

II ACKNOWLEDGEMENTS

I would firstly like to thank the Almighty God for the wonderful gift called life, wisdom, strength and the ability to complete this project in good health. Indeed there is a living God.

I would also like to extend my deepest and sincere gratitude to my supervisor Dr EL Viljoen for her generous support, constructive criticism, guidance and input to this project work. A special thank you as well to my co-supervisor Prof Ofomaja and Dr Peleyeju for their valuable input.

My heartfelt appreciation goes to my siblings, Takalani, Mpho and Abigail Makamu for the support you gave me throughout the duration of this project. I'd also like to give a special thank you to my friends Mudau Zwavhudi, Mulaudzi Nduvho, Vele Mulayo, Nwendamutswu Khangale, Muthivhi Rudzani and Rudzani Muruge your support meant the world to me at times when I felt like giving up and also tolerated my countless complaints you guys are indeed God sent. To Dimakatso Moshoeu and Sentse Oyandi thank you guys for making those night shifts much easier.

I would also like to thank the Vaal University of Technology, Department of Chemistry for giving me the opportunity to pursue my degree of Magister Technologiae Chemistry and also allowing me to use their facilities and equipment's for my project work.

I would like to thank the National Research Foundation (NRF) and Sasol for their financial support throughout this study.

III ABTRACT

Organic water pollutants such as dyes are difficult to biodegrade. In this study Fenton, photo-Fenton and photocatalysis were used to degrade methylene blue dye in the presence of copper oxide catalysts. The copper oxide catalysts were prepared with a precipitation reduction method. The effect of different preparation parameters on the catalyst properties and catalytic activity were investigated.

The reducing agents, ascorbic acid (ASC, $C_6H_8O_6$), hydrazine (N_2H_4), sodium boron hydride ($NaBH_4$) and glucose ($C_6H_{12}O_6$) could be used to obtain the desired Cu_2O phase. ASC, N_2H_4 and $NaBH_4$ were able to reduce copper (II) to copper (I) at room temperature whereas glucose required a higher reduction temperature. Stoichiometric amounts of the reducing agents ASC, N_2H_4 and glucose and double the stoichiometric amount of $NaBH_4$ were required to obtain Cu_2O. A further increase in the amounts of $NaBH_4$ and N_2H_4 resulted in the formation of copper metal (Cu (0)). High amounts of ASC did not over-reduce the copper. ASC also functioned as capping molecule and anti-oxidant preventing the oxidation of the Cu_2O to CuO in air after preparation. Hydrazine was thus not able to protect the Cu_2O against oxidation.

The SEM results showed that an increase in the amount of the precipitating agent, NaOH, resulted in an increase in the particle sizes. The particle shapes changed from spherical to cubic when a high amount of NaOH was used with hydrazine as reducing agent. Smaller particle sizes were obtained when $CuCl_2$ was used instead of $CuSO_4$ and $Cu(NO_3)_2$. Larger crystallites formed when the preparation temperature was increased from room temperature to 100°C with glucose as reducing agent.

TEM and XRD analyses showed that the micro-particles seen in SEM analyses are made up of nano-particles. The catalysts were not active for photocatalysis which may be explained by the oxidation of these nano-particles to form the photocatalytic inactive CuO. The catalysts were shown to be active for Fenton and photo-Fenton degradation.

The addition of graphene and activated carbon to the Cu_2O catalysts were detrimental to the catalytic activity. The percentage degradation of methylene blue by the Fenton reaction increased with an increase in the BET surface area from 1.5 m^2/g to 10 m^2/g and a further increase in the surface area resulted in a decrease in the percentage degradation. A direct correlation between the Fenton catalytic activity and the pore size were found which indicate that the reaction was mass transfer limited.

Keywords: methylene blue, Fenton degradation, photo-Fenton degradation, photodegradation, ASC, N_2H_4**,** $NaBH_4$, glucose, catalytic activity.

TABLE OF CONTENTS

I LIST OF FIGURES

II LIST OF TABLES

III ABBREVIATIONS

AC	Activated charcoal
AFM	Atomic force microscope
AOP	Advanced oxidation processes
ASC	Ascorbic acid
BET	Brunauer-Emmett-Teller
FTIR	Fourier transformation infrared
MB	Methylene blue
PL	Photoluminiscence
SEM	Scanning electron microscope
TEM	Transmission electron microscopy
UV-vis	Ultraviolet-visible spectroscopy
XRD	X-ray diffraction

IV CONFERENCES AND SYMPOSIUM PRESENTATIONS

- MAKAMU,A.R.,VILJOEN,E.L.,OFOMAJA,A. The effect of preparation parameters on the morphology and phase of copper oxide catalyst. 2017. 19-22 November. Catalysis Society of South Africa, Pilanesberg, South Africa. *Poster presentation.*
- MAKAMU,A.*R.,*VILJOEN,E.L.,OFOMAJA,A. Cu_2O catalyst for the Fenton degradation of methylene blue. 2018. 2-7 December. 43rd South African Chemistry Institute national convention, CSIR-International convention center, Tshwane, South Africa. *Poster presentation*.
- MAKAMU,A.R.,VILJOEN,E.L.,OFOMAJA,A.Cu_2O catalysts for the Fenton degradation of methylene blue. 2018. 17-18th December.3rd Vaal University of Technology interdisciplinary conference, Quest conference center, Vanderbijlpark, South Africa. *Oral presentation*.

Chapter 1

1.1 INTRODUCTION

Over seven million tons of products produced using dye are manufactured every year. Dyes are used in many different industries such as textile, paper, cosmetics, leather, food and pharmaceutical industries (Xavier et al., 2015; Jouari et al., 2019; Aguilar & Rosas 2019). Dyes can be used to colour many natural and synthetic products (Xavier et al., 2015). It is noteworthy that some amount of a dye is lost in the process of producing the dye and also during its use (Xavier et al., 2015, Abdelrahman et al., 2019). Thus, effluents from industries where dyes are produced or utilized cause pollution of water bodies (Saeed et al., 2019).

Synthetic dyes can cause considerable amount of environmental pollution and health hazards (Xavier et al., 2015, Sirajudheen et al., 2019; Nie et al. 2019). Waste waters from dyeing industries are often coloured and can pose serious environmental hazards (Xavier et al., 2015). Discharging untreated effluent into water bodies results in water pollution and constitutes threat to the aquatic ecosystems (Houas et al., 2001, Benzaouak et al., 2018).It is therefore important to remove synthetic dyes from industrial wastewaters prior to their release into the environment (Dutta et al., 2001). To do this, ways to remove these dyes need to be investigated.

Dyes like methylene blue (MB) are difficult to biodegrade and oxidation reactions, like oxidative photocatalysis, Fenton and photo-Fenton reactions are required to chemically degrade these dyes. During oxidative degradation reactions metal oxides such as ZnO, TiO_2 and Cu_2O are used as catalysts (Umar and Aziz 2013, Ischenko et al., 2016).

Cu_2O was used because it is affordable, environmentally friendly and it absorbs light in the visible-light region of the spectrum since it has a small band gap. The drawbacks associated with Cu_2O is that Cu_2O is not stable under illumination in aqueous solutions, and the edge of the valence band is not positive enough to provide sufficient over potential for water oxidation (Wang et al., 2016). Carbon materials are used as support for the copper oxide catalyst to improve its stability and activity (Zhang et al., 2016). Also, studies have shown that addition of carbon to Cu_xO catalyst can increase the activity by

increasing the dispersion of the copper oxide phase (Gau et al., 2012). It can also hinder the recombination of photo electrons and holes by electron transfer between carbon and the copper oxide (Zhang et al., 2016; Ma et al., 2016). On the other hand, the presence of carbon can decrease the activity of the Cu_xO, as it can consume the radicals that are supposed to degrade the pollutant (Zubir et al., 2015).

1.2 Problem statement

Water is often polluted by organic compounds that are resistant to biodegradation and therefore powerful oxidative processes are required to degrade these difficult compounds. In this regard, advanced oxidation processes such as heterogeneous photocatalysis, Fenton and photo-Fenton processes have been reported to be effective. As stated earlier, Cu_2O is a promising catalyst in the degradation of organic pollutants via heterogeneous photocatalysis or photo-Fenton process.

The phase, size and shape of the copper oxide particles affect its activity. The copper oxide particles are often prepared using a precipitation and reduction method and the phases, size and shape can be controlled by varying the precipitation parameters like amount of the precipitating agent, type and amount of reducing agent. Various types and amounts of reducing agents have been used in literature and it is not clear which reducing agent yields the most active catalyst and therefore research is required to compare the different reducing agents.

Often copper oxide crystals are supported on support like silica, alumina, activated carbon and graphene. There are conflicting results in literature on the influence of carbon based supports on the catalytic activity and therefore research is required to establish if the addition of carbon will be beneficial for the catalytic activity.

1.3 Aim

The aim of this research was to study the effects of preparation parameters and different salt precursors on the synthesized copper oxide catalysts, their characteristics and catalytic activities during photocatalysis, Fenton and photo-Fenton reactions.

1.4 Objectives

In this study the main object was to prepare the Cu_xO catalysts using the following preparation parameters:

- Using **ascorbic acid** as reducing agent and capping molecules (the amount of reducing agent, NaOH, different copper precursor).
- Using hydrazine as reducing agent (varying reaction time, amount of $\mathbf{N_2H_4}$ and amount of NaOH).
- Using $\mathbf{NaBH_4}$ as reducing agent (amount of reducing agent).
- Using **glucose** as reducing agent and capping molecules (the amount of reducing agent, and temperature).
- By the addition of carbon materials (graphene and activated charcoal).

The subsequent object was to characterize the prepared copper oxide particles using XRD, BET, SEM, UV-vis spectroscopy and FTIR.

The final objective was to degrade MB with the prepared copper oxide particles using Fenton, photocatalytic and photo-Fenton degradation.

1.5 Thesis outline

This work is divided into five different chapters which make up the whole thesis. Each chapter will be briefly described.

Chapter 1: Introduction

This chapter gives the background information related to the topic. It highlights the problem statement, aim and objectives of this research.

Chapter 2: Literature review

In this chapter the literature review is explained in more detail topics such as the synthesis of the copper oxide catalysts, degradation methods of methylene blue, different reducing agents that can be used to prepare the catalysts are discussed.

Chapter 3: Materials and methods

In this chapter the materials and methodology procedure are described in detail. These includes the chemicals and, the characterization techniques used. The synthesis of copper oxide catalysts and the application of the prepared catalysts in the degradation of MB by Fenton and photo-Fenton and photodegradation are also discussed.

Chapter 4: Results and discussion

This chapter focuses on the results obtained from the characterization techniques when different parameters were varied for the different reducing agents used. It also gives more details on the application of the prepared copper oxide nanoparticles for the degradation of MB.

Chapter 5: Conclusion

This chapter gives general conclusions drawn from the research with respect to the aim and objectives.

Chapter 2

2.1 Literature review

A lot of dye products are produced in different industries and their waste water are released into different water bodies which results in water pollution which affects our health and the environment. Different ways of removing the dyes from the waste waters were studied.

2.2 Organic pollutants

Dyes are stable chemical compounds, easy to produce and have a wide range of colors (Benzaouak et al., 2018). The uncontrolled release of pollutants into different water bodies is a big threat to the health of human beings and sustainable development and this is because of their poisonous and cancer causing attributes (Yang et al., 2018).

Methylene blue is one of the most known and used organic dyes. It is a cyclic compound with a chemical formula $C1_6H1_8N_3SCl$ and produces $C_6H_{18}N_3S^+$ cations in aqueous medium. It is tricky to degrade dyes such as methylene blue because they are stable to light, heat and oxidation reactions (Silva Junior et al., 2019). Methylene blue is a synthetic basic dye that is used in the manufacturing of paper, plastic and textile industries. It has harmful side effects on human beings and animals if congested and can result in a burning effect on the eyes which can lead to permanent injury (Kumar et al., 2018).

2.3 Removal of organic pollutants

Several methods have been used to remove organic waste from different water bodies such as adsorption and catalytic degradation (Yang et al., 2018).

2.3.1 Adsorption

Organic and inorganic pollutants can be removed from water by adsorption utilizing solid adsorbents (Rashed, 2013). When a solution containing the pollutant comes into contact with a porous solid, liquid–solid intermolecular forces of attraction cause some of the pollutant molecules to be adsorbed and concentrated on the solid surface (Rashed, 2013). The way the bonding happens depends on the characteristics of the species involved, but the process is normally classified as physisorption or chemisorption. During

adsorption an equilibrium between the adsorbent and pollutant is obtained (Rashed, 2013).

2.3.2 Fenton reaction

Catalytic oxidation processes have become a popular solution for treating industrial waste waters containing dyes, since the pollutant is degraded. One of the methods of removing organic pollutants is the Fenton process which uses catalysts. The Fenton reactions have been a convenient way to treat chemical wastes (Pignatello et al., 2006). The catalyst typically used is a heterogeneous catalyst since it can easily be separated from the water.

During the Fenton reaction, radicals are produced. The production of the radicals is formed when hydrogen peroxide and the Fe ions react with each other and form active oxygen radicals and hydroxyl (OH) radicals (Pignatello et al., 2006). These radicals then react with the organic pollutant and oxidize it into less harmful products (Pignatello et al., 2006).

These are classical free radical mechanisms for the decomposition of H_2O_2 during the Fenton reaction:

$Fe^{2+} + H_20_2 \rightarrow Fe^{3+} + OH^- + HO^\bullet$ reaction 1

$Fe^{3+} + H_2O_2 \rightarrow Fe^{2+} + HO^\bullet{}_2 + H^+$ reaction 2

$HO^\bullet + H_2O_2 \rightarrow HO^\bullet{}_2 + H_2O$ reaction 3

$HO^\bullet + Fe^{2+} \rightarrow Fe^{3+} + OH^-$ reaction 4

$Fe^{3+} + HO^\bullet{}_2 \rightarrow Fe^{2+} + O_2H^+$ reaction 5

$Fe^{2+} + HO^\bullet{}_2 + H^+ \rightarrow Fe^{3+} + H_2O_2$ reaction 6

$HO^\bullet{}_2 + HO^\bullet{}_2 \rightarrow H_2O_2 + O_2$ reaction 7

Because hydrogen peroxide decomposes to water and oxygen it poses no harm to human beings and the environment which makes it safe to use (Pignatello et al., 2006). The disadvantage of the Fenton process is that it requires the use of hydrogen peroxide which comes with a cost.

Traditionally iron ions and iron oxide has been used for the Fenton reaction. However, copper-based catalyst may be preferred since the rate of reaction to produce the hydroxyl radical is higher as shown by the rate constants in reactions 8-11 (Fang et al., 2019) which resulted in a higher activity for copper catalyst than iron catalysts (Wang et al., 2017). Furthermore copper-based catalysts can work at a broader range of pH than iron-based catalysts (Fang et al., 2019).

$Cu^{2+} + H_2O_2 \rightarrow Cu^{+} + HO_2\bullet + OH^{-}$ ($k = 4.6 \times 10^2\ M^{-1}\ s^{-1}$) reaction 8

$Cu^{+} + H_2O_2 \rightarrow Cu^{2+} + OH\bullet + OH^{-}$ ($k = 1.0 \times 10^4\ M^{-1}\ s^{-1}$) reaction 9

$Fe^{3+} + H_2O_2 \rightarrow Fe^{2+} + HO_2\bullet + H^{+}$ ($k = 0.001 - 0.01\ M^{-1}\ s^{-1}$) reaction 10

$Fe^{2+} + H_2O_2 \rightarrow Fe^{3+} + HO\bullet + OH^{-}$ ($k = 63 - 76\ M^{-1\ s-1}$) reaction 11

2.3.2.1 ***Influence of the phase of Cu-based catalyst on its activity in the Fenton process***

Different copper phases with different oxidation states can be formed for example Cu, Cu_2O, and CuO. Catalyst containing Cu (I) is more active than Cu (II) and Cu (0) for activation of H_2O_2 to produce hydroxyl radicals (Sun et al., 2018; Yang et al., 2015). This may be explained by the Fenton reactions that show that Cu(I) is necessary to produce the hydroxyl radical and that the rate determining step is the reduction of Cu(II) to Cu(I) (Sun et al., 2018).

2.3.2.2 ***The influence of the shape of Cu-based catalyst on its activity in Fenton process***

It has been shown that the shape of a catalyst may have effect on its activity in Fenton reaction. For instance, the Fenton catalytic activity of octahedral Cu (I) oxide was higher than the cubic and spherical shapes (Kang et al., 2019). This may be explained by {100} faces of the octahedral shape having more Cu(I) dangling bonds which is believed to aid adsorption on the surface during reaction (Kang et al., 2019).

2.3.3 Photo-Fenton

Fang et al. (2019) and Miao et al. (2018) showed that the combination of photocatalysis and Fenton process outperforms the individual reactions. Fang et al. (2019) found that visible light photodegradation of phenol on CuO is negligible, whereas about 50% of the

pollutant was degraded using the semiconductor in a Fenton process carried out in the dark. Interestingly, 100% of the phenol were degraded with the combination of CuO catalyst with visible light as well as H_2O_2. Literature indicates that CuO is not active for photocatalysis (Fang et al., 2019; Nguyen et al., 2015) and one may argue that the presence of H_2O_2 is required to activate the catalyst for photocatalysis by reducing the surface CuO to Cu_2O as shown by reaction 8.

This may explain why the photo-Fenton reaction percentage degradation is greater than the sum of the individual reactions. Miao et al. (2018) used an iron based catalyst and argued that the direct photolysis of H_2O_2 (reaction 12) under UV irradiation may have given rise to the synergistic effect since H_2O_2 with UV light without a catalyst could degrade methyl orange dye. The excited electron formed from the photocatalysis can also react with the H_2O_2 used for the Fenton reaction. Therefore, there are two additional reactions (12 and 13) in photo-Fenton catalysis to produce the hydroxyl radicals.

$H_2O_2 + hv \rightarrow 2HO\bullet$ reaction 12

$e^- + H_2O_2 \rightarrow HO\bullet + OH^-$ reaction 13

2.3.4 Photocatalysis

In photocatalysis, a metal oxide semiconductor that absorbs light which gives rise to a chemical reaction is known as a photocatalyst (Umar and Aziz, 2013). Semiconductors used in photocatalysis have the ability to adsorb organic pollutants in water and oxidize them into less harmful products such as H_2O and CO_2 (Lee et al., 2016).

The photocatalytic reactions are shown in Figure 1. The catalyst absorbs light which results in the excitation of an electron from the valence band to the conduction band and the formation of a hole (Ibhadon and Fitzpatrick, 2013, Kumar et al., 2016). The electron reacts with oxygen to form superoxide radicals ($O_2^{-}\bullet$) and the hole reacts with water to form hydroxyl radicals (OH•) (Ibhadon and Fitzpatrick, 2013; Kumar et al., 2018). These radicals are responsible for the degradation of the pollutant (Ibhadon and Fitzpatrick, 2013; Kumar et al., 2018).

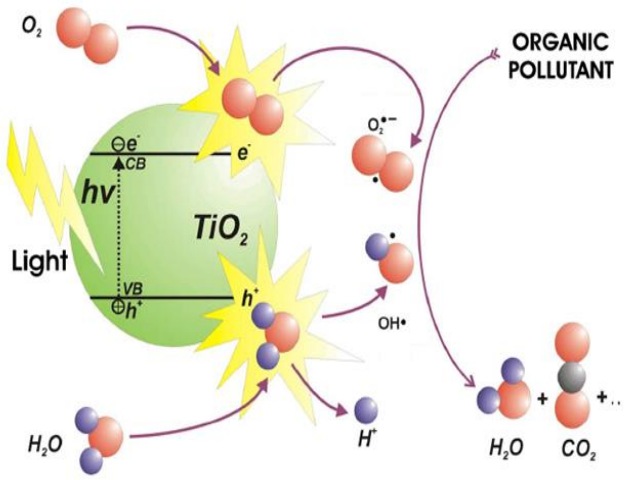

$$Cu_2O + h\nu \rightarrow Cu_2O^*(e^-_{CB} + h^+_{VB})$$

$$h^+_{VB} + H_2O \rightarrow {}^\bullet OH + H^+$$

$$O_2 + e^-_{CB} \rightarrow O_2^{\bullet -}$$

$$O_2^{\bullet -} + H^+ \rightarrow HO_2^\bullet$$

$$HO_2^\bullet + HO_2^\bullet \rightarrow H_2O_2 + O_2$$

$$O_2^{\bullet -} + HO_2^\bullet \rightarrow O_2 + HO_2^-$$

$$HO_2^- + H^+ \rightarrow H_2O_2$$

Figure 1: Scheme explaining photocatalysis (Ibhadon and Fitzpatrick,2013;Kumar et al.,2016)

The process of advanced oxidation can be applied on a large number of different organic pollutants and it is of high interest because of its efficiency in degrading organic pollutants (Umar and Aziz, 2013). The advantage of photocatalysis is that it does not require the expensive reagents like hydrogen peroxide as in the case of the Fenton process.

2.3.4.1 ***Catalysts for photocatalysis***

The two most popular catalysts that are used in photocatalysis are TiO_2 and ZnO because of their properties such as high catalytic activity, chemical stability, low cost and low toxicity (Ishchenko et al., 2016). Both TiO_2 and ZnO have the same catalytic property limitations since they both have a large band gap of about 3.1 ev which means that they both cannot absorb light in the visible range of the spectrum (Lee et al., 2016).

TiO_2 as a catalyst has one of the best advantages as it can photo-catalytically degrade organic compounds with ease. For example, if it is added into an organic polluted pool of water and light is shined on it, it can oxidise the organic pollutants and the water becomes cleaned (Fujishima et al., 2000). It has also been found that the smaller the particle size of the titanium dioxide catalyst the higher the efficiency of the catalytic reaction (Fujishima et al., 2000).

Some of the limitations of using both TiO_2 and ZnO are their lack of performance in the visible range of the spectrum (Ishchenko et al., 2016). Zinc oxide is an n-type semiconductor which means it has a larger electron concentration than the hole concentration which means it has poor electrical conductivity (Lee et al., 2016).

2.3.4.2 ***Copper oxides for photocatalysis***

Sunlight contains only about 3-5% ultra violet light (Ibhadon and Fitzpatrick, 2013), which means a large amount of energy is not utilized when ZnO and TiO_2 are used as photocatalysts. A catalyst that can adsorb visible light is of great interest because it enables better utilisation of the sun's energy.

Copper oxide catalyst has been reported to outperform zinc oxide and titania in a photocatalytic reaction because it absorbs light in the visible-light region of the spectrum since it has a small band gap of about 2.0-2.2 eV (Zhou et al., 2013). Copper oxide is abundant, its toxicity is very low and it is cheap to prepare (Ma et al., 2016). Copper oxide is a p-type semiconductor which means it has a higher hole concentration than the electron concentration.

There are various parameters that affect the band gap size and the rate of electron and hole recombination of the copper oxide and the resulting photocatalytic activity of the catalyst. The effect of the copper oxide size and shape, oxidation state and supporting the catalyst on carbon on the band gap and activity will be discussed.

2.3.4.3 ***Effect of size and shape on the photocatalytic behaviour***

Physical and chemical properties are significantly influenced by the shape and sizes of inorganic material. Therefore, there has been extensive research to prepare copper oxide with different shapes and sizes over the past years (Zhou et al., 2013). It has been suggested that Cu_2O in the nanoscale size is more stable than Cu_2O in micrometer range and it has been found that properties such as crystallite size and crystal facet-dependent properties play important roles in making the nanoscale Cu_2O more stable (Wang et al., 2016). A decrease in the copper particle sizes results in an increase in the band gap (Ke et al., 2016; Kuo et al., 2007; Wang et al., 2016). For example, nanoparticles with a size

of 4 µm had a band gap of about 1.9 eV and when the size was decreased to about 10 nm the band gap increased to 2.6 eV (Wang et al., 2016). This may indicate that large particles may be more desirable as a photocatalysts. Table 1 shows that for a similar copper oxide particle size, different shapes absorb light at different wavenumbers. Cubic particles absorbed light at the lowest wavenumber (largest band gap) and truncated octahedral particles absorbed light at the highest wavenumber. The shape as well as the size thus influence the band gap.

Table 1: Effect of size on the absorption of light.

Size (nm)	**Shape**	**λ max**	**Reference**
45	Cubic	460	Xiong et al., (2016)
45	Spherical	584	He et al., (2005)
47	Nanorod-nanoparticles	597	Sabbaghan et al., (2015)
41	Nanosheet	620	Sabbaghan et al., (2015)
46	Truncated octahedral	862	Sabbaghan et al., (2015)

Ouyang et al. (2016) studied the effect of shape (spheres, sheets and octahedron) on the photocatalytic activity of the Cu_2O particles. They showed that pure spherical Cu_2O exhibited the best photocatalytic activity and about 96% of the methyl orange dye was decolorized after 1 hour irradiation.

Sheets had lower photocatalytic activity and about 85% of the dye was removed in 1 hour. Octahedrons showed the lowest efficiency for dye decolorization and only about 50% of the dye was decolorized. Different reaction rate constants were obtained for the various shapes. The maximum reaction rate constant was obtained for the spheres and the minimum reaction rate constant was obtained from the octahedrons. This showed the spherical pure Cu_2O had the best catalytic performance.

The micro-spheres have a narrow band gap which may explain the better photocatalytic performance in comparison to that of the octahedron particles (Ouyang et al., 2016). Xu

et al. (2006) compared the photocatalytic activity of cubic Cu_2O with octahedral Cu_2O particles and found the octahedral Cu_2O is significantly more active than that of the cubic Cu_2O. Based on the literature discussed one may argue that the desired shape for the most active catalyst may be spherical.

2.3.4.4 ***Influence of the oxidation state of copper on the photocatalytic activity of copper oxide***

The band gap of CuO is 1.3-2.1 eV which is smaller than the band gap of Cu_2O that is 2.1-2.6 eV (Deng et al., 2017). One may thus argue that CuO might be the favoured copper oxide phase for photocatalytic degradation of organic pollutants.

In a study by Deng et al.2017, Copper oxide was prepared with a precipitation reduction method in which the amount of the reducing agent, hydroxylamine hydrochloride, was varied. In the absence of the reducing agent, only CuO formed and the amount of Cu_2O increased with an increase in the amount of reducing agent. The morphology also changed from nanosheets to octahedrons with an increase in the amount of reducing agent. The activity for the photodegradation of methyl orange also increased with an increase in the amount of reducing agent used. Therefore one may argue that the observed increase in the activity may have been due to the decrease in the oxidation state and that Cu_2O may be more active than CuO.

In a study by Scuderi et al. (2016), CuO was annealed in vacuum at 400 °C for 3 h which resulted in a decrease in the photodegradation activity. The annealing caused the formation of Cu_2O and a change in the morphology where the straight rods became crinkled with defects. It is thus not clear to which factor (oxidation state or morphology) the decrease in the activity may be attributed to.

In a study by Haung et al. (2009), methyl orange was degraded using Cu_2O nanoparticles and Cu_2O micro particles. The Cu_2O was oxidized to CuO which is an inactive phase in photocatalysis, which resulted in no catalytic activity. Nguyen et al. (2015) also reported that Cu_2O was a more active phase for photodegradation.

2.4 Combining carbon with copper-based material

Carbon can be used as support to facilitate the dispersion of Cu_2O (Gao et al., 2012), to improve the stability of the Cu_2O photocatalysts (Ma et al., 2016; Yurderi et al., 2015), to increase the adsorption of the reagent (pollutant) on the catalyst (Ma et al., 2016; Gao et al., 2012; Zhou et al., 2013) and to serve as excellent electron acceptors or electron donors (Ma et al., 2016). Electron transfer between carbon and the copper oxide occurs and thus hindering the recombination of photo generated electrons and holes on the semiconductors (Ma et al., 2016; Gao et al., 2012; Yang et al., 2016; Zhou et al., 2013; Zhang et al.,2016). The use of a support will thus increase the activity as demonstrated in the studies discussed.

The addition of carbon spheres to Cu_2O increased the methylene blue degradation from 27% to 55% as measured after 120 min (Zhou et al., 2013). Zhang et al. (2016) found 100% conversion of methyl orange after 2 h for reduced graphene oxide copper oxide nanocomposite which is 20% more than that obtained when the pure copper oxide crystals was used. UV-vis spectroscopy showed that the reduced graphene oxide increased the absorption of light and decreased the band gap and the PL indicated that the reduced graphene oxide decreased the recombination of electrons and hole.

Carbon supported Cu_2O nanoparticles exhibits a much higher photocatalytic activity than pure Cu_2O (Ma et. al., 2016). The structure and morphology of pure Cu_2O nanoparticles is a cubic structure with a smooth surface but after introducing carbon it shows a shape evolution to a rough cube which eventually becomes a smooth sphere (Ma et al., 2016). UV-vis spectroscopy showed that the addition of carbon dots to the copper oxide particles increased the absorption of light and the PL spectroscopy indicated that the addition of carbon dots decreased the recombination of electrons and holes (Ma et al., 2016).

Gao et al. (2012) added different amounts of graphene to the copper oxide particles. The copper oxide particle size decreased with an increase in the amount of graphene added. The copper oxide particles were very agglomerated when no graphene was present in the catalyst. When enough graphene was added no agglomeration was observed and the copper oxide particles were evenly spread on the support surface. One may argue

that the graphene acted like a capping molecule during the catalyst preparation. The activity of the catalyst was significantly enhanced with an increase in the amount of graphene added to the catalyst composition.

Composites of copper oxide and carbon have been used as Fenton catalysts to degrade organic pollutants (Priyanka et al., 2014; Xiong et al., 2019, Wang et al., 2017; Sun et al., 2018; Wang et al., 2019). Xiong et al. (2018) reported the preparation and application of a composite of copper oxide-carbon composite for degradation of organic pollutant via Fenton reaction. The carbon was obtained from calcination of metal organic frameworks and it was reported that different calcination temperatures used yielded catalyst with different surface areas and carbon with different crystallinities (Xiong et al., 2018). The catalysts with the higher surface areas and more crystalline carbon were more active for Fenton reaction than those with the lower surface areas and amorphous carbon (Xiong et al., 2018).

In another study, it was reported that CuFe supported on carbon nanofibers were more active than CuFe supported on carbon and the enhanced activity was ascribed to the higher electron transfer rate of carbon nanofibers in comparison to carbon (Wang et al., 2017). The increase in Fenton catalytic activity by the addition of a hydrophobic support such as carbon-base support was explained by the support concentrating the organic pollutant on the surface near the metal oxide active species producing hydroxyl radicals (He et al., 2016; He et al., 2011). In contrast, Georgi and Kopinke (2005) found that hydroxyl radical attach on the organic pollutant occurs in the solution and that the adsorbed pollutant on the surface of the activated carbon were unreactive towards hydroxyl radicals. Based on the findings of Georgi and Kopinke (2005), the addition of carbon could be detrimental for the Fenton catalytic activity.

During the formation of the hydroxyl radicals, the metal ion is oxidised and needs to be reduced again to regenerate the catalytic active site (reaction 1-4). The rate of reduction of the metal ions is slower than the oxidation of the metal ions (reactions 1 - 4). Zubir et al. (2015) found than the Fe (III)/Fe (II) ratio increase with each cycle of the process, leading to a decrease in the activity of the catalyst with each reaction cycle. However, when the iron oxide is supported on graphene oxide, the Fe (III)/Fe (II) ratio remained

constant and the catalyst activity did not decrease with each cycle. This finding was explained by the graphene oxide C=C bonds being oxidized to reduce the Fe (III) to Fe (II). A similar catalytic activity enhancement effect is expected when adding graphene to the copper oxide-based Fenton catalyst in this study. However, one could also argue that if Fe (III) can oxidize the C=C bond then the hydrogen peroxide and hydroxyl radicals which are stronger oxidizing agents (see standard reduction half potentials in reaction 15 to 18) than Fe (III) should also be able to oxidize the C=C bond which would be a competing reaction during the degradation of dye and therefore a decrease in the rate of dye degradation may be observed. This argument is supported by the research findings of Xing et al. (2014). These authors have determined with TEM, Raman and AFM that H_2O_2 can break carbon-carbon bonds and cause holes in the graphene platelets.

$Fe^{3+} + 3e^- = Fe$	-0.04 E° (V)	reaction 14
$Fe^{2+} + 2e^- = Fe$	-0.44 E° (V)	reaction 15
$HO^\bullet + e^- + H^+ = H_2O$	-2.73 E° (V)	reaction 16
$H_2O_2 + 2\ H^+ + 2e- = 2H_2O$	1.763 E° (V)	reaction 17
$2H_2O_2 \rightarrow O_2 + 2H_2O$		reaction 18

The undesirable reaction where the H_2O_2 is decomposed to form oxygen (reaction 18) was found to be catalyzed by carbon-based material such as carbon nanotubes (Voitco et al., 2015) and activated carbon (Rey et al., 2008; Khalil et al., 2001). This reaction will lead to less H_2O_2 being available for the formation of hydroxyl radicals by the Fenton reaction and therefore a decrease in the rate of the degradation of the MB may be expected.

The effect that carbon and graphene will have on the activity of copper oxide based Fenton reaction is thus not clear and further research is required.

2.5 Copper oxide nanoparticles preparation

In a review article by Gawande et al. (2016), it was indicated that there are five main groups of preparation methods for preparation of copper oxide nanoparticles which are:

chemical methods, electrochemical synthesis, photochemical techniques, sonochemical methods, and thermal treatment. A chemical precipitation reduction method is chosen for this study since the size and shape can be controlled (Gawande et al., 2016). Only this method will be discussed in more detail. The copper (II) salt is precipitated with a base like NaOH and thereafter reduced with a reducing agent like hydrazine and $NaBH_4$ in the presence or absence of capping agents (Gawande et al., 2016). Ouyang et al. (2016) manipulated the phase, size and shape by changing the amount of precipitating agent (NaOH), amount of reducing agent (N_2H_4), capping agent (PVP) and temperature. The size of copper oxide particles can be controlled by the amount of base added. For instance, an increase in size was observed with an increase in the volume of NaOH used (Ke et al., 2016).

The type of precipitating agent can also influence the shape and size of the copper oxide crystals. Xu et al. (2006) varied the relative amounts of NH_4OH and NaOH (both precipitating agents were used simultaneously) and spheres, cubic and octahedral crystals with different sizes were formed.

The amount of reducing agent can also affect the size, shape and copper/copper oxide phase ($Cu/Cu(OH)_2/CuO/Cu_2O$) (Deng et al.,2017). An increase in the amount of hydroxylamine hydrochloride as reducing agent resulted in increase in the amount of Cu_2O and a decrease in the amount of CuO and the morphology change from sheets to octahedral shapes (Deng et al., 2017). Not all the copper hydroxide is converted to copper oxide when not enough reducing agent is used (Ouyang et al., 2016).

In this study hydrazine hydrate ($N_2H_4.H_2O$), ascorbic acid, sodium borohydride and glucose were used as reductants to prepare the copper oxide particles. Cu_2O particles formed through the reduction of $Cu(OH)_2$ or $Cu(OH)_4^{2-}$ by hydrazine hydrate, ascorbic acid, sodium borohydride and glucose (Ke et al., 2016; Zhang et al., 2010).

The precipitation reduction producing copper oxide crystals could happen in the presence or absence of a capping molecule. Some organic molecules like ascorbic acid (Ke et al., 2016) and phytochemicals (Gawande et al., 2016) can have dual functionality by being a capping molecule as well as a reducing agent. The advantage of a capping molecule is

that it decreases agglomeration and assist in shape and size control. The disadvantage is that the capping molecule may be strongly adsorbed on the surface, thereby decreasing the catalytic activity of the catalyst (Lee et al., 2011).

2.6 Different reducing agents

Reducing agents such as hydrazine hydrate (N_2H_4), ascorbic acid (ASC), sodium borohydride and glucose can be used in the preparation steps of copper oxide particles to reduce $Cu(OH)_2$ precipitate into Cu_xO.

2.6.1 Hydrazine hydrate

Hydrazine is an inorganic compound with the chemical formula N_2H_4. It is a colorless liquid with an ammonia-like odour. N_2H_4 is highly toxic and getting exposed to it can result in conditions such as irritation of the nose, eyes, temporary blindness, liver and kidney failure and nausea. (Ejaz and Jeon, 2019). Hydrazine hydrate has been reported to be a very strong reducing agent and gives rise to a much faster reduction process during the preparation of nanoparticles (Andal and Buvaneswari, 2017).

Reactions 19-22 are the proposed reactions for the formation of Cu_2O using hydrazine as a reducing agent.

$4Cu^{2+} + N_2H_4 \rightarrow N_2 + 4H^+ + 4Cu^+$ reaction 19

$4Cu(OH)_2 + N_2H_4 \rightarrow N_2 + 4OH^- + 4H_2O + 4Cu^+$ reaction 20

$4Cu(OH)_2 + N_2H_4 \rightarrow N_2 + 4OH^- + 2H_2O + 2Cu_2O + 4H^-$ reaction 21

$4Cu(OH)_2 + N_2H_4 \rightarrow N_2 + 6H_2O + 2Cu_2O$ (Ke et al.,2016). reaction 22

Wang et al. (2010) reported the use of hydrazine hydrate as a reducing agent during the preparation of copper oxide particles. An increase in the concentration of N_2H_4 resulted in the formation of larger particles and a decrease in the concentration of N_2H_4 resulted in the formation of smaller particles.

Rahmatolahzadeh et al. (2016) reported large agglomerated particles when 1 mL of N_2H_4 was used, at lower concentrations of N_2H_4 (0.25 mL) more uniform particles were obtained.

2.6.2 Ascorbic acid

The discovery of ascorbic acid was made about 80 years ago, and its biological use continues to grow (Du et al., 2012). In its impure form ascorbic acid is yellow in color. Its purity and concentration can be determined by its molar absorptivity ε_{265} =14,500 $M^{-1}S^{-1}$ at pH values between 6 and 7.8 and it contains two ionizable hydroxyl groups.

There are advantages and disadvantages of using ascorbic acid as a reducing agent and one of its disadvantage is that it's a weak reducing agent (Qing-Ming et al., 2012). The advantage of using ascorbic acid as a reducing agent is that it is a cheap, abundant and non-toxic (Umer et al., 2014). Also, ascorbic acid functions as both reducing and capping agent, this makes the process of synthesizing nanoparticles less costly and not harmful to the environment. As a capping agent, ascorbic acid protects the synthesized nanoparticles from their external environment and also from coming together to form aggregation of the nanoparticles (Umer et al 2014, Ramos et al., 2018).

Ascorbic acid has antioxidant properties which come from its ability to scavenge free radicals and reactive oxygen molecules, accompanying the donation of electrons to give the semi-dehydroascorbate radical and dehydroascorbic acid (Dang et al., 2011).

Proposed reduction reactions by ascorbic acid (Wu. 2007, Rabastabi et al., 2015)

$2Cu^{2+} + C_6H_8O_6 + H_2O \rightarrow C_6H_6O_6 + 2H^+ + 2Cu^+$ reaction 23

$2Cu(OH)_2 + C_6H_8O_6 \rightarrow C_6H_6O_6 + 4OH^- + 2H^+ + 2Cu^+$ reaction 24

$2Cu(OH)_2 + C_6H_8O_6 \rightarrow C_6H_6O_6 + 2H_2O + 2OH^- + 2Cu^+$ reaction 25

$2Cu(OH)_2 + C_6H_8O_6 \rightarrow C_6H_6O_6 + H_2O + 2H^+ + 2OH^- + Cu_2O$ reaction 26

$2Cu(OH)_2 + C_6H_8O_6 \rightarrow C_6H_6O_6 + Cu_2O + 3H_2O$ reaction 27

In a study by Ramos et al. (2018), copper oxide nanoparticles were prepared and ascorbic acid was used as a capping agent and reducing agent and it was observed that better capping reduced the amount of oxides particularly in samples prepared at higher temperature and with a higher reducing agent concentration-to-lower copper precursor concentration ratio. During the preparation of copper nanoparticles it was observed that the nanoparticles decreased in size as the concentration of the reducing agent (ascorbic acid) was increased. It was explained that the Cu^{2+} encapsulated in ascorbic acid molecules decreases with increasing concentration of ascorbic acid. The reducing agent was also used as a capping agent which prevented the oxidation of the copper oxide particles and increased the stability of the particles (Jain et al., 2015).

2.6.3 Glucose

Glucose, also known as dextrose, is a group of carbohydrates known as simple sugars. Chunfa et al.(2016) described glucose as a non-toxic sugar.Glucose can be used as an environment-friendly reducing agent, it also plays an important role as a reducing agent during the synthesis of nanoparticles because it does not gelatinize or become adhesive (sticky) at low temperatures (Han et al., 2018 and Chen et al., 2017).

The advantage of using glucose as a reducing agent are that it is low-priced, broadly used in many biomaterials, glucose can be obtained from many different sources, it does not cause any harm to human health and its efficiency of conversion is high (Chen et al.,2017). The disadvantage of using glucose as a reducing agent is that it is a weak reducing agent and it requires high temperatures in order for it to reduce metal oxides (Sharma & Sharma 2012).

Proposed reduction reactions by glucose is described as reaction 28-32 (Andal and Buvaneswani .2017):

$2Cu^{2+} + C_6H_{12}O_6 + H_2O \rightarrow C_6H_{12}O_7 + 2H^+ + 2Cu^+$ reaction 28

$2Cu(OH)_2 + C_6H_{12}O_6 + H_2O \rightarrow C_6H_{12}O_7 + 4OH^- + 2H^+ + 2Cu^+$ reaction 29

$2Cu(OH)_2 + C_6H_{12}O_6 + H_2O \rightarrow C_6H_{12}O_7 + 2H_2O + 2OH^- + 2Cu^+$ reaction 30

$2Cu(OH)_2 + C_6H_{12}O_6 + H_2O \rightarrow C_6H_{12}O_7 + H_2O + 2H^+ + 2OH^- + Cu_2O$ reaction 31

$2Cu(OH)_2 + C_6H_{12}O_6 \rightarrow C_6H_{12}O_7 + 2H_2O + Cu_2O$ reaction 32

The rate of reduction of glucose can be controlled based on the glucose isomerization (Nguyen et al., 2015).

Chunfa et al. (2016) reported the use of glucose as a reducing agent during the synthesis of monodispersed silver nanoparticles and it was reported that the amount of reducing agent (glucose) played an important role in the size of the nanoparticles produced and amount produced of the silver nanoparticles. As the concentration of the reducing agent was increased the silver nanoparticles became smaller and the yield improved.

Sharma and Sharma (2012) reported the microscopic investigation of Cu_2O nanostructures using both hydrazine and glucose as reducing agents to determine the different morphologies of Cu_2O. It was reported that glucose was a very weak reducing agent and its strength was enhanced by increasing the reaction temperature from 25°C to 80°C.

2.6.4 Sodium borohydride

Sodium borohydride is a white powder chemical with a chemical formula $NaBH_4$. It is soluble in water and reacts exothermically with water to produce a hydrogen gas.Sodium borohydride is a strong reducing agent used worldwide (Liu et al., 2012). When used as a reducing agent, it can also act as a stabilizer (Banne et al., 2017). Due to its strong reducing ability it may result in side reactions occurring, an ice bath is used to slow down the reaction (Banne et al., 2017 & Mavani et al.,2013).

Reaction 33-36 are the suggested reduction reactions when sodium borohydride is used (Liu et al.,2011):

$BH_4^- + 8OH^- + 8Cu^{2+} \rightarrow B(OH)4^- + 4H_2O + + 8Cu^+$ reaction 33

$8Cu(OH)_2 + BH_4^- \rightarrow B(OH)_4^- + 4H_2O + 8Cu^+ + 8OH^-$ reaction 34

$8Cu(OH)_2 + BH_4^- \rightarrow B(OH)_4^- + 4Cu_2O + 8H^+ + 8OH^-$ reaction 35

$8Cu(OH)_2 + BH_4^- \rightarrow B(OH)_4^- + 4Cu_2O + 8H_2O$ reaction 36

Song et al. (2009) reported the use of $NaBH_4$ as a reducing agent during the preparation of colloidal silver nanoparticles using the reduction method. It was observed that less agglomerated silver nanoparticles were obtained when more than the stoichiometric amount of the reducing agent was used because sodium borohydride could not adsorb onto the surface of the nanoparticles due to a thick BH_4^- layer.

Liu et al. (2012) reported the preparation of Cu nanoparticles with $NaBH_4$ by aqueous reduction method and observed that the increase of sodium borohydride resulted in a decrease in the average size of the nanoparticles.

Aguilar and Rosas. (2019) reported the synthesis of Cu_2O spherical nanoparticles using $NaBH_4$ as a reducing agent for the degradation of methylene blue dye. Spherical Cu_2O nanoparticles with an average size of 90 and 200 nm were obtained and it was observed that the particles with a size of 90 nm had a removal of about 63% and particles with a size of 200 nm had a removal of 44% indicating that spherical Cu_2O nanoparticles prepared using $NaBH_4$ can be used in the degradation of methylene blue dye.

Chapter 3

3.1 MATERIALS AND METHODS

This chapter describes the preparation of Cu_2O nanoparticles using hydrazine and ascorbic acid as reducing agents. It also presents how different parameters were varied during the preparation and how the different catalysts were used in the degradation of methylene blue.

3.1.1 Chemicals

Table 2: List of chemicals used, purity and suppliers.

chemicals	**Purity (%)**	**Supplier**
Hydrazine hydrate	78-82 %	Sigma-Aldrich
Sodium hydroxide	98 %	Glass world
Ammonium solution	25 %	Glass world
Ascorbic acid	99 %	Sigma-Aldrich
Copper chloride	99 %	Sigma-Aldrich
Isopropanol	99%	Glass world
Methanol	99%	Glass world
Hydrogen peroxide	30 %	Glass world
Methylene blue	82 %	Sigma-Aldrich
Sodium borohydride	96%	Sigma-Aldrich
Glucose	99.5 %	Sigma-Aldrich
Copper sulphate	98.5 -101 %	Sigma-Aldrich
Copper nitrate	99 – 104 %	Sigma-Aldrich

All chemicals were of analytical grade and were used as received without further purification. All glassware used in the experiment were cleaned and washed thoroughly with de-ionized water and dried before use. The degradation was carried out in a glass reactor vessel connected to a water bath.

3.1.2 Apparatus

Beakers, weighing boat, hot plate, volumetric flasks, weighing balance, measuring cylinders, micropipettes (100 to 5000 µL), pasture pipettes, stirrer bars, pipette tips, centrifuge tubes, centrifuge machine, sonicator, vacuum oven, sample vials, aluminum foil, cuvettes, water bottle, water bath, glass reactor vessel, magnetic stirrer bars, UV lamp, LED lights were used for the synthesis of the nanoparticles.

3.1.3 Synthesis

Copper oxide crystals were prepared using precipitation reduction methods. The methods were based on the articles of Xu et al. (2006) and Zhang et al. (2010).

3.1.4 Preparation of Cu_xO particles using hydrazine as reducing agent.

The method of Xu et al.(2006) was used for the preparation of Cu_2O particles using hydrazine as the reducing agent with slight modifications. The amount of hydrazine used was changed, the solvent used to wash the precipitate was changed from ethanol to methanol and the precipitate was dried in a fume hood instead of vacuum oven.

A mass of 0.852 g of $CuCl_2 \bullet 2H_2O$ was weighed and dissolved in a 100 mL of de-ionized water. Ammonia solution (2.5 mL, 14 M) was then added into the $CuCl_2$ solution under constant stirring. A blue soluble complex:

$[Cu(OH_2)_6]^{2+} + 4NH_3 \rightarrow [Cu(NH_3)_4(OH_2)_2]^{2+} + 4H_2O$ reaction 37 then

$[Cu(NH_3)_4(OH_2)_2] + 2NaOH \rightarrow + Na_2(Cu(OH)_4 + 4NH_3$ reaction 38, was formed.

A blue precipitate of $Cu(OH)_2$ was produced when (10 mL, 1 M) NaOH was added drop-wise to the above solution. After stirring for 10 minutes (1 mL, 85 %) $N_2H_4.H_20$ was added drop-wise to the $Cu(OH)_2$ precipitate suspension with constant stirring for another 10 minutes. The $Cu(OH)_2$ precipitate gradually turned yellow and then red. The red precipitate was centrifuged at 5000 rpm for 5 minutes and washed with deionized water and methanol several times and dried in a fume hood.

3.1.5 Preparation of Cu_xO particles using ascorbic acid, $NaBH_4$ and glucose as reducing agent

The method of Zhang et al. (2010) was used for the preparation of copper oxides with ascorbic acid, sodium borohydride and glucose as reducing agents (with slight modification).The method used $CuSO_4$ as the precursor salt however $CuCl_2$ was used as the precursor salt in this study. Aqueous solution of NaOH (40 mL, 0.5 mol L^{-1}) was added into an aqueous solution of $CuCl_2$ (20 mL, 0.5 mol L^{-1}) with constant stirring as shown in reaction 39-40:

$CuCl_2.2H_2O + 4H_2O \rightarrow [Cu(OH_2)_6]^{2+} + 2Cl^-$ then reaction 39

$[Cu(H_2O)_6]^{2+} + 2OH^- \rightarrow [Cu(OH)_2(H_2O)_4] + 2H_2O$ reaction 40.

The aqueous solution of ascorbic acid (50 mL, 0.1 mol L^{-1}) was added drop-wise into the copper-solution and stirred vigorously at room temperature. After 30 min of stirring, a yellow precipitate was observed, the particles were separated from the solution using centrifugation at 5000 rpm for 5 minutes. The precipitate was then washed with de-ionized water and methanol. The final product was dried in a fume hood.

3.1.6 Preparation of copper oxide graphene and AC composites

The method of Zhang et al. (2010) was used with slight modifications for the preparation of copper oxide-graphene/AC composites. ASC was used as a reducing agent. $CuCl_2$ as a precursor salt and NaOH as a precipitation agent. Aqueous solution of NaOH (40 mL, 0.5 mol L^{-1}) was added into an aqueous solution of $CuCl_2$ (20 mL, 0.5 mol L^{-1}). Different percentages of graphene and AC 1 and 5% (0.0066 g and 0.0344 g) was added into the reaction. ASC (50 mL, 0.4 nol L^{-1}) was added dropwise and stirred vigorously at room temperature. After 30 minutes a grey precipitate was observed. The precipitate was then separated using centrifugation at 5000 rpm for 5 minutes. The precipitated was then washed with de-ionized water and methanol. The final product was dried in the fume hood.

3.1.7 Fenton degradation of methylene blue using the prepared Cu_xO particles as catalyst

A mass of 0.1000 g of the copper oxide was weighed and transferred into a jacketed glass reactor which was connected to a water bath that was kept at a constant temperature of 27 ^{o}C. A volume of 10 mL (1000 ppm) methylene blue stock solution was then added into the reactor. De-ionized water (70 mL) was added. The MB solution had a concentration of 100 ppm. The MB solution was stirred for 1 hour in the dark in order for adsorption equilibrium to be reached. After an hour, 20 mL of H_2O_2 was added into the solution to initiate the Fenton oxidation reaction. Samples (1 mL) were taken at different time intervals. The samples were each transferred into a 100 mL volumetric flask, 1 mL of isopropanol was added and diluted with cold water to the mark. Isopropanol was added into the volumetric flask to quench the reaction. The diluted solutions were then transferred to centrifuge tubes and centrifuged at 3500 rpm for two minutes to remove the catalyst. The clear solutions were analyzed with UV-Vis spectroscopy.

3.1.8 Photo-Fenton degradation of MB using the prepared copper oxide particles as catalysts

A mass of 0.1000 g was weighed and transferred into a jacketed glass reactor which was connected to a water bath that was kept at a constant temperature of 27 ^{o}C. A volume of 10 mL (1000 ppm) of methylene blue stock solution was then added into the reactor. De-ionized water (70 mL) was added then the solution was stirred for 1 hour in the dark in order for adsorption equilibrium to be reached. After an hour, 20 mL of H_2O_2 was added into the solution to initiate the Fenton oxidation reaction and the UV lamp was switched on to initiate the photo-degradation oxidation reaction. Samples (1mL) were taken at different time intervals. The samples were each transferred into a 100 mL volumetric flask, 1 mL of isopropanol were added and diluted with cold water to the mark. Isopropanol was added into the volumetric flask to quench the reaction. The diluted samples were then transferred to centrifuge tubes and centrifuged at 3500 rpm for two minutes to remove the catalyst. The diluted samples were analyzed with UV-Vis spectroscopy.

3.1.9 Photodegradation of methylene blue using the prepared Cu_xO particles as catalyst

Methylene blue solution (20 ppm), prepared from a stock solution of 1000 ppm, was used in the photodegradation experiment. A mass of 0.075 g of the Cu_2O catalyst was weighed and transferred to an Erlenmeyer flask that was covered in foil to prevent degradation from the light. A volume of 150 mL of MB from the 20 ppm solution was measured and poured into the flask. The solution was sonicated for 10 minutes to ensure that the solution and catalyst had fully mixed. The solution was transferred to a beaker with LED lights with wavelength of around 200- 800 nm. The experiments were conducted in the dark to prevent photocatalysis from the ambient light. The solution was stirred for an hour in the dark in order for adsorption equilibrium to be reached. Thereafter the light was turned on and at different time intervals samples (3 ml) were taken and filtered and 3 mL of isopropanol was added to quench the reaction. The samples were analyzed with UV-Vis spectroscopy.

3.2 Characterization of the Cu_xO particles

3.2.1 X-ray diffraction (XRD)

XRD analyses were done using the Shimadzu-XRD 700, X-ray diffractometer with Cu Ka radiation (λ-1.154056 Å). A scan speed of 1˚/minute, current 30 mA and voltage of 40 kV was used.

3.2.2 UV-Visible spectroscopy (UV-Vis)

UV-Vis spectroscopy analyses were performed with a double beam spectrometer-Perkin Elmer Lambda 25 UV/Vis with a tungsten and deuterium lamp. It collects spectra from 180-1100 nm using a bandwidth of 1 nm with a fixed slit. A baseline setting was done by using de-ionized water as a reference sample. To estimate optical absorption edges the $(\alpha h\nu)^n$ versus hv curves (Tauc plot) were plotted for n=1/2 (direct) and n=2 indirect transitions. In this cases n=2 was chosen for the Tauc plot because all data showed a linear relationship indicating an indirect transition.

3.2.3 Scanning electron microscope (SEM)

SEM analysis was performed as follows. A small amount of the sample was sprinkled onto an aluminum SEM stub coated with carbon glue. Excess sample was gently blown

off with compressed air. The samples were then coated in an evaporation coater with a thin layer of carbon, this was to make the samples conductive. The samples were viewed in an FEI Nova NanoSEM 230 with a field emission gun. The viewing conditions (Kv, working distance and spot size are all on the data bar on the bottom of the images). The elemental analysis was carried out using an Oxford X-max detector and Inca software. The crystallite sizes were estimated using ImageJ.

3.2.4 Transmission Electron Microscopy (TEM)

The size and shape of the dried nanoparticles were determined using TEM, LEO TEM 912, with an acceleration voltage of 120 kW and a tungsten wire filament. The nanoparticles dispersed in methanol were pipetted onto carbon coated, copper grids and allowed to dry. The nanoparticles' sizes were measured using the software program ImageJ

3.2.5 Fourier Transform Infrared (FTIR)

The FTIR spectrum of Cu_xO nanoparticles was recorded on a Thermo Scientific NICOLET iS50 FT-IR spectrometer in the range 400-4000 cm^{-1} to interpret the functional groups present on the catalyst.

3.2.6 Brunauer- Emmet-Teller (BET)

The specific surface area, pore volume and pore size were measured using Nitrogen physisorption at 77 K. A micrometrics TRISTA 3020 analyzer (USA) was used for the measurements. The sample was degassed by evacuation at 150 °C for 2 hours.

Table 3: Copper oxide crystal preparation parameters.

Code	Mass of $CuCl_2.2H_2O$ in g	Amount of 14M NH_3 in ml	Conc [NaOH] in M	Amount of NaOH in ml	Reducing agent	Amount of reducing agent	Conc of reducing agent in M	Stirring/reaction time in minutes	Temperature in °C
H1	0.852	2.5	1.0	10	H_2H_4	1	0.1	10	26
H2	0.852	2.5	1.0	10	H_2H_4	1	0.1	20	26
H3	0.852	2.5	1.0	10	H_2H_4	0.1	0.1	20	28
H4	0.852	2.5	1.0	10	H_2H_4	0.1	0.1	20	40
H5	0.852	2.5	1.0	10	H_2H_4	0.1	0.1	20	65
A1	8.524	-	0.5	40	ASC	50	0.1	30	27
A2	8.524	-	1.0	40	ASC	50	0.1	30	27
A3	8.524	-	1.5	40	ASC	50	0.1	30	27
A4	8.524	-	0.5	40	ASC	50	0.1	30	27
A5	8.524	-	0.5	40	ASC	50	0.2	30	27
A6	8.524	-	0.5	40	ASC	50	0.4	30	27
G1	8.524	-	0.5	40	Glucose	50	0.1	30	27
G2	8.524	-	0.5	40	Glucose	50	0.4	30	27
G3	8.524	-	0.5	40	Glucose	50	0.1	30	85
G4	8.524	-	0.5	40	Glucose	50	0.1	30	90
G5	8.524	-	0.5	40	Glucose	50	0.1	30	95
G6	8.524	-	0.5	40	Glucose	50	0.1	30	100
B1	8.524	-	0.5	40	$NaBH_4$	50	0.1	30	27
B2	8.524	-	0.5	40	$NaBH_4$	50	0.5	30	27
B3	8.524	-	0.5	40	$NaBH_4$	50	0.0125	30	27

Table 4: Cu_2O catalyst supported on graphene and activated charcoal

Code	Mass of $CuCl_2.2H_2O$ in g	Mass of Carbon in g	Conc of NaOH in M	Amount of NaOH in mL	Reducing agent	Amount of reducing agent in mL	Concentration of reducing agent in M	Stirring/reaction time in minutes	Temperature in °C
G1	8.524	0.0066 (1%)	0.5	40	ASC	50	0.4	30	27
G2	8.524	0.0344 (5%)	0.5	40	ASC	50	0.4	30	27
AC1	8.524	0.0066 (1%)	0.5	40	ASC	50	0.4	30	27
AC2	8.524	0.0344 (5%)	0.5	40	ASC	50	0.4	30	27

Table 5: Preparation of Cu_2O catalyst using copper sulphate and copper nitrate salts.

code	Mass of $CuSO_4.5H_2O$ in g	Conc of $CuSO_4.5H_2O$ M	Amount of NaOH in mL	Conc of NaOH in M	Reducing agent	Amount of reducing agent in mL	Conc of reducing agent in M	Stirring/reaction time in minutes	Temperature in °C
S1	7.9805	0.5	40	1.5	ASC	50	0.1	30	27
code	Mass of $Cu(NO_3)_2.3H_2O$ in g	Conc of $Cu(NO_3)_2.3$ in M	Amount of NaOH in mL	Conc of NaOH in M	Reducing agent	Amount of reducing agent in mL	Conc of reducing agent in M	Stirring/reaction time in minutes	Temperature in °C
N1	9.9825	0.5	40	1.5	ASC	50	0.1	30	27

Chapter 4

4.1 RESULTS AND DISCUSSIONS

4.2 Preparation of copper oxide catalysts with ascorbic acid as reducing agent.

A precipitation reduction method was used to prepare the copper oxide crystallites. The preparation method used was based on the method of Zhang et al. (2010) with slight modification, $CuCl_2$ was used as a precursor instead of $CuSO_4$. NaOH was used as the precipitating agent and ascorbic acid (ASC) was used as reducing agent. The amount of ASC was varied to see the effect on the size, shape, copper phase of the crystals and catalytic activity.

4.2.1 Preparation of Cu_2O particles varying ASC

Different concentrations of ASC was varied during the preparation of copper oxide which were 0.1, 0.2 and 0.4 mol L^{-1} , 0.5 mol L^{-1} $CuCl_2$ and 0.5 mol L^{-1} NaOH were used in all reactions.

$2Cu(OH)_2 + C_6H_8O_6 \rightarrow Cu_2O + C_6H_6O_6 + 3H_2O$ (Reaction 27)

Based on reaction 27, 1 mol of ASC reacts with 2 mols of Cu^{2+}, the stoichiometric amount was calculated to be 0.005 mols (50 ml of 0.1 mol.L^{-1}) ASC reacting 0.01 mol of Cu^{2+} (20 ml of 0.5 mol.L^{-1}). The 0.1 mol.L^{-1} ASC was thus the stoichiometric concentration and two times and four times the stoichiometric amounts were used.

4.2.1.1 ***XRD analyses***

The prepared copper oxide particles were analyzed with XRD to determine the crystallite size and the phases of the particles prepared (Figure 2). The calculated sizes of the particles are shown in Table 6. The smallest crystallites were formed at an ASC concentration of 0.1 mol.L^{-1}. The amount of ascorbic acid did not have a strong effect on the crystallite sizes. At low concentrations of the reducing agent both CuO and Cu_2O phases were obtained but the Cu_2O was the predominant phase. As the concentration of ascorbic acid was increased only the Cu_2O phase was observed in the XRD pattern. The stoichiometric amount of ASC was thus not sufficient to enable reduction of all the copper (II) to copper (I) since more ASC is required to achieve only the Cu_2O phase.

Table 6: XRD sizes calculations of copper oxide particles prepared using 0.1, 0.2 and 0.4 mol L^{-1} ASC.

0.1 mol L^{-1} ASC			
Phase	**Angle (2θ°)**	**FWHM (2θ°)**	**Size (nm)**
CuO	43.33	0.63	13.5
Cu_2O	36.29	0.42	19.8
0.2 mol L^{-1} ASC			
Phase	**Angle (2θ°)**	**FWHM (2θ°)**	**Size (nm)**
Cu_2O	36.36	0.35	23.8
0.4 mol L^{-1} ASC			
Phase	**Angle (2θ°)**	**FWHM (2θ°)**	**Size (nm)**
Cu_2O	36.43	0.49	17.0

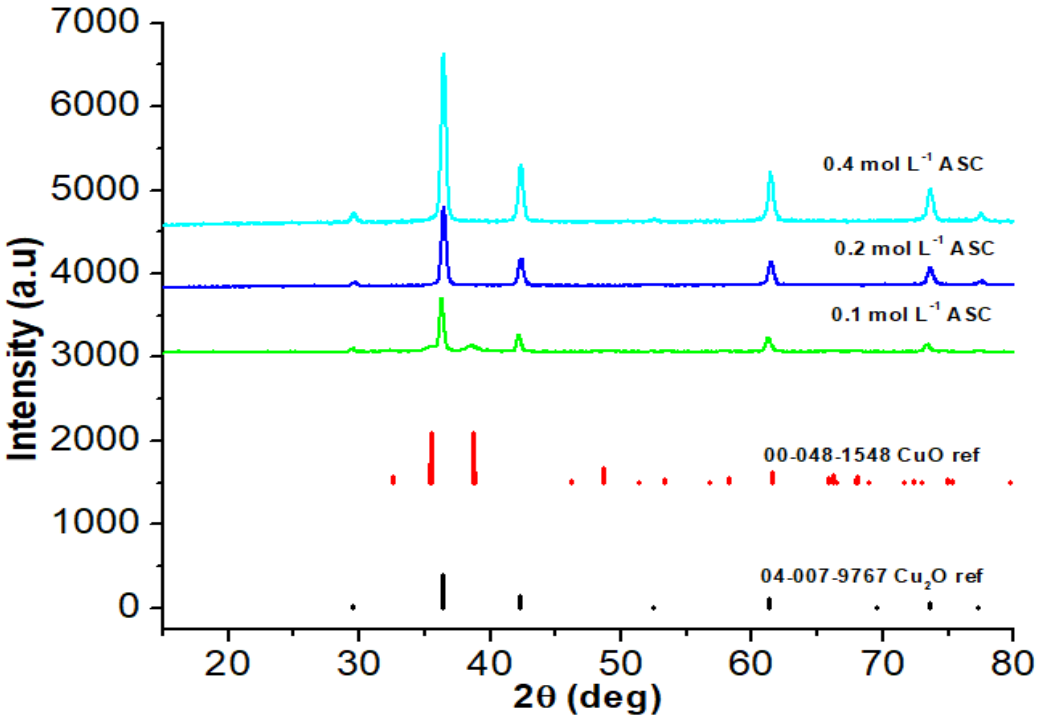

Figure 2: XRD diffraction pattern of copper oxide particles prepared using 0.1, 0.2 and 0.4 mol L^{-1} ASC as reducing agent. 0.5 mol L^{-1} NaOH and 0.5 mol L^{-1} $CuCl_2$.

4.2.1.2 ***Stability of copper oxide particles prepared using ASC as reducing agent***

The Copper oxide particles prepared using ASC were analyzed using XRD (Figure 3) after preparation and it was observed that the particles were in-line with Cu_2O reference spectra indicating that pure Cu_2O particles were obtained. After a month of storage, the same particles were analyzed again with XRD and it was observed that the particles were still in-line with Cu_2O reference spectra. The Cu2O particles did not oxidize to CuO in the presence of air. This indicated that ASC plays a dual role as a reducing agent and antioxidant of copper nanoparticles.

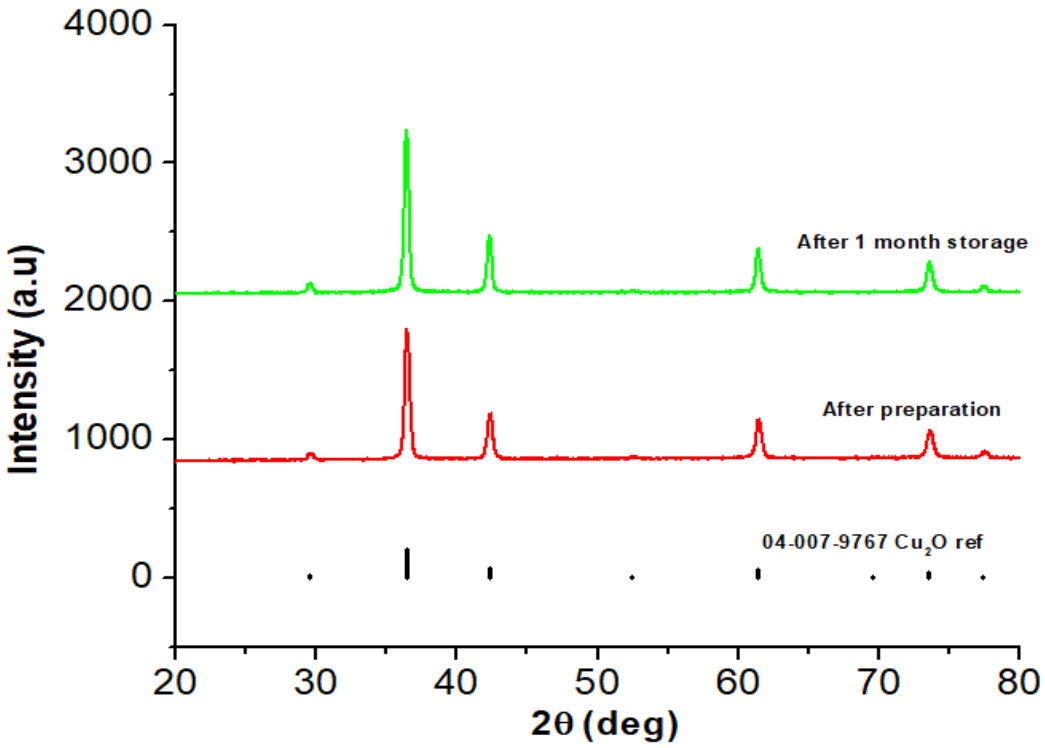

Figure 3: XRD diffraction patterns of the stability of copper oxide particles prepared using 0.2 mol L^{-1} ASC as reducing agent, 0.5 mol L^{-1} $CuCl_2$ and 0.5 mol L^{-1} NaOH.

4.2.1.3 ***BET analyses***

The specific surface area of the 0.1 mol L^{-1} ASC catalyst was investigated using adsorption and desorption isotherms. The BET surface area was 23.7 m^2/g and the isotherm corresponded to the type IV according to IUPAC classification. The BJH pore size distribution was used to determine the pore size distribution of the particles. The pore

size peak was from 260-450 nm which indicated that the particles are microporous structures. Average pore size was 54.6 Å.

4.2.1.4 ***SEM analyses***

SEM analyses (Figure 4) show a,b and c that the copper oxide particle formed were spherical and agglomerated. At a low ASC concentration (0.1 mol L^{-1}) there particles had a size of about 119 nm. And at concentrations of 0.2 mol L^{-1} and 0.4 mol L^{-1}, the particles size was estimated to be a 130 and 104 nm respectively. The smallest particles size were obtained at the highest concentration of ASC used.

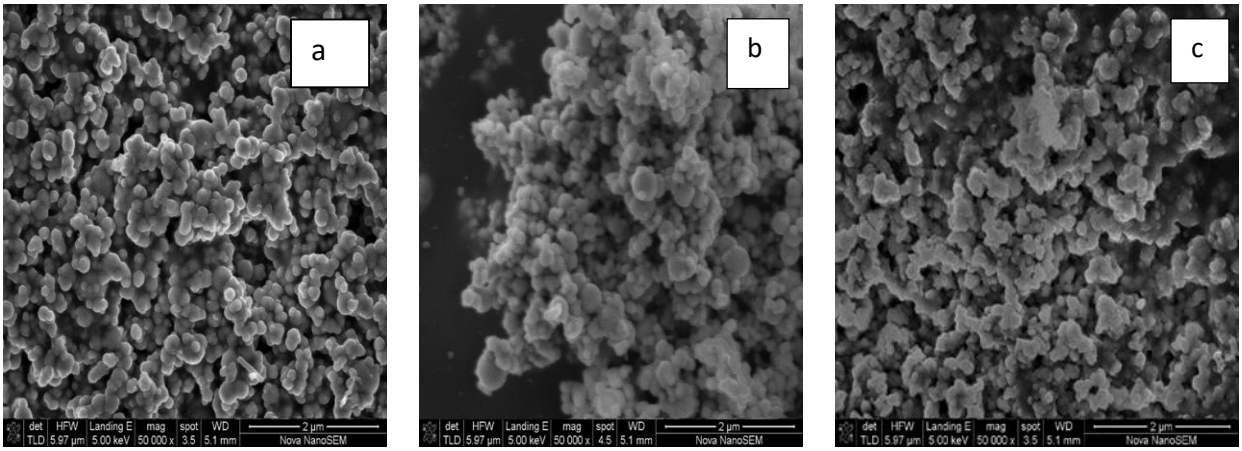

Figure 4: SEM images of copper oxide particles prepared using (a) 0.1, (b) 0.2 and 0.4 mol L^{-1} ASC as reducing agent.

4.2.1.5 ***UV-vis spectroscopy analyses***

The copper (I) oxide particles prepared using 0.1, 0.2 and 0.4 mol L^{-1} ASC solutions were characterized using UV-vis. There was observable difference between the optical absorption profiles of the catalysts prepared using the concentrations given above. It can be observed from the UV-vis spectrum in Figure 5(A1) that the particles prepared using 0.1 mol L^{-1} ASC exhibit optical absorption over UV and visible regions of the solar spectrum. The absorption is higher over visible region, this is advantageous for visible light utilization. The particles prepared using 0.2 and 0.4 mol L^{-1} ASC showed an optical absorption at 500 nm and 495 nm. The indirect band gap was estimated using the $(\alpha h\nu)^2$ versus hv plots for the catalysts prepared using 0.1, 0.2 and 0.4 mol L^{-1} ASC were 1.33, 1.80 and 1.89 eV respectively. These values are lower than the 2.137 eV commonly

reported for bulk Cu_2O, indicating that the particles of the prepared Cu_2O in this study are larger in size.

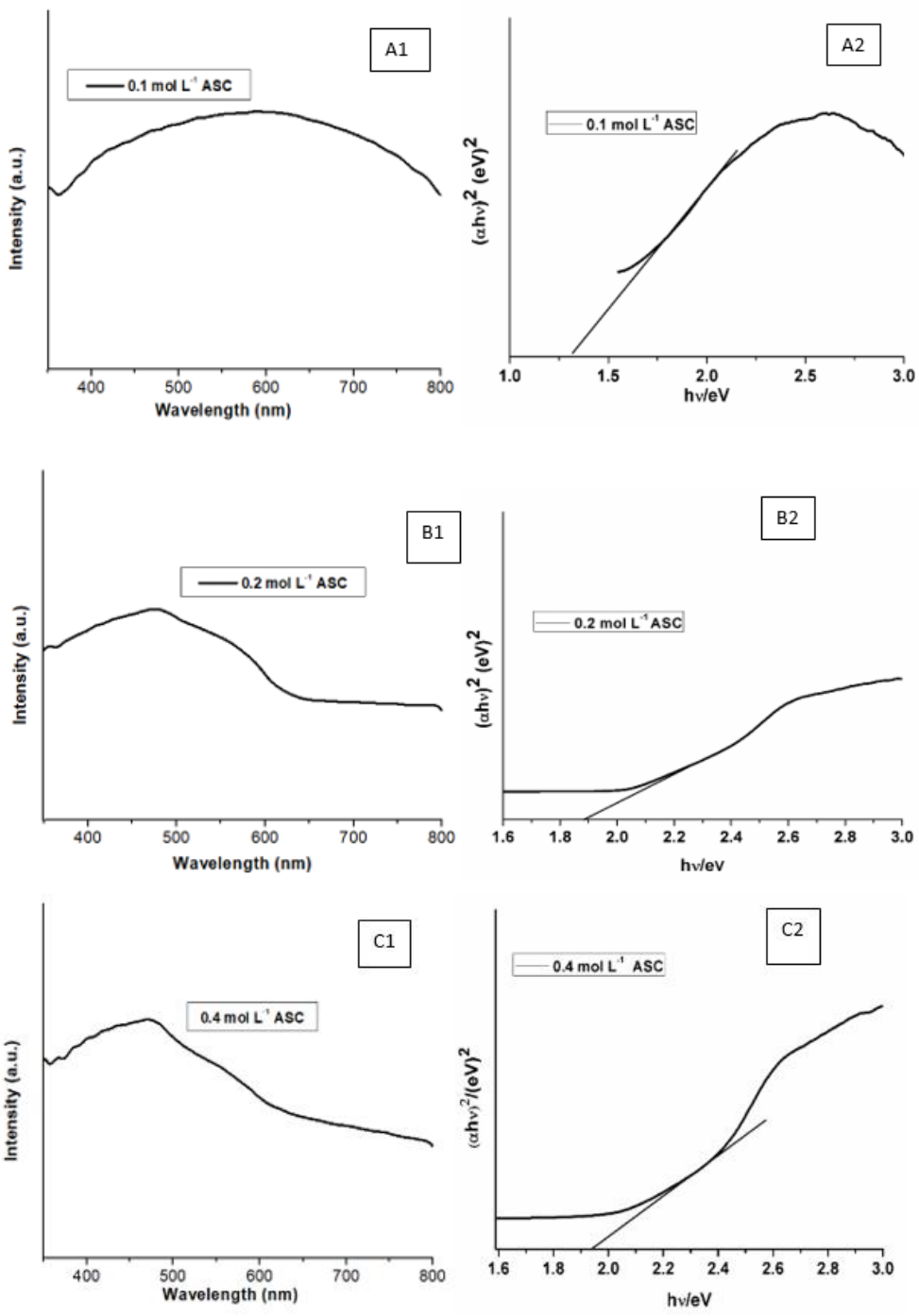

Figure 5: (A1,B1 & C1) UV-vis absorption spectra and (A2,B2 & C2) Tauc plot of the prepared copper oxide particles prepared with 0.1,0.2 & 0.4 mol L^{-1} ASC as reducing agent ,0.5 mol L^{-1} NaOH, 0.5 mol L^{-1} $CuCl_2$.

4.2.1.6 ***FTIR analyses***

As it can be seen in Figure 6 ascorbic acid consists of O-H stretching at around 3500-3200 cm^{-1}, a carbonyl C=O stretching at around 1760-1665 cm^{-1}, C=C stretching around 1680-1640 cm^{-1} , a =C-H alkene stretching around 3100-3000 cm^{-1} and an alkane C-H stretching around 3000-2850 cm-1 . These peaks characteristic of ascorbic acid were observed in all the copper oxide catalysts that were prepared using ASC as a reducing agent. This suggested that the ASC had capped the prepared copper oxide particles which might have attributed to the oxidation stability of the particles. This was observed in a study done by Shakina et al.(2015) where ASC was observed on the surface of the prepared copper oxide particles and this suggested that ascorbic acid was both a reducing agent and capping agent of the prepared copper oxide nanoparticles.

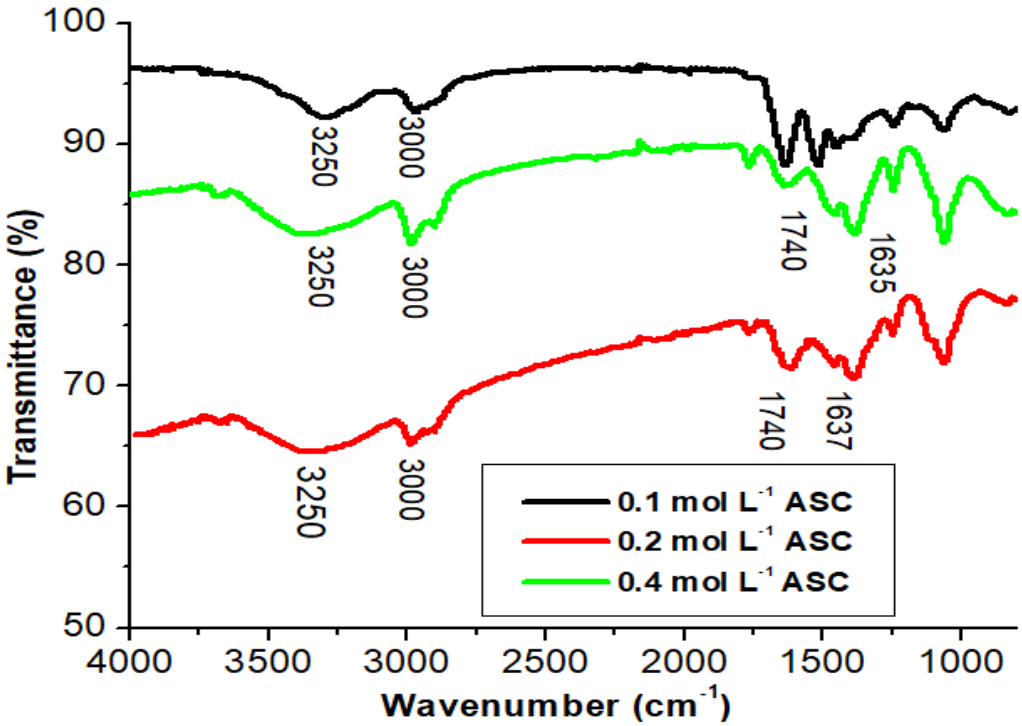

Figure 6: FTIR spectra of copper oxide particles prepared with 0.1, 0.2 and 0.4 mol L^{-1} ASC. 0.5 mol L^{-1} $CuCl_2$. 0.5 mol L^{-1} NaOH.

4.2.2 Degradation of methylene blue using copper oxide particles prepared using ASC as the reducing agent.

4.2.2.1 ***Fenton and Photo-Fenton degradation***

The catalyst was added into the MB and reacted for 1 hour to reach adsorption equilibrium, different catalysts adsorbed different concentrations of MB hence the Fenton and Photo-Fenton degradations started at different concentrations. The rate of the photocatalytic reaction was the highest when the highest ascorbic acid concentration was used during preparation (see Figure 7 and Table 7). The Fenton catalysis was compared with the photo-Fenton catalysis as shown in Figure 7. In the case where the catalyst was prepared using the lowest concentration of ascorbic acid, the rate of reaction of the Fenton reaction was higher than the photo-Fenton. The opposite was observed for the catalyst prepared using the higher concentration of ascorbic acid.

Photo-Fenton reaction can either have a high reaction rate than the Fenton reaction due to the additional pathways of $OH^{\bullet}$ generation during degradation (Mia et al.,2018) or a lower reaction rate due to photo-corrosion which can be caused by photo oxidation in the presence of photo induced hole resulting in the oxidation of Cu_2O to CuO which is an inactive phase of photocatalysis (Toe et al., 2018).

The low reaction rate of the Photo-Fenton reaction of the particles prepared using 0.1 and 0.2 mol L^{-1} ASC can be attributed to photo-corrosion (photo oxidation). This was reported in a study by Toe et al. 2018 where by Cu_2O is oxidized into CuO during degradation by the photo induced holes. The photo oxidation process is shown in reaction 41:

$$Cu_2O + 2OH^- + 2h^+ \rightarrow 2CuO + H_2O \qquad \text{Reaction 41}$$

Table 7: Rate constants of degradation of methylene blue using Fenton and Photo-Fenton degradation.

Fenton degradation					
Catalyst (mol L^{-1} ASC)	**k-values (1^{st} order) (s^{-1})**	**k-values (2^{nd} order) (m^{-1} s^{-1})**	**R^2 (1^{st} order)**	**R^2 (2^{nd} order)**	**percentage (%) removal (after 60 min degradation)**
0.1	0.0222	0.0011	0.9567	0.9888	77
0.2	0.0316	0.0010	0.9712	0.9493	88
0.4	0.0307	0.0006	0.9633	0.9461	88
Photo-Fenton degradation					
Catalyst (mol L^{-1} ASC)	**k-values (1^{st} order) (s^{-1})**	**k-values (2^{nd} order) (m^{-1} s^{-1})**	**R^2 (1^{st} order)**	**R^2 (2^{nd} order)**	**percentage (%) removal (after 60 min degradation)**
0.1	0.0179	0.0004	0.9974	0.9872	66
0.2	0.0141	0.0003	0.9938	0.9946	56
0.4	0.0380	0.0018	0.9327	0.9864	91

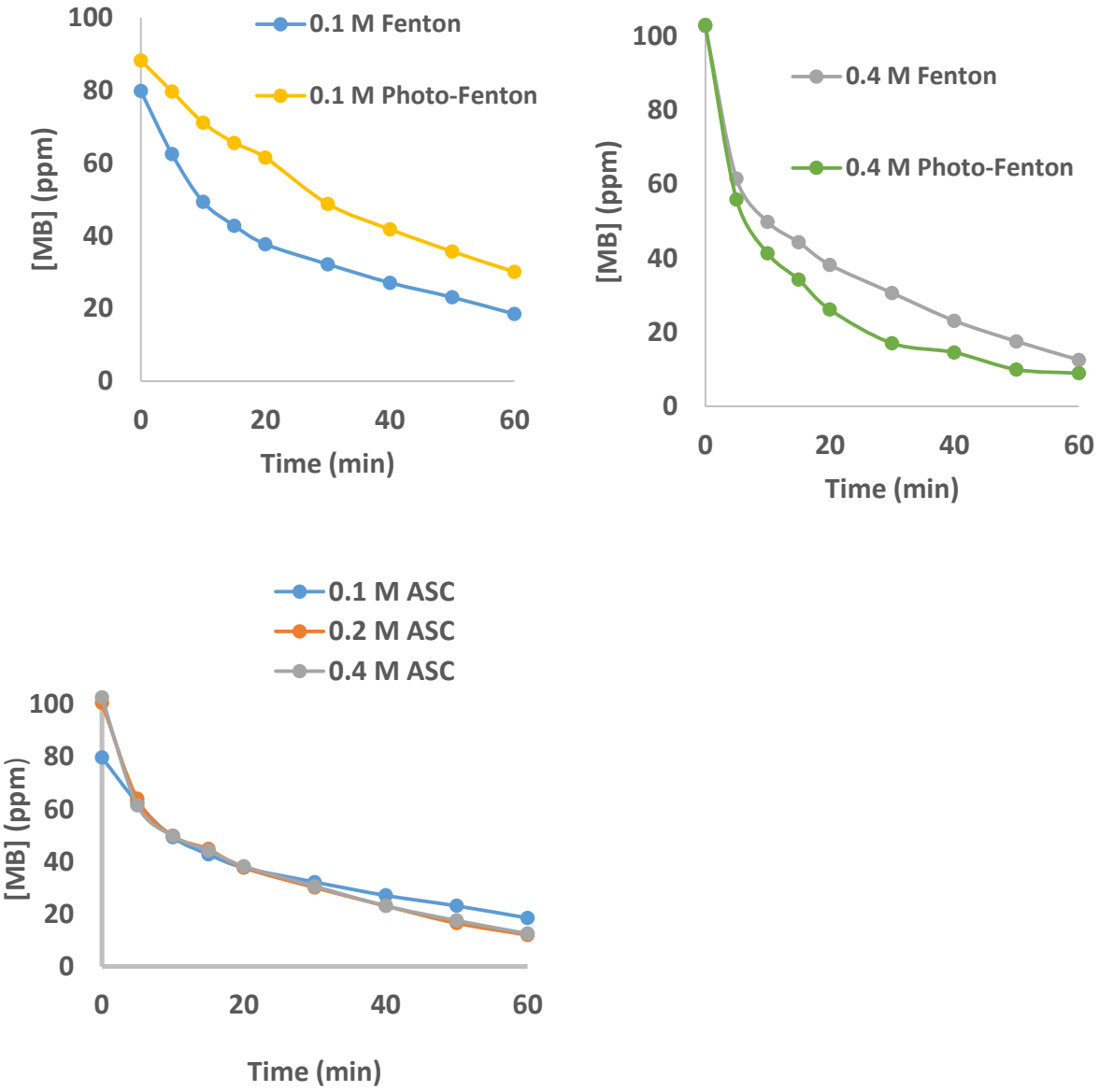

Figure 7: Fenton and Photo-Fenton degradation of MB using particles prepared with 0.1, 0.2 and 0.4 mol L^{-1}ASC as reducing agent.

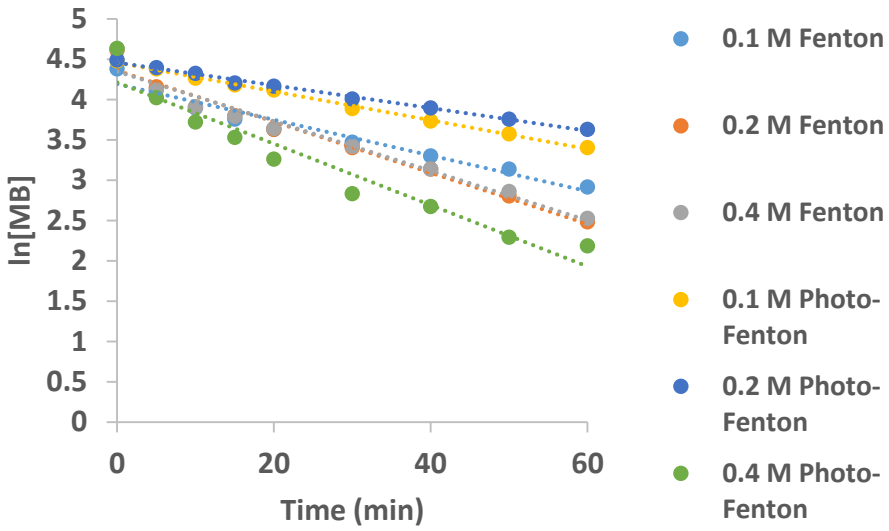

Figure 8: First order plots of the degradation of MB using copper oxide particles prepared with 0.1, 0.2 and 0.4 mol L^{-1} ASC.

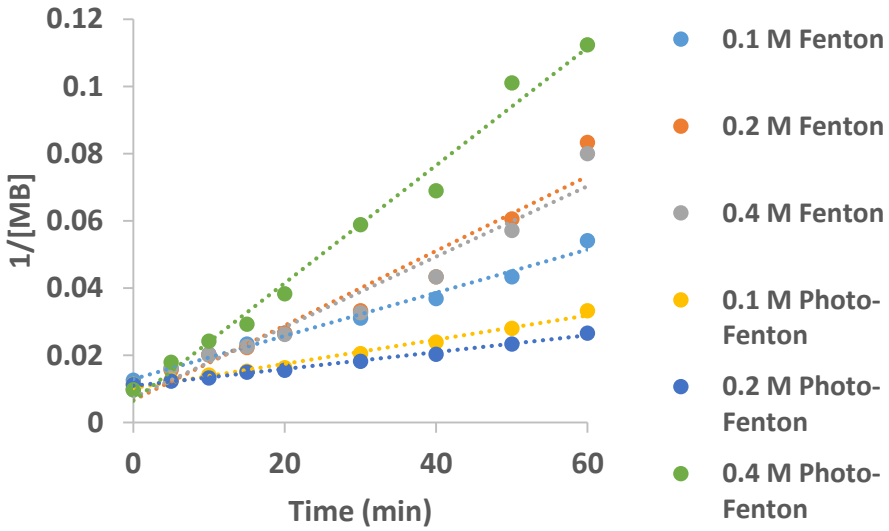

Figure 9: Second order plots of the degradation of MB using copper oxide particles prepared with 0.1, 0.2 and 0.4 mol L^{-1} ASC as reducing agent.

4.2.3 Preparation of Cu_2O particles varying NaOH

Different concentrations of NaOH were used which were 0.5, 1 and 1.5 mol L^{-1}. Concentrations of 0.5 mol L^{-1} $CuCl_2$ and 0.1 mol L^{-1} ASC were used in the preparations.

4.2.3.1 ***XRD analyses***

The sizes of the particles were calculated are shown in Table 8 and the crystallite sizes increased from 13 nm to 20 nm with an increase in the NaOH concentration. The particles prepared using 0.5 mol L^{-1} NaOH consisted of a mixture of Cu_2O and CuO and the particles mostly consisted of the Cu_2O phase (Figure 10). At higher NaOH concentrations only the Cu_2O phase was observed.

Table 8: XRD sizes and phase of copper oxide particles prepared varying different concentrations of NaOH.

Catalyst (mol L^{-1} NaOH)	Phase	Angle (2θ°)	FWHM (2θ°)	Size (nm)
1.5	Cu_2O	36.57	0.42	19.8
1	Cu_2O	36.29	0.49	17.0
0.5	Cu_2O	36.15	0.63	13.2
	CuO	38.40	0.63	13.3

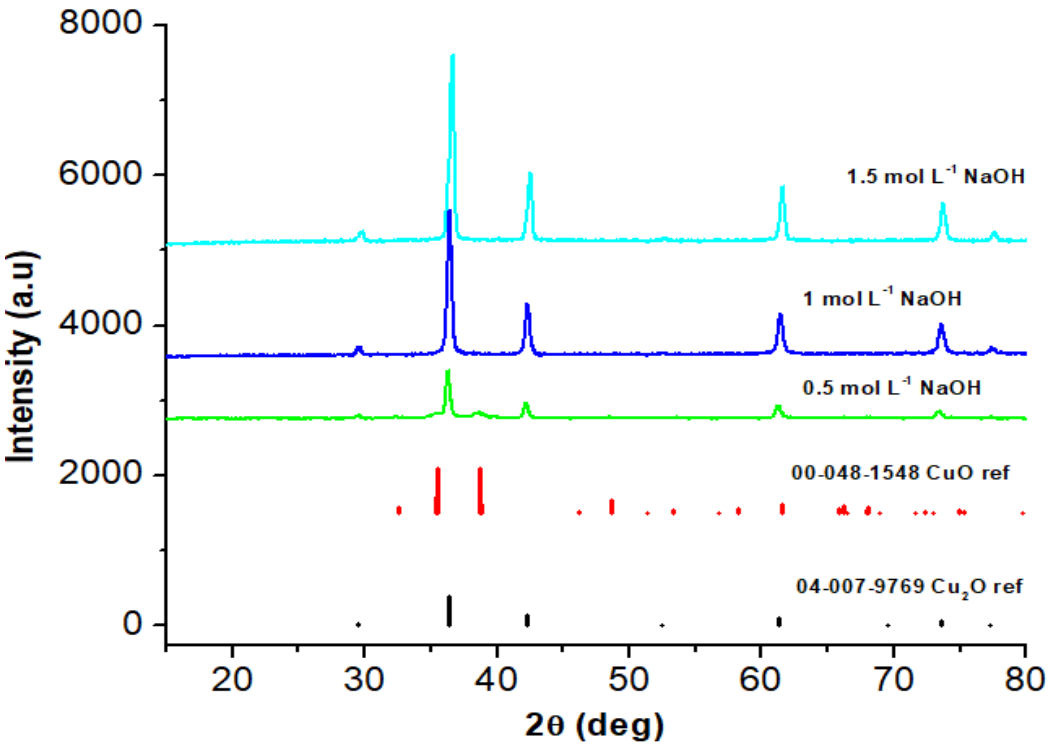

Figure 10: XRD diffraction patterns of copper oxide particles prepared with 0.5, 1 and 0.5 NaOH. 0.1 mol L^{-1} ASC. 0.5 mol L^{-1} $CuCl_2$.

4.2.3.2 ***BET analyses***

The specific surface area and pore size distribution of particles prepared with 0.5,1 and 1.5 mol L^{-1} NaOH were characterized using adsorption and desorption isotherms and BJH pore size distribution. The catalyst prepared using 0.5 mol L^{-1} NaOH had the highest surface area (Table 9). The average pore size was 54.6 Å. As the concentration increased the surface area of the particles also decreased and this may be attributed to the increase in the concentration. The pore size distribution at a NaOH concentration 0.5 mol L^{-1} was around 400 nm and for the catalysts at concentrations 0.1 and 1.5 mol L^{-1} NaOH the pore size distribution was around 150 nm which indicated that the particles were microporous structures. The average pore size for the particles prepared with 1 and 1.5 mol L^{-1} NaOH was 66.1 and 38.4 Å respectively.

Table 9: Specific surface area of the copper oxide particles prepared with 0.5, 1 and1.5 mol L^{-1} NaOH, 0.1 mol L^{-1} ASC, 0.5 mol L^{-1} $CuCl_2$ at 27 °C.

Sample	**Surface area (m^2/g)**
0.5 mol L^{-1} NaOH	23.7212
1 mol L^{-1} NaOH	9.6174
1.5 mol L^{-1} NaOH	2.2784

4.2.3.3 ***UV-vis spectroscopy analyses***

The prepared copper (I) oxide particles varying 1.5, 1 and 0.5 mol L^{-1} NaOH were characterized using UV-visisible spectroscopy. For the particles prepared using 1.5 and 0.5 mol L^{-1} NaOH as it can be seen Figure 11(A1 & C1), it is observed that the particles exhibited optical absorption over UV and visible regions of the spectrum however a higher absorption was observed in the visible region. The particle prepared using 1 mol L^{-1} NaOH exhibited optical absorption at 500 nm. The indirect band gap was estimated using the $(\alpha hv)^2$ versus hv plots for the catalysts prepared using 1,5, 1 and 0.5 mol L^{-1} NaOH were 1.83, 1.92 and 1.33 eV, respectively. These values are lower than the 2.137 eV commonly reported for bulk Cu_2O, indicating that the particles of the prepared Cu_2O in this study are larger in size.

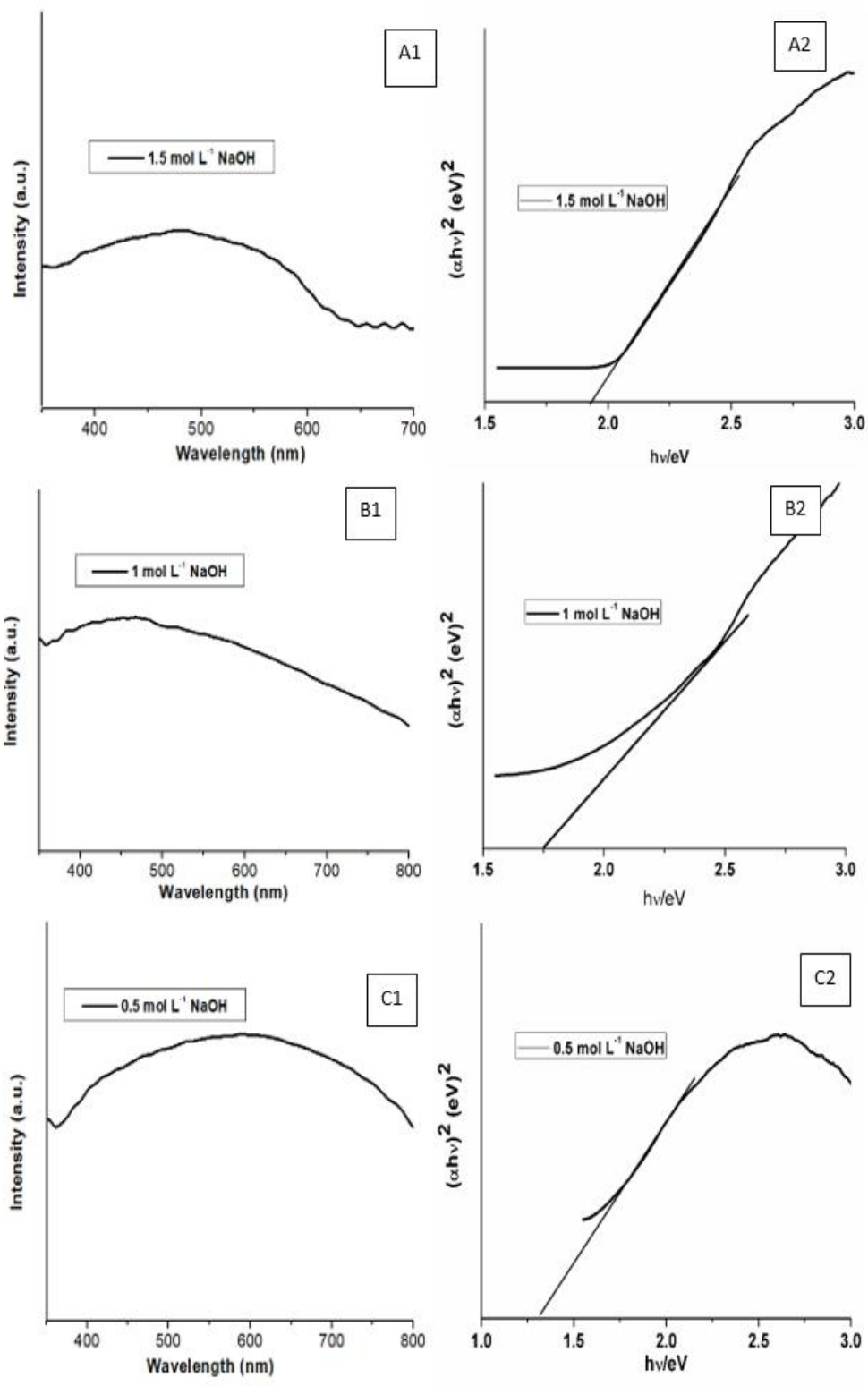

Figure 11: (A1,B1 & C1) UV-vis spectrum and (A2,B2 & C2) Tauc plot of copper oxide particles prepared using 1.5, 1 and 0.5 mol L^{-1} NaOH.

4.2.3.4 ***SEM analyses***

SEM analyses (Figure 12) was done on the prepared particles and it was observed that an increase in the concentration of NaOH has an effect on both the particle size and the morphology of the particles. At the concentration of 0.5 mol L^{-1} it was observed that the particles were more agglomerated and there was a mixture shapes, the size was estimated to be 119 nm. At the concentration of 1 mol L^{-1} the particles became less agglomerated and were spherical in shape, the size was about 150 nm. As the concentration was increased to 1.5 mol L^{-1} it was observed that there was a mixture of both large and small particles, the size was estimated to be 300 nm. The sizes of the particles increased as the concentrations of NaOH were increased. The same size trend was observed by Zhang et al. (2010). At a low concentration of NaOH, there may have been less hydroxyl groups on the surface in comparison when higher concentrations of NaOH have been used. An increase in the hydroxyl concentration may have led to an increase in Cu_2O nanoparticles combining forming larger particles by a condensation type of reaction (Yang et al., 2007).

(Cu_2O particle)-OH + (Cu_2O particle)-OH → (Cu_2O particle)-O-(Cu_2O particle) + H_2O

However, Zhang et al. (2010) found that the shape changed from spherical to cubic with an increase in the NaOH concentration which was not observed in this study. The difference in the shape may be attributed to the different precursor salts that were used. In this study $CuCl_2$ was used as a precursor salt whereas Zhang et al (2010) used $CuSO_4$.

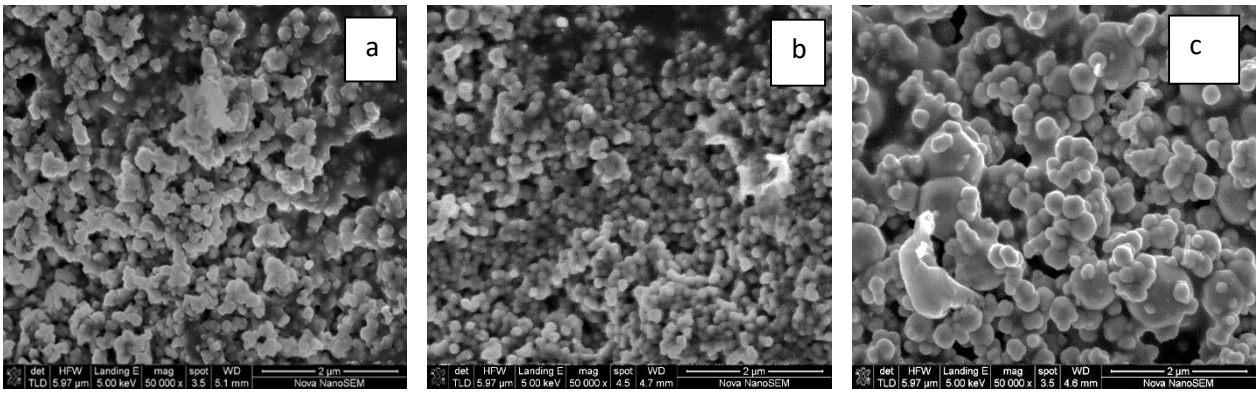

Figure 12: SEM images of copper oxide particles prepared with(a) 0.5,(b) 1 and (c)1.5 mol L^{-1} NaOH, 0.1 mol L^{-1} ASC, 0.5 mol L^{-1} $CuCl_2$ at 27 °C.

4.2.3.5 ***TEM analysis***

TEM analysis (Figure 13) was performed on the prepared particles and it was observed that the particles consisted of large particles and small particles. The size was calculated to be 120 nm for the large particles and 13 nm for the small particles.

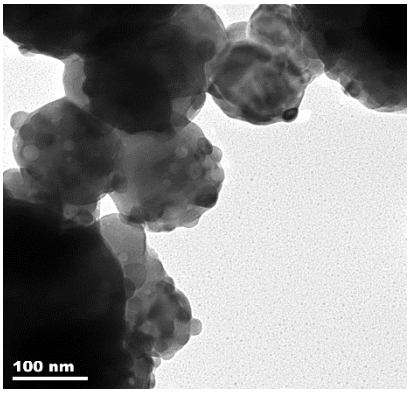

Figure 13: TEM analyses of copper oxide particle prepared with 1.5 mol L^{-1} NaOH, 0.1 mol L^{-1} ASC, 0.5 mol L^{-1} $CuCl_2$ at 27 °C.

4.2.4 Degradation of methylene blue using copper oxide particles prepared using different concentrations of NaOH and ASC as the reducing agent.

4.2.4.1 ***Fenton degradation and Photo-Fenton degradation***

The copper oxide particles prepared using 0.5, 1 and 1.5 mol L^{-1} of NaOH were used as catalysts during the Fenton degradation of MB as shown in Figure 14 and Table 10. The reaction of all the catalysts fitted the pseudo first order and this was based on the R^2 values as shown in Table 10. The rate of the Fenton reaction was significantly higher (see Appendix B for repeatability) when the catalyst was prepared using 1.0 mol L^{-1} of NaOH with a removal of 94% of the MB in comparison to the other two catalysts which had 77 and 61%, respectively (see Table 6 and Figure 14). The rates of the photo-Fenton reaction were only slightly different for the catalysts prepared at different NaOH concentrations.

When comparing the Fenton and Photo-Fenton degradation it was observed that the Fenton degradation was more active than the Photo-Fenton degradation method. A study by Miao et al.,(2018) showed that the, Photo-Fenton reaction has a higher reaction rate

because of additional pathways for $OH^{\bullet}$ generation. However the low reaction rate of Photo-Fenton might be attributed to photocorrosion (photo-oxidation) by the induced holes. Cu_2O is oxidized to CuO which is an inactive phase for both photodegradation and Fenton degradation thus resulting in the low activity of photo-Fenton degradation. (Toe et al., 2018).

Table 10: Rate constants of degradation of methylene blue using Fenton and Photo-Fenton degradation.

Fenton degradation					
Catalyst (mol L^{-1} NaOH)	**k-values (1^{st} order) (s^{-1})**	**k-values (2^{nd} order) (m^{-1} s^{-1})**	**R^2 (1^{st} order)**	**R^2 (2^{nd} order)**	**Percentage (%) removal (after 60 min of degradation)**
0.5	0.0222	0.0006	0.9567	0.9888	77
1	0.0431	0.0025	0.9723	0.9438	94
1.5	0.0131	0.0002	0.9163	0.9716	61
Photo-Fenton degradation					
Catalyst (mol L^{-1} NaOH)	**k-values (1^{st} order) (s^{-1})**	**k-values (2^{nd} order) (m^{-1} s^{-1})**	**R^2 (1^{st} order)**	**R^2 (2^{nd} order)**	**percentage (%) removal (after 60 min of degradation)**
0.5	0.0179	0.0004	0.9974	0.9872	66
1	0.0177 -	0.0003	0.9926	0.9930	66
1.5	0.0098	0.0002	0.9613	0.9820	49

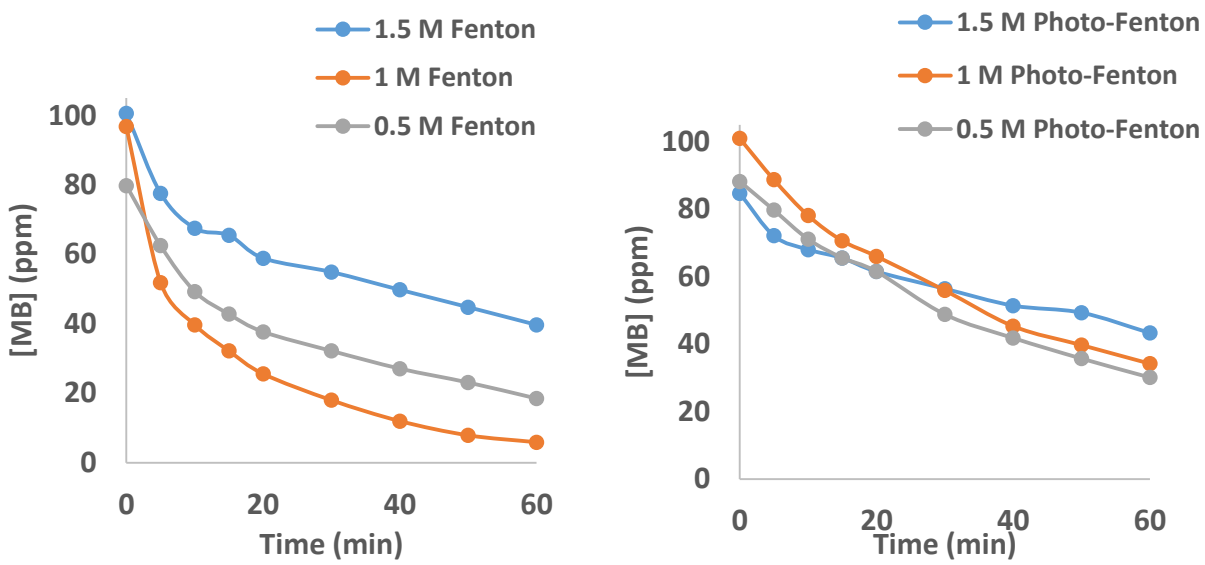

Figure 14: Fenton and Photo-Fenton degradation plots of the degradation of MB using copper oxide particles prepared with 0.5 mol L^{-1}, 1 mol L^{-1} and 1.5 mol L^{-1} NaOH , 0.1 mol L^{-1} ASC, 0.5 mol L^{-1} $CuCl_2$ at 27 °C.

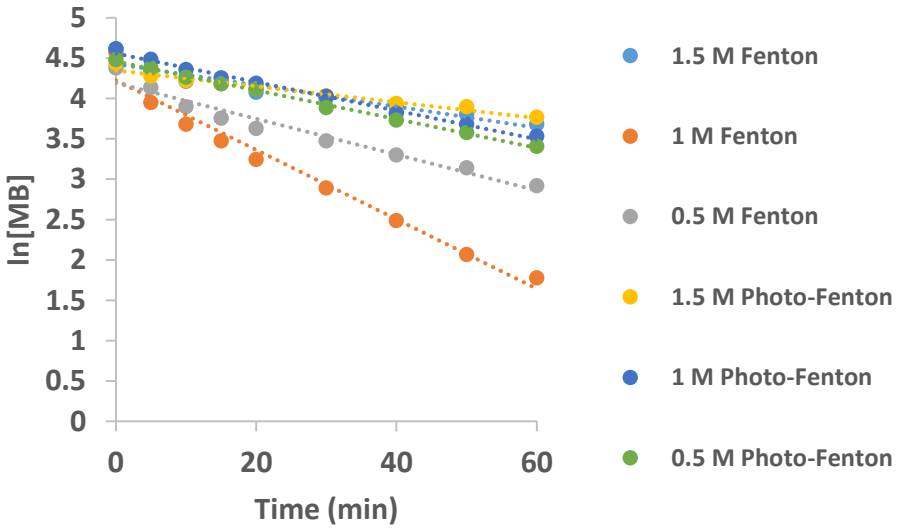

Figure 15: First order plots of the degradation of MB using copper oxide particles prepared with 0.5 mol L^{-1}, 1 mol L^{-1} and 1.5 mol L^{-1} NaOH, 0.1 mol L^{-1} ASC, 0.5 mol L^{-1} $CuCl_2$ at 27 °C.

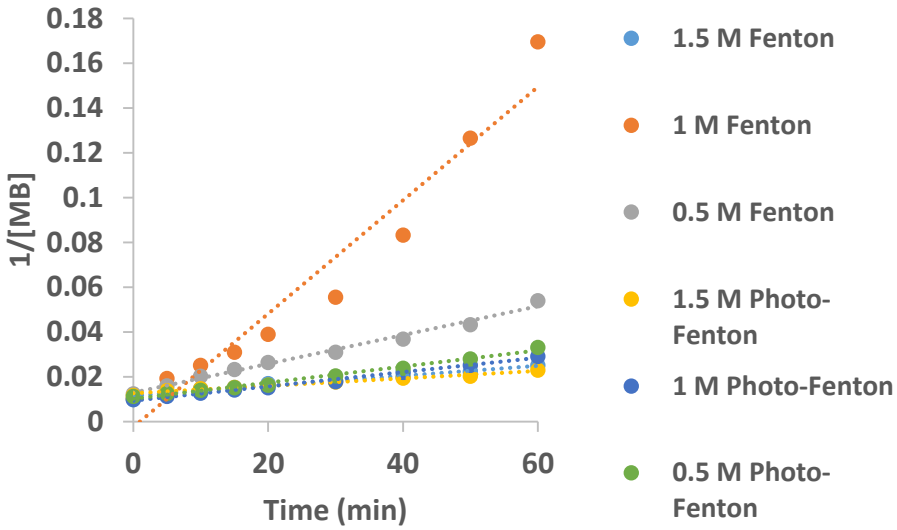

Figure 16: Second order plots of the degradation of MB using copper oxide particles prepared with 0.5 mol L^{-1}, 1 mol L^{-1} and 1.5 mol L^{-1} NaOH, 0.1 mol L^{-1} ASC, 0.5 mol L^{-1} $CuCl_2$ at 27 °C.

4.2.5 Preparation of copper oxide particles using different precursor salts

Copper oxide particles were prepared using 3 different precursor salts which were $CuCl_2$, $Cu(NO_3)_2$ and $CuSO_4$. The preparation method used were based on the method of Zhang et al. (2010) with slight modification $CuSO_4$ where used as the precursor salt, however in this study $CuCl_2$ and $Cu(NO_3)_2$ were used as well. The copper (II) ions were precipitated with NaOH (40 mL, 1.5 mol L^{-1}), 0.1 mol L^{-1} ASC was used as reducing agent and (20 ml, 0.5 mol L^{-1}) $CuCl_2$, $Cu(NO_3)_2$ and $CuSO_4$ were used as precursor salts.

4.2.5.1 ***XRD analyses***

The phase of the particles were determined using XRD (Figure 17). The same Cu_2O phase was obtained for all the Cu_2O catalysts made with the different copper precursors. The crystallite size of all the particles were the same (Table 11).

Table 11: XRD sizes and phase of copper oxide particles prepared using different copper salts 0.5 mol L^{-1} of $CuCl_2$, $Cu(NO_3)_2$ and $CuSO_4$, 1.5mol L^{-1} NaOH and 0.1 mol L^{-1} ASC.

Catalyst	Phase	Angle (2θ°)	FWHM (2θ°)	Size (nm)
$CuCl_2$	Cu_2O	36.57	0.42	19.8
$Cu(NO_3)_2$	Cu_2O	36.36	0.42	19.8
$CuSO_4$	Cu_2O	36.42	0.42	19.8

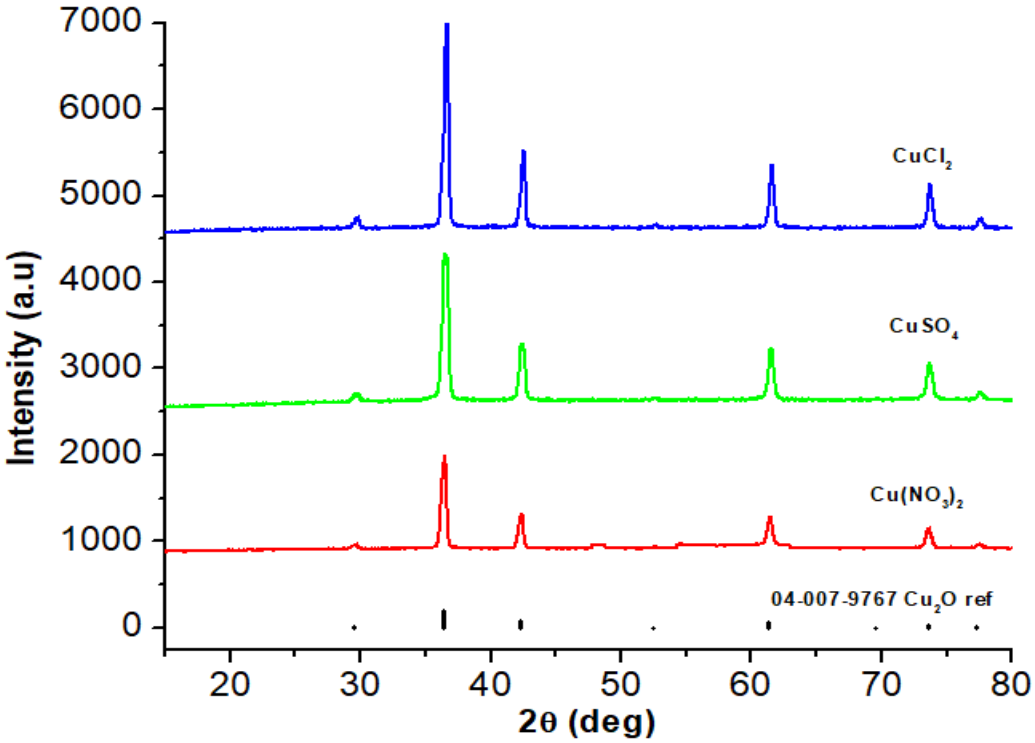

Figure 17: XRD diffraction pattern of copper oxide particles prepared using different copper salts 0.5 mol L^{-1} of $CuCl_2$, $Cu(NO_3)_2$ and $CuSO_4$, 1.5 mol L^{-1} NaOH and 0.1 mol L^{-1} ASC.

4.2.5.2 ***SEM analyses***

The Cu_2O catalysts prepared using $CuCl_2$, $CuSO_4$ and $Cu(NO_3)_2$ were analyzed using SEM (Figure 18) to determine the morphology and size of the particles. For the catalysts prepared using $CuCl_2$ the particles were spherical in shape and the size was estimated to be 300 nm. Mostly spherical and a few cubic particles with a size of around 910 nm

were obtained for the Cu_2O catalysts prepared using $CuSO_4$. Large agglomerated spherical particles with an estimated size of 659 nm were observed for particles prepared using $Cu(NO_3)_2$ salt.

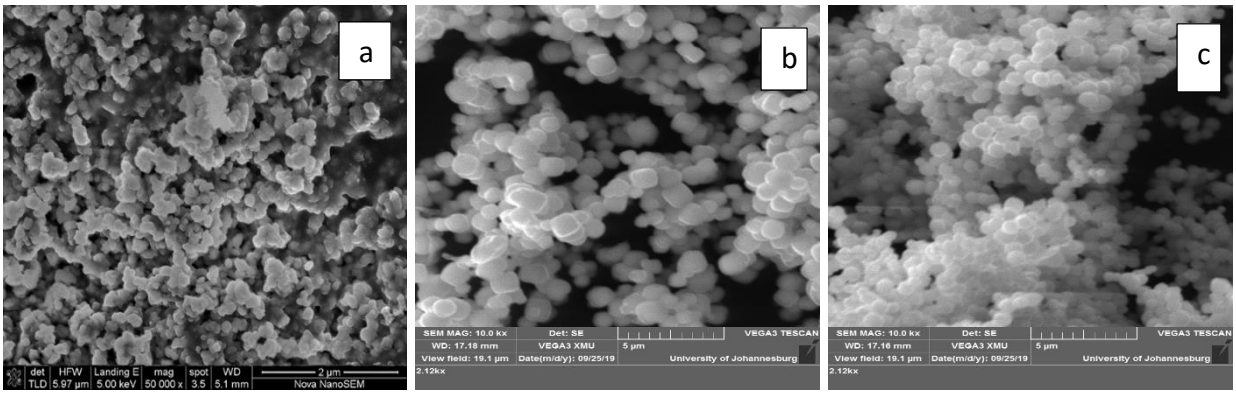

Figure 18: SEM images of copper oxide particles prepared using different copper salts 0.5 mol L^{-1} of (a) $CuCl_2$, (b) $CuSO_4$ and (c) $Cu(NO_3)_2$ and, 1.5mol L^{-1} NaOH and 0.1 mol L^{-1} ASC.

4.2.5.3 ***BET analyses***

The total surface area and pore volume of the particles prepared using $CuCl_2$, $CuSO_4$ and $Cu(NO_3)_2$ were investigated using BET (Table 12). The copper oxide particles prepared with $CuCl_2$ had the highest surface area and pore volume and copper oxide particles prepared with $CuSO_4$ had the lowest surface area and pore volume. The pore size distribution was in the range of 150-200 nm which represented microporous. The average pore sizes were 38.4, 27.4 and 28.1 Å for the particles prepared using $CuCl_2$, $CuSO_4$ and $Cu(NO_3)_2$.

Table 12: specific surface area and pore volume of the copper oxide particles prepared using different copper salts 0.5 mol L^{-1} of $CuCl_2$, $Cu(NO_3)_2$ and $CuSO_4$, 1.5mol L^{-1} NaOH and 0.1 mol L^{-1} ASC.

Sample	**Surface area (m^2/g)**	**Pore volume (cm^3/g)**
$CuCl_2$	2.2784	0.002191
$CuSO_4$	1.3312	0.000915
$Cu(NO_3)_2$	1.5444	0.001085

4.2.5.4 ***Degradation of MB using copper oxide particles prepared using different copper salts***

Fenton degradation method was used to degrade MB using the copper oxide particles prepared using different copper salts. The highest reaction rate for the degradation of MB was obtained when the copper oxide catalyst prepared using $CuCl_2$ was used. The particles prepared using $Cu(NO_3)_2$ and $CuSO_4$ had the lowest reaction rate.

Table 13: Rate constants of degradation of methylene blue by copper oxide particles prepared using different copper salts 0.5 mol L^{-1} of $CuCl_2$, $Cu(NO_3)_2$ and $CuSO_4$, 1.5 mol L^{-1} NaOH and 0.1 mol L^{-1} ASC using Fenton degradation.

Catalyst	**k-value (1^{st} order) (s^{-1})**	**k-values (2^{nd} order) (m^{-1} s^{-1})**	**R^2 (1^{st} order)**	**R^2 (2^{nd} order)**	**Percentage (%) removal (after 60 min degradation)**
0.5 mol L^{-1} $CuCl_2$ (1.5 mol L^{-1} NaOH, 0.1 mol L^{-1} ASC 27 °C)	0.01310	0.00020	0.9163	0.9716	61
0.5 mol L^{-1} $Cu(NO_3)_2$ (1.5 mol L^{-1} NaOH, 0.1 mol L^{-1} ASC, 27 °C)	0.00680	0.00009	0.9806	0.9869	33
0.5 mol L^{-1} $CuSO_4$ (1.5 mol L^{-1} NaOH, 0.1 mol L^{-1} ASC, 27 °C)	0.00550	0.00007	0.8868	0.8516	33

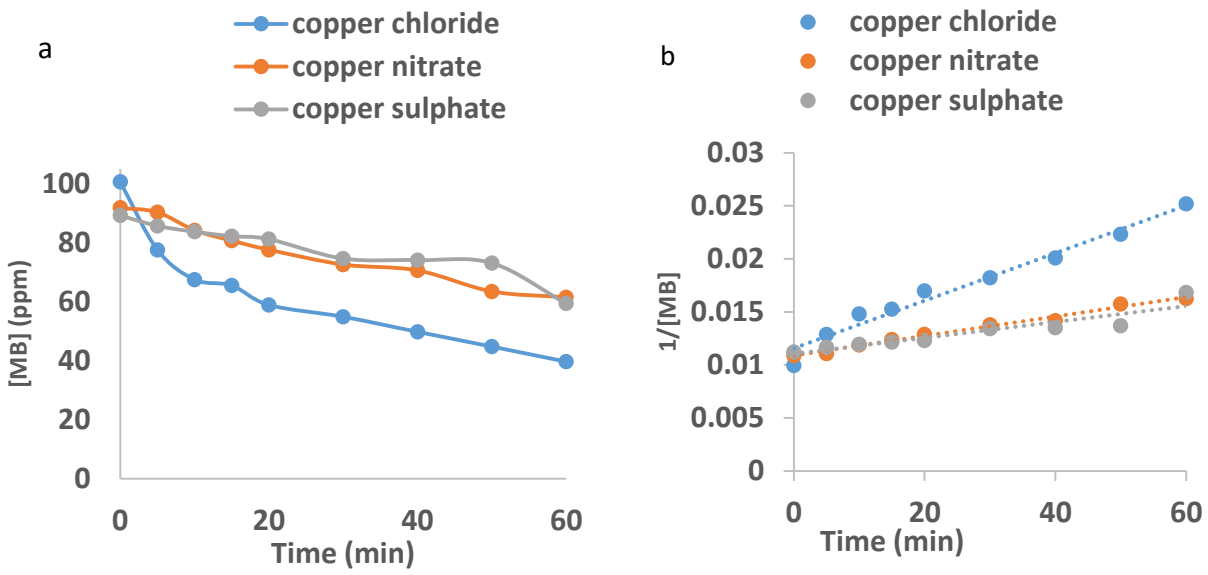

Figure 19: (a) Fenton degradation and (b) 2nd order plot of copper oxide particles prepared using different copper salts 0.5 mol L^{-1} of $CuCl_2$, $Cu(NO_3)_2$ and $CuSO_4$, 1.5 mol L^{-1} NaOH and 0.1 mol L^{-1} ASC.

4.2.6 Discussion

The XRD and SEM sizes were different for all the catalysts prepared. TEM showed that the size difference was because the particles were made up of an agglomeration of smaller particles.

The particles prepared using ASC as a reducing agent were stable and did not oxidize as verified by XRD. FTIR spectra showed that all the functional groups of ASC were present on the surface of the catalyst and one could argue that the reducing agent was acting as a capping agent preventing oxidation.

The particle prepared using 1 mol L^{-1} of NaOH had the highest Fenton catalytic activity. And from the SEM images it was observed that the particles were smaller and less agglomerated in comparison to the other samples which may explain the high catalytic activity.

From the XRD results (Table 11) the catalyst prepared using $CuCl_2$, $Cu(NO_3)_2$ and $CuSO_4$ had the same phase Cu_2O which is an active/desired phase for Fenton degradation. The

particles also had the same size however the particles prepared using $CuCl_2$ had the highest reaction rate. The XRD size may not be attributed to the activity of the catalysts.

Copper oxide prepared using $CuCl_2$ had the highest reaction rate and the lowest reaction rate was from the copper oxide catalyst prepared using $CuSO_4$ and $Cu(NO_3)_2$. The high reaction rate may be attributed to size. The Cu_2O catalyst made with $CuCl_2$ had the smallest size compared to Cu_2O catalysts made with $CuSO_4$ and $Cu(NO_3)_2$. Smaller size particles show high specific surface area while larger size/ aggregated particles show lower specific surface area (Karekar et al., 2017). BET analyses confirmed that the Cu_2O catalysts made with $CuCl_2$ had the highest surface area which might have attributed to its higher reaction rate. However Cu_2O catalysts made with $CuSO_4$ and $Cu(NO_3)_2$ had smaller surface area hence the lower reaction rate.

4.3 Preparation of copper oxide catalysts with hydrazine as reducing agent.

A precipitation reduction method was used to prepare the copper oxide crystallites. The preparation method used were based on the method of Xu et al. (2006). NaOH was used as the precipitating agent and hydrazine was used as reducing agent. The reaction time, the amount of hydrazine, amount of NaOH and temperature were varied to see the effect on the size, shape, copper phase of the crystals.

4.3.1 Preparation of copper oxide particles varying the reaction time

Cu_2O was prepared and during the preparation process the reaction time was varied. A preparation reaction time of 10 minutes and 20 minutes were used.

4.3.1.1 ***XRD analyses***

For the sample that had the reaction time of 20 minutes it was observed that when the $Cu(OH)_2$ solution was stirred during preparation the reducing agent reduced it into copper metal instead of the desired Cu_2O. The crystallite size was 14 nm as determined by the Scherrer equation (Appendix A). When the reaction time was reduced to 10 minutes the diffraction peaks were in line with both the diffraction patterns of copper metal and Cu_2O which suggested that in less reaction time the reducing agent reduces the $Cu(OH)_2$ solution into both copper metal and Cu_2O and there is a mixture of phases. The crystallite size was 10 nm.

The same amount of hydrazine was used as Xu et al. (2006). The amount is ten times more than the stoichiometric amount of hydrazine required. Andal and Buvaneswari (2017) have shown that hydrazine can reduce copper oxide to copper metal. Reactions 42 and 43 are proposed showing that the copper reduction may happen in two steps. After 10 minutes the copper (II) was converted to Cu_2O and Cu and with an increase in reaction time to 20 minutes some of the Cu_2O was converted to Cu. The XRD results indicated that 10 minutes reaction time was long enough to form Cu_2O and that less hydrazine should be used to limit over reduction to Cu.

$4Cu(OH)_2 + N_2H_4 \rightarrow N_2 + 6H_2O + 2Cu_2O$ reaction 42

$2Cu_2O + N_2H_4 \rightarrow 4Cu + N_2 + 2H_2O$ reaction 43

Table 14: XRD sizes calculations of copper oxide particles prepared using 10 and 20 minutes reaction time, 0.1 mL N_2H_4, 10 mL NaOH, 0.852 g $CuCl_2$, 2.5 mL NH_3.

10 minutes reaction time				**20 minutes reaction time**			
phase	**Angle (2θ°)**	**FWHM (2θ°)**	**Size (nm)**	**Phase**	**Angle (2θ°)**	**FWHM (2θ°)**	**Size (nm)**
Cu	43.41	0.84	10.1	Cu	42.70	0.63	13.5
Cu_2O	36.99	0.98	8.5	Cu_2O	36.71	0.63	13.2

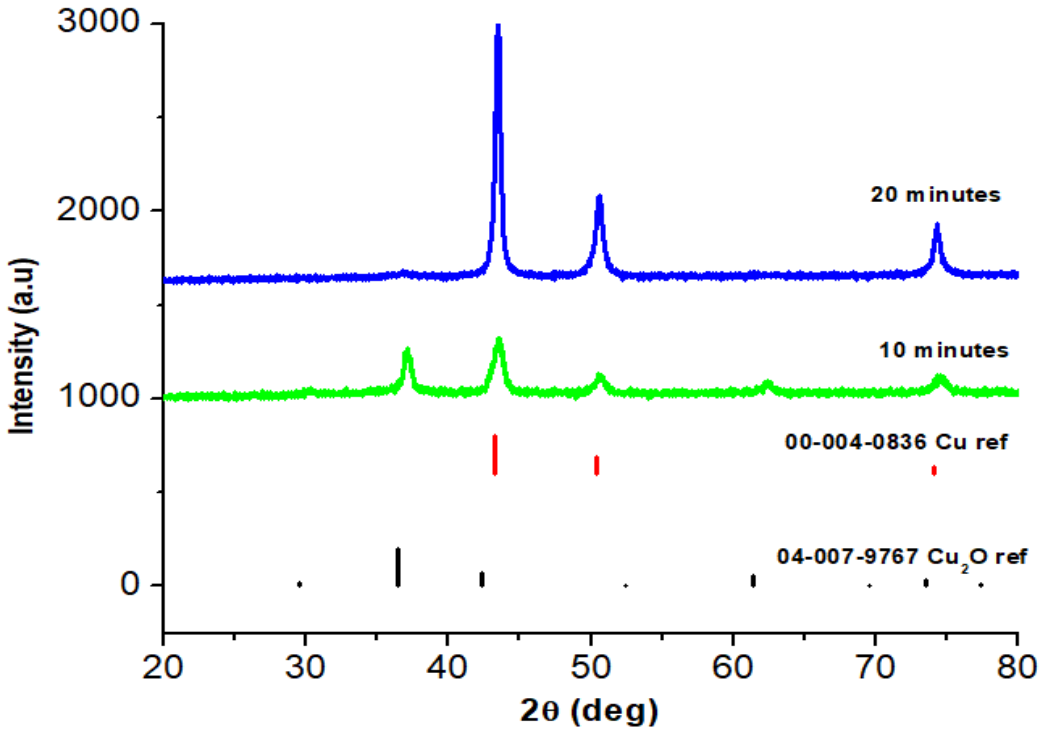

Figure 20: XRD diffraction patterns of copper oxide particles prepared using 10 and 20 minutes reaction time, 0.1 mL N_2H_4, 10 mL NaOH, 0.852 g $CuCl_2$, 2.5 mL NH_3.

4.3.1.2 ***SEM analyses***

SEM analyses was performed on the two Cu_2O particles that were prepared by varying the reaction time. Figure 21(a) shows the Cu_2O particles prepared by reacting the solution for 20 minutes, and it showed that the longer reaction time resulted in the particles becoming more agglomerated. A shorter reaction time of 10 minutes resulted in flat Cu_2O sheets Figure 21(a). A shorter reaction time resulted in particles which had rough spherical morphology and the particles were less agglomerated when compared to the particles that were reacted for 20 minutes.

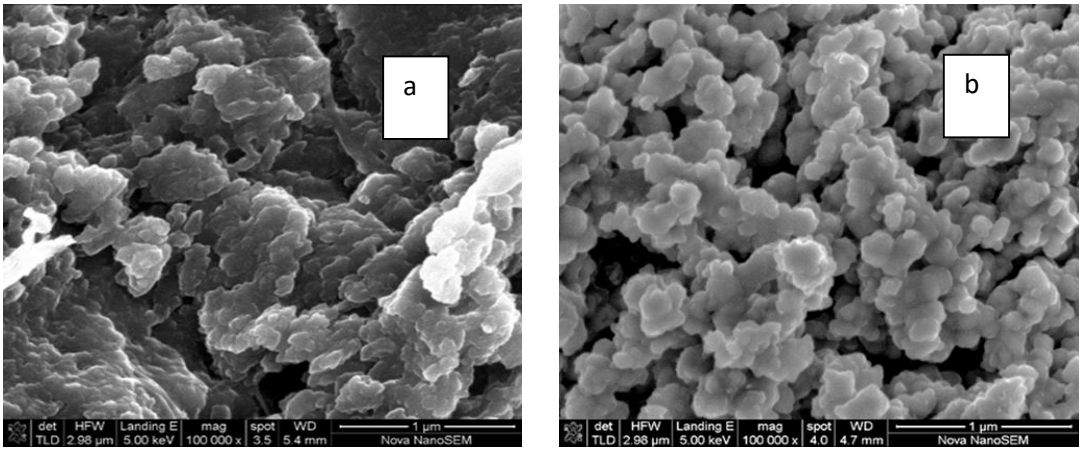

Figure 21: SEM images of copper oxide particles prepared by varying different reaction time (a) 20 minutes and (b) 10 minutes, 0.1 mL N_2H_4, 10 mL NaOH, 0.852 g $CuCl_2$, 2.5 mL NH_3.

4.3.2 Preparation of copper oxide varying hydrazine

Cu_2O particles were prepared varying different amounts of hydrazine which were 0.1 mL and 1mL. The amount of hydrazine has been lowered since over reduction has been observed when the preparation time was varied. The volume of 1 mL of hydrazine is more than the stoichiometric amount required to reduce the copper (II) to copper (1). This amount of hydrazine was used based on the preparation method of Xu et al. (2006). A volume of 0.1 mL corresponds to the stoichiometric amount.

4.3.2.1 ***XRD analyses***

The sizes of the particles were calculated as shown in Appendix A and are shown in Table 15. For the particle prepared using 1 mL of H_2N_4 it was observed that Cu_2O and Cu phases were obtained. It was observed that when a higher amount of H_2N_4 was used during preparation of Cu_2O particles it led to an over reduction and the formation of Cu_2O and Cu. The calculated crystallite size was found to be around 9 nm. The particles prepared using 0.1 mL of hydrazine, it was observed that the diffraction peaks were in-line with the reference spectra of Cu_2O and CuO. When 0.1 mL of H_2N_4 was used it was observed that the major phase was Cu_2O with small amounts of CuO was formed. The crystallite size was 17 nm. When the amount of hydrazine added exceeds the

stoichiometric amounts required to form Cu_2O then the hydrazine reduces the $Cu(OH)_2$ during preparation to a mixture of Cu metal and Cu_2O. When a stoichiometric amount was used, the H_2N_4 reduced the $Cu(OH)_2$ during preparation to Cu_2O as shown in Figure 22. Similar findings were obtained in a study done by Rahnatolahzadeh et al. (2017) where by the effect of amount of H_2N_4 was varied during preparation of Cu_2O particles. They observed that at 1 mL of H_2N_4 the diffraction peaks in XRD were indexed to pure Cu cubic phase of Cu metal and no other impurities where observed indicating high purity Cu nanostructures. When the amount of H_2N_4 was reduced to 0.1 mL there was a mixture of Cu and Cu_2O diffraction peaks which meant that at a lower amount of H_2N_4 there can be a mixture of crystalline phases.

Table 15: XRD sizes calculations of copper oxide particles prepared using, 0.1 and 1 mL N_2H_4, 10 mL NaOH, 0.852 g $CuCl_2$, 2.5 mL NH_3.

0.1 mL N_2H_4				**1 mL N_2H_4**			
phase	**Angle (2θ°)**	**FWHM (2θ°)**	**Size (nm)**	**Phase**	**Angle (2θ°)**	**FWHM (2θ°)**	**Size (nm)**
Cu	42.70	0.42	20.2	Cu	50.51	0.98	8.9
Cu_2O	36.78	0.49	17.0	Cu_2O	36.99	0.77	10.8

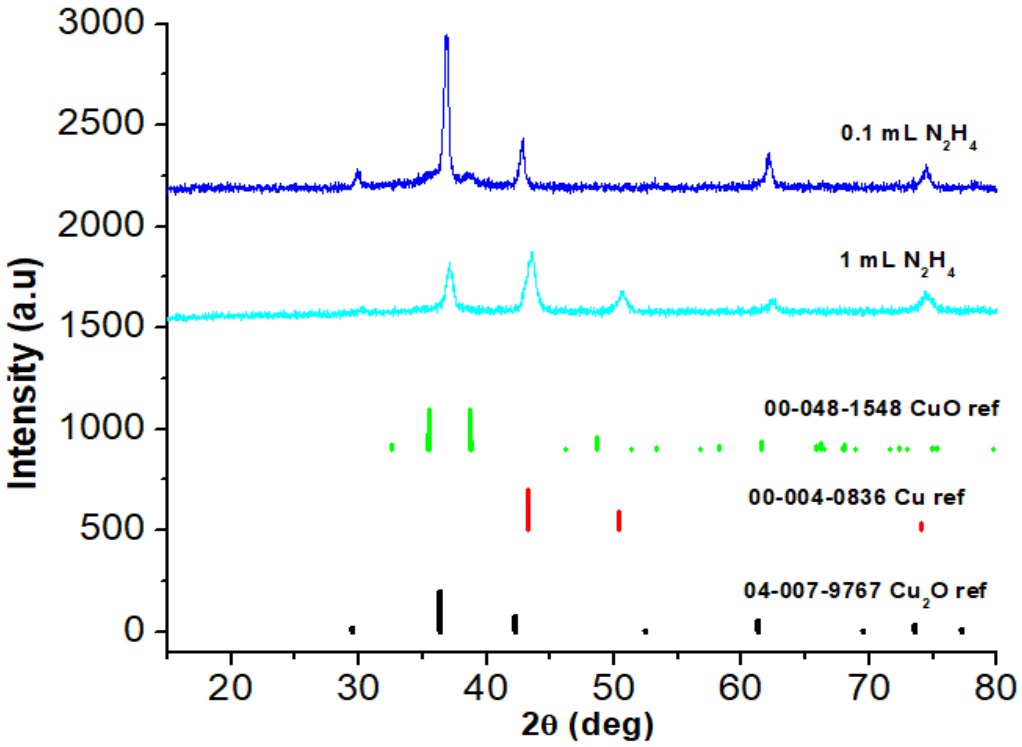

Figure 22: XRD diffraction patterns of copper oxide catalyst prepared with 0.1 and 1 mL N_2H_4 as reducing agents, 10 mL NaOH, 2.5 mL NH_3, 0.852 g $CuCl_2$.

4.3.2.2 ***Stability of copper oxide particles prepared using hydrazine as reducing agent.***

After 1 week a color change was observed from the bright yellow color to a very dark brown color after the sample was kept in the sample vials. XRD analyses showed that the Cu_2O oxidized to CuO (Figure 23). The crystallite size was 14 nm just after the particles were prepared. The crystallite size decreased to 6 nm after the sample was stored for a for a few days in a closed sample vial.

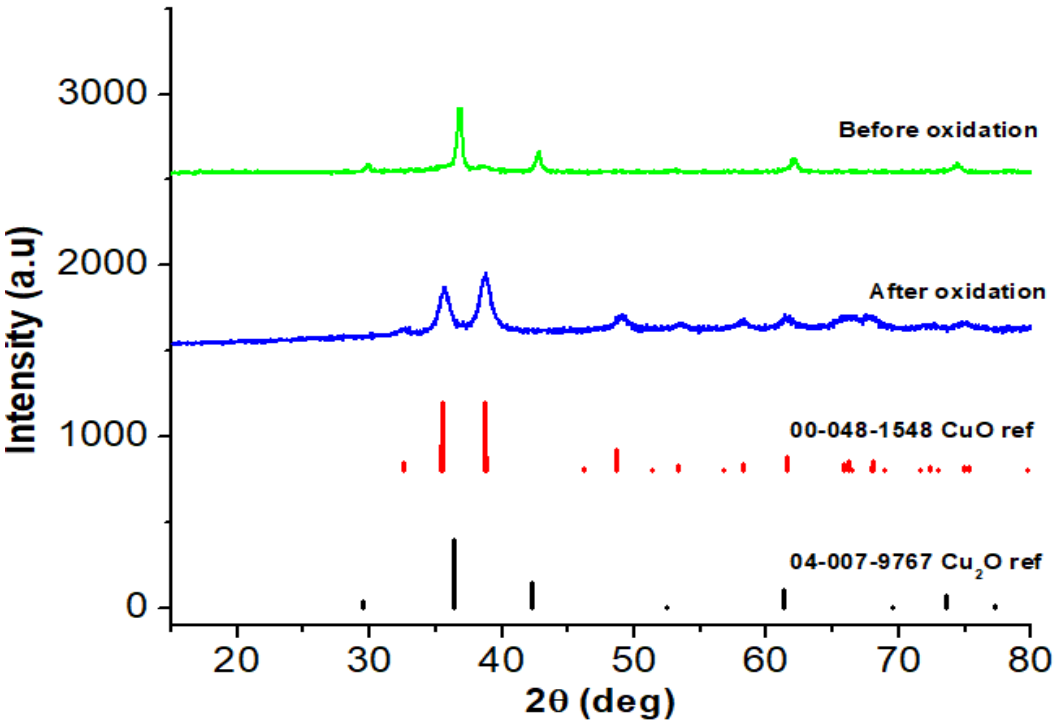

Figure 23: XRD diffraction patterns of copper oxide particle before oxidation and after oxidation.

4.3.2.3 ***BET analyses***

The total surface area and pore volume of the particles prepared with 0.1 mL N_2H_4 was investigated using the adsorption and desorption isotherms and BJH pore size distribution. The surface area was 37.6 m^2/g and the pore volume 0.0457 cm^3/g. Macro porous structures with a pore size distribution in the range of 50-100 nm were obtained. The average pore size was 48.7 Å.

4.3.2.4 ***UV-vis spectroscopy analyses***

The Cu_2O particles prepared using 0.1 and 1 mL N_2H_4 solutions were characterized using UV-visible spectroscopy Figure 24 (A1 & B1). It can be observed that the particles exhibit optical absorption over the UV and visible light regions of the spectrum. A higher absorption was observed in the visible light region for both catalysts prepared. The indirect band gap was estimated using the $(\alpha hv)^2$ versus hv plots for the catalysts prepared using 0.1 and 1 mL N_2H_4 and were 1.29 and 1.47 eV, respectively. These values

are considerably lower than the 2.137 eV commonly reported for bulk Cu_2O, indicating that the particles of the prepared Cu_2O in this study are larger in size.

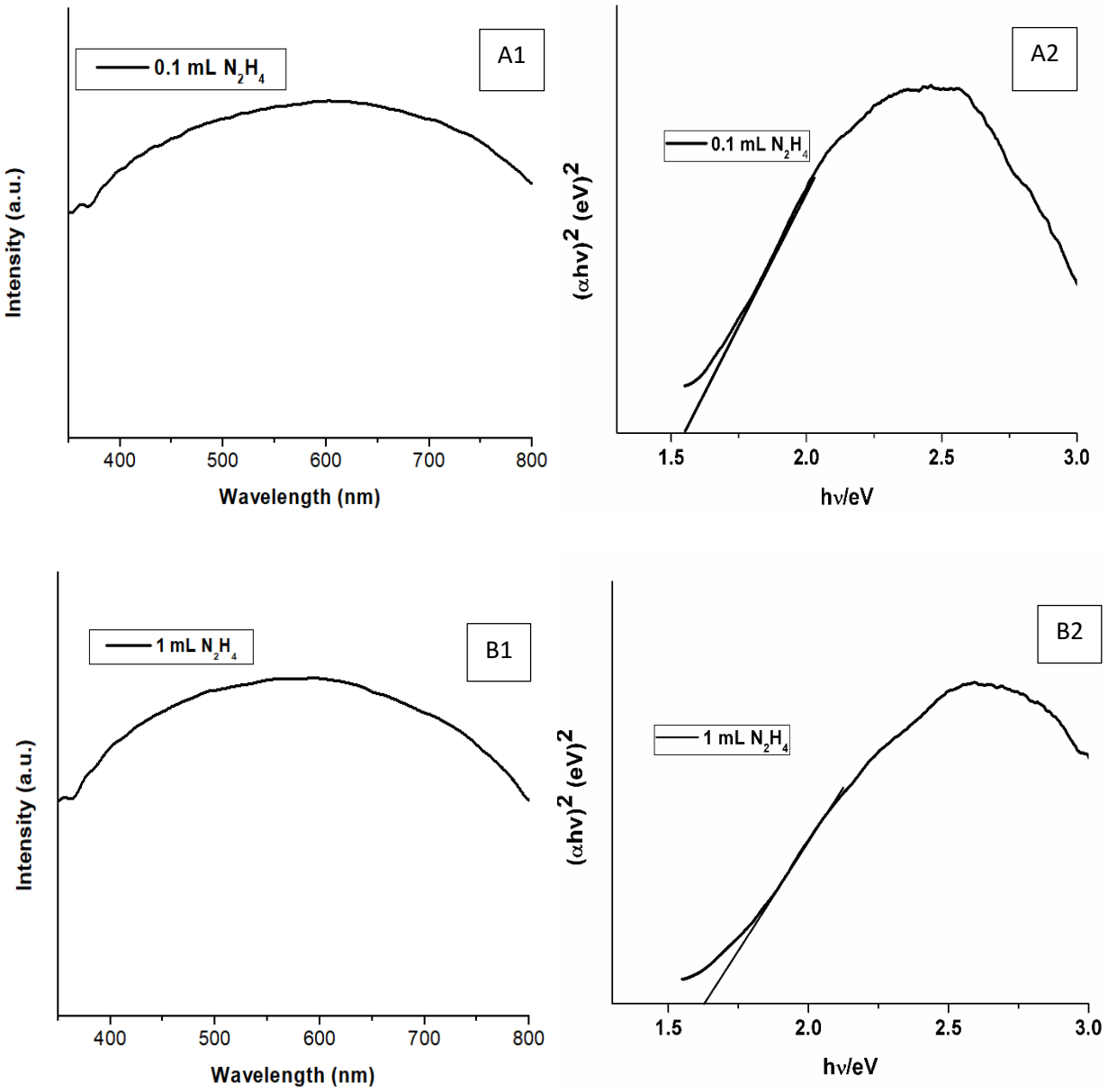

Figure 24: (A1 & B1) UV-vis and (A2 & B2) Tauc plot of copper oxide particles prepared using 0.1 and 1 mL N_2H_4, 10 mL NaOH and reacted for 10 minutes.

4.3.2.5 ***FTIR analyses***

Hydrazine has C-N stretching around 1335-1250 cm^{-1} a N-H stretching around 3400-3250 cm^{-1}. An alkane C-H stretching was observed at 3000 cm^{-1}, N-H stretching around 3350 cm^{-1} was observed, C-N stretching around 1330 cm^{-1} was observed and C-O (alcohol) stretching at 1020 cm^{-1} was observed. The peaks that were observed were from the hydrazine used during the preparation of the particles as well as the reducing agent, the methanol used during the washing process and copper oxide particles.

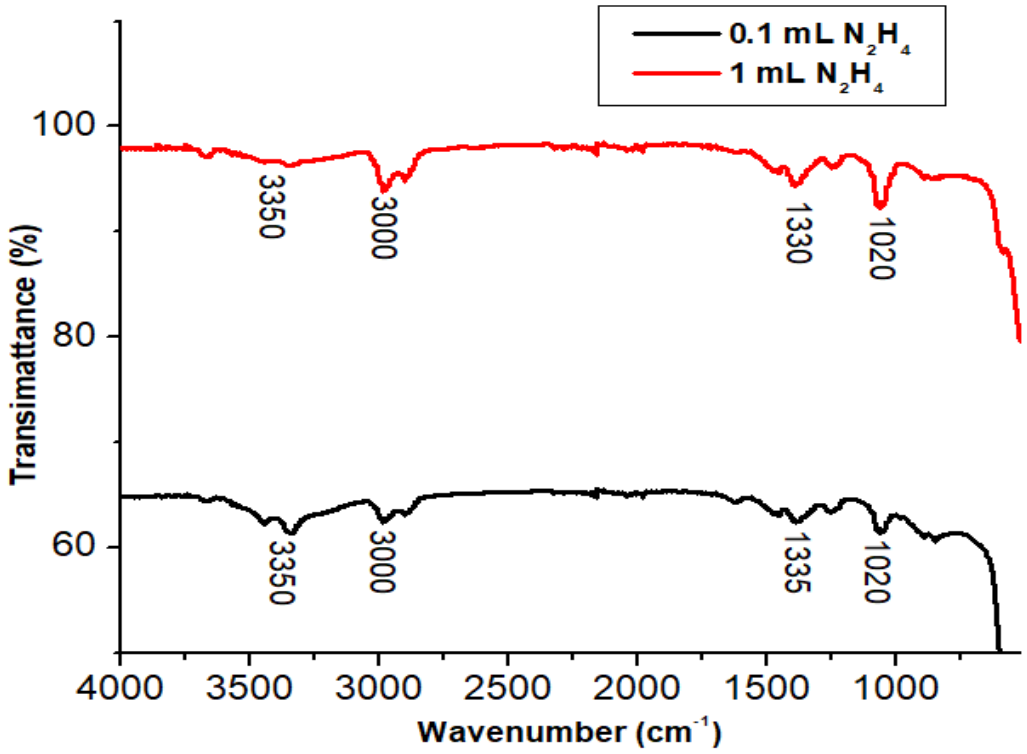

Figure 25: FTIR spectra of copper oxide particles prepared with 0.1 and 1 mL N_2H_4, 10 mL NaOH, 0.852 g $CuCl_2$ and 2.5 mL NH_3 at 10 minutes reaction time.

4.3.2.6 ***SEM analyses***

SEM analyses were performed on the Cu_2O particles to determine the morphology of the particles. The Cu_2O particles prepared using 1mL H_2N_4 (Figure 26a) were more agglomerated and formed flat-like sheets. The particle size could also not be calculated due to the agglomeration. When less amount of H_2N_4 was used which was 0.1 ml (Figure 26b) and there was a mixture of spheres and cubic particles formed during the preparation process.

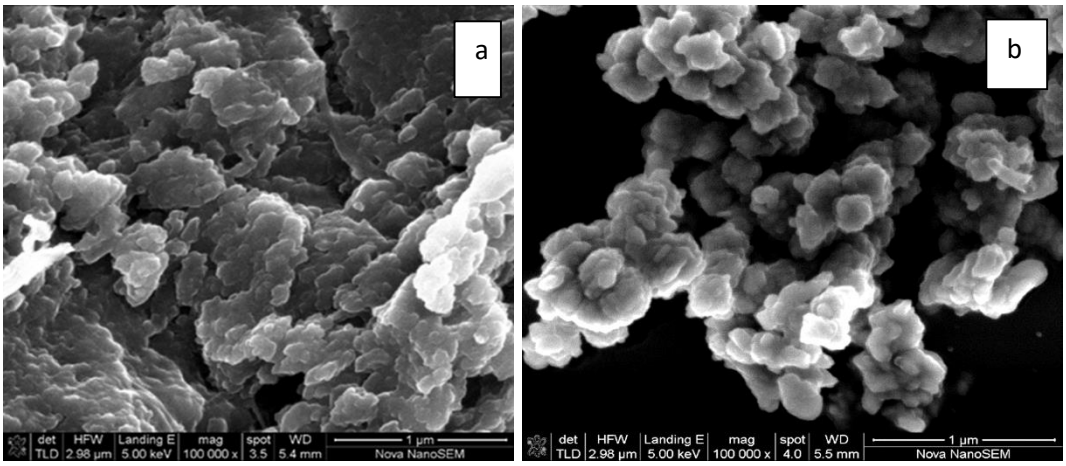

Figure 26: SEM images of copper oxide particles prepared using (a) 1 mL and (b) 0.1 mL hydrazine.

4.3.3 Degradation of methylene blue using copper oxide particles prepared using different amounts of hydrazine.

4.3.3.1 ***Fenton degradation***

The MB removal of 42% after 1 hour was obtained when the catalyst prepared using 0.1 mL N_2H_4 was used and MB removal of 40% after 1 hour was obtained when the catalyst prepared using 1 mL N_2H_4. There was not a significant difference in the reaction rate of the catalysts prepared using 0.1 mL N_2H_4 followed the pseudo 2^{nd} order suggesting that the degradation of the pollutant was from both adsorption and Fenton reaction. The 1 mL N_2H_4 followed the pseudo 1^{st} order suggesting that the degradation of the MB was mainly from the Fenton reaction.

Table 16: Rate constants of degradation of methylene blue using Fenton degradation.

Fenton degradation					
Catalyst (mL N_2H_4)	**k-values (1^{st} order) (s^{-1})**	**k-values (2^{nd} order) ($m^{-1}s^{-1}$)**	**R^2 (1^{st} order)**	**R^2 (2^{nd} order)**	**Percentage (%) removal (after 60 min degradation)**
0.1	0.0091	0.0001	0.9682	0.9781	42
1	0.0084	0.0001	0.9875	0.9860	40

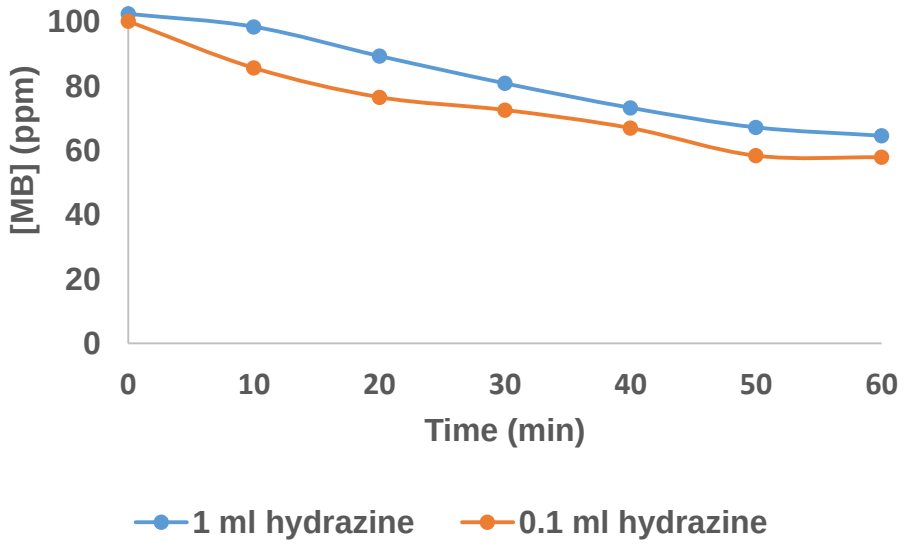

Figure 27: Fenton degradation of MB using 0.1 mL and 1 mL N_2H_4 copper oxide particles, 10 mL NaOH, 0.852 g $CuCl_2$ and 2.5 mL NH_3 at 10 minutes reaction time.

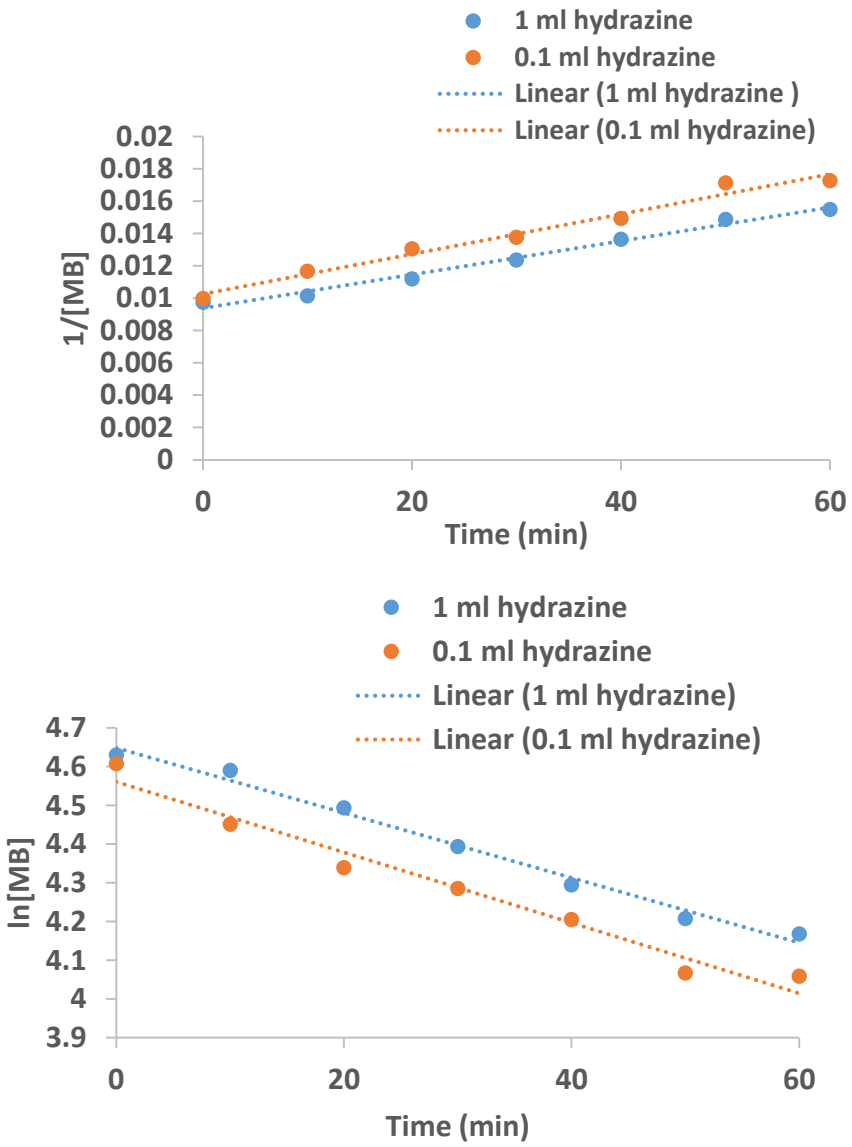

Figure 28: 1st and 2nd order fits of the degradation of MB using 0.1 mL and 1 mL N_2H_4 copper oxide particles, 10 mL NaOH, 0.852 g $CuCl_2$ and 2.5 mL NH_3 at 10 minutes reaction time.

4.3.4 Preparation copper oxide particles varying the amount of NaOH

The amounts of NaOH (10 mL and 15 mL) were varied during the preparation of the Cu_2O particles using H_2N_4 (0.1 mL) as the reducing agent.

4.3.4.1 ***XRD analyses***

The calculated sizes of the nanoparticles are shown in Table 17. The phases that were obtained were Cu_2O and Cu for the particles prepared using 10 mL NaOH as shown in Figure 29. At low amounts of NaOH, the copper was more reduced. For the particles prepared using 15 mL of NaOH Cu_2O and CuO phase were obtained. It was observed that as the amount of NaOH was increased from 10 to 15 mL the size of the Cu_2O phase particles increased.

Table 17: Rate constants of copper oxide particles prepared using 10 and 15 mL NaOH and hydrazine as a reducing agent.

10 mL NaOH				**15 mL NaOH**			
phase	**Angle (2θ°)**	**FWHM (2θ°)**	**Size (nm)**	**Phase**	**Angle (2θ°)**	**FWHM (2θ°)**	**Size (nm)**
Cu	43.47	0.63	13.5	CuO	39.04	1.64	5.1
Cu_2O	36.78	0.77	10.8	Cu_2O	36.96	0.52	16.1

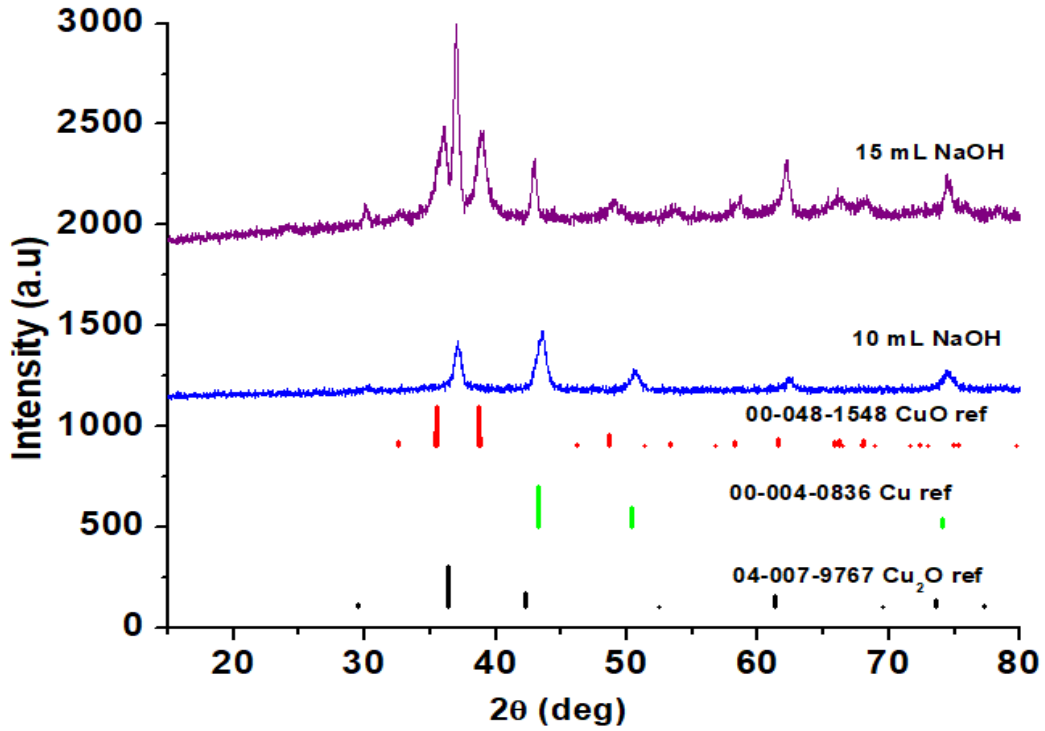

Figure 29: XRD patterns of copper oxide particles prepared by varying 10 mL and 15 mL of NaOH, 0.1 mL N_2H_4, 2.5 mL NH_3, 0.852 g $CuCl_2$.

4.3.4.2 ***BET analyses***

The pore size distribution of the particles prepared with 10 and 15 mL NaOH was characterized using BJH pore size distribution. The pore size peak of the 10 mL NaOH catalyst was in the range of 20-30 nm indicating that the catalyst was mesoporous. The 15 mL NaOH catalyst indicated a pore size distribution in the range 50-100 nm indicating that the catalyst was macro porous. At lower amounts of NaOH the surface area was 37.6 m^2/g and the pore volume was 0.4573 cm^3/g. As the amount of NaOH was increased to 15 mL there was a decrease in the surface area and pore volume of the catalyst of 12.3 m^2/g and 0.0201 cm^3/g. The average pore size for the particles prepared with 10 mL and 15 mL NaOH were 48.7 Å and 63.4 Å, respectively.

4.3.4.3 ***UV-vis spectroscopy analyses***

The copper (I) oxide particles prepared using 10 and 15 mL of 0.1 M NaOH solutions were characterized using UV-vis. There was observable difference between the optical

absorption profiles of the catalysts prepared using 10 and 15 mL NaOH. It can be observed from the UV-vis spectrum in Figure 30(A1 & B1) that the particles exhibit optical absorption over UV and visible regions of the solar spectrum. The absorption is higher over visible region and this is advantageous for visible light utilization. The indirect band gap was estimated using the $(\alpha hv)^2$ versus hv plots for the catalysts prepared using 10 and 15 mL NaOH were 1.29 and 1.44 eV respectively. These values are considerably lower than the 2.137 eV commonly reported for bulk Cu_2O, indicating that the particles of the prepared Cu_2O in this study are larger in size.

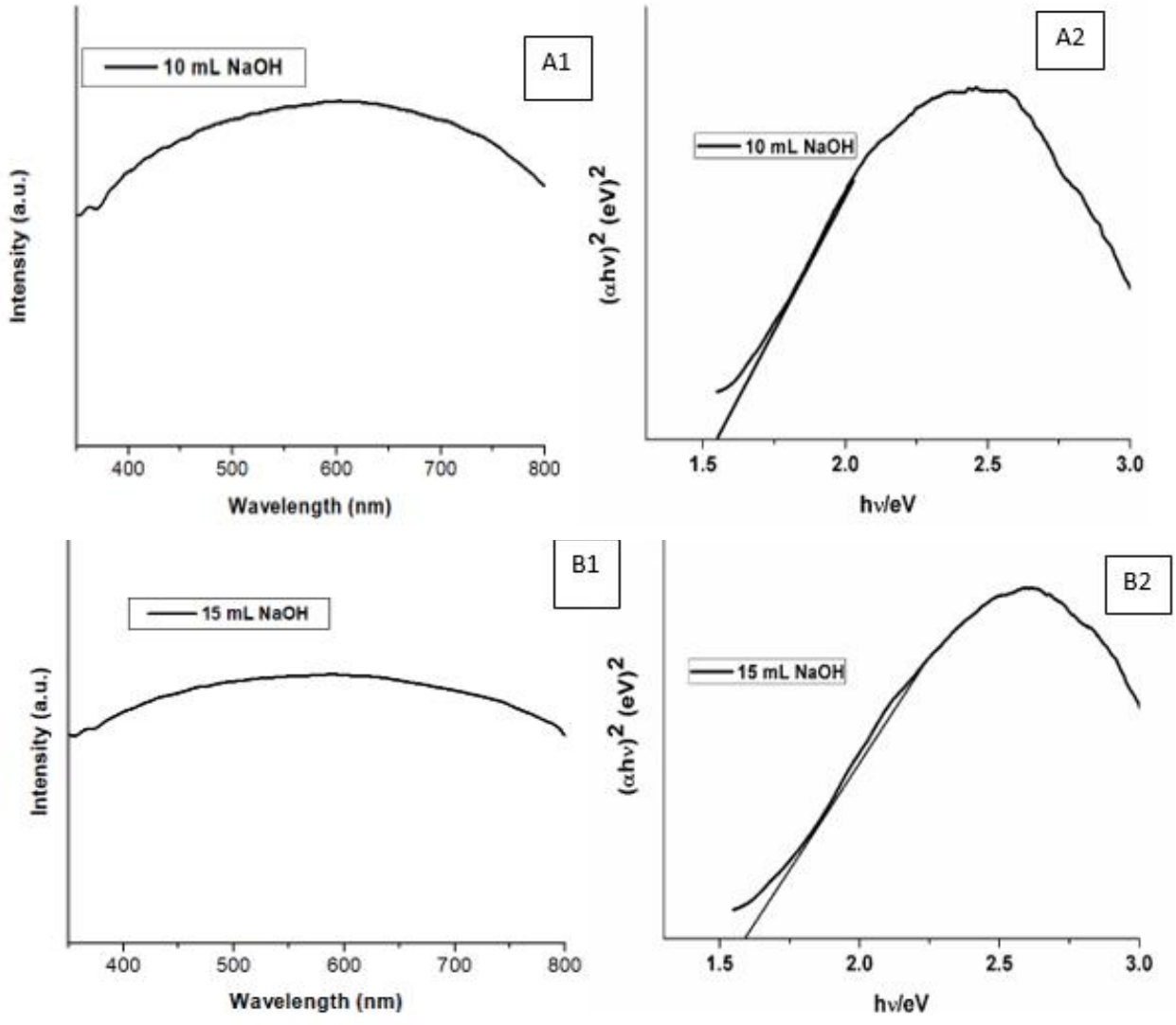

Figure 30: UV-vis (A1 & B1) and Tauc plots (A2 & B2) of copper (I) oxide particles prepared using 10 and 15 mL NaOH, 0.1 mL hydrazine.

4.3.4.4 ***SEM analyses***

SEM analyses shows that the amount of NaOH affects both the size and the morphology of the copper oxide crystallites. Figure 31 shows that when a lower amount (10 mL) of NaOH is used, the particles are smaller in size (290 nm), more agglomerated and irregular in shape. When the amount is increased to 15 mL (Figure 31) the particles size increased (407 nm) and were less agglomerated. A mixture of spheres and cubic morphology were observed. In a study by Zhang et al. (2010) the shape changed from spherical to cubic and increased in size as the NaOH concentration was increased.

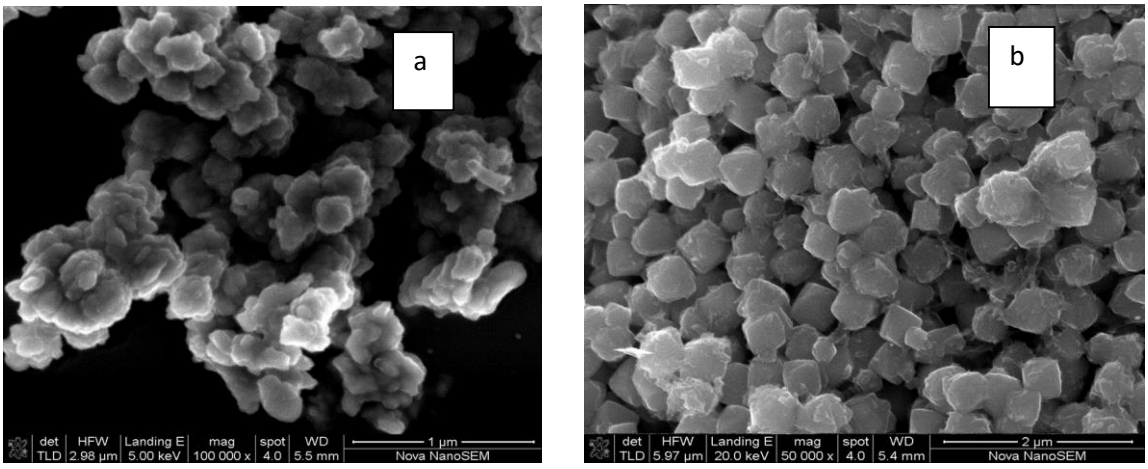

Figure 31: SEM images of copper oxide particles varying NaOH 10 mL (a) and 15 mL (b), 0.1 mL N_2H_4, 0.852 g $CuCl_2$ and 2.5 mL NH_3.

4.3.5 Degradation of methylene blue using copper oxide particles prepared using different concentrations of NaOH.

4.3.5.1 ***Fenton degradation***

The rate of the Fenton reaction was higher when the catalyst prepared using 15 mL NaOH was used to degrade MB (Figure 32 and Table 18) compared to the rate of the Fenton reaction of the catalyst prepared using 10 mL NaOH. The catalyst prepared using 15 mL NaOH had a removal of 81% of the MB after an hour of degradation. The catalyst prepared using 10 mL NaOH had a removal of 42% of the MB. The degradation fitted the pseudo 1st order reaction (Figure 33).

Table 18: XRD sizes calculations of copper oxide particles prepared using, 10 and 15 mL NaOH,0.1 mL N_2H_4 at 10 minutes reaction time.

Fenton degradation					
Catalyst (mL NaOH)	**k-values (1^{st} order) (s^{-1})**	**k-values (2^{nd} order) (m^{-1} s^{-1})**	**R^2 (1^{st} order)**	**R^2 (2^{nd} order)**	**Percentage (%) removal (after 60 min degradation)**
10	0.0091	0.0001	0.9682	0.9781	42
15	0.0284	0.0008	0.9974	0.9642	81

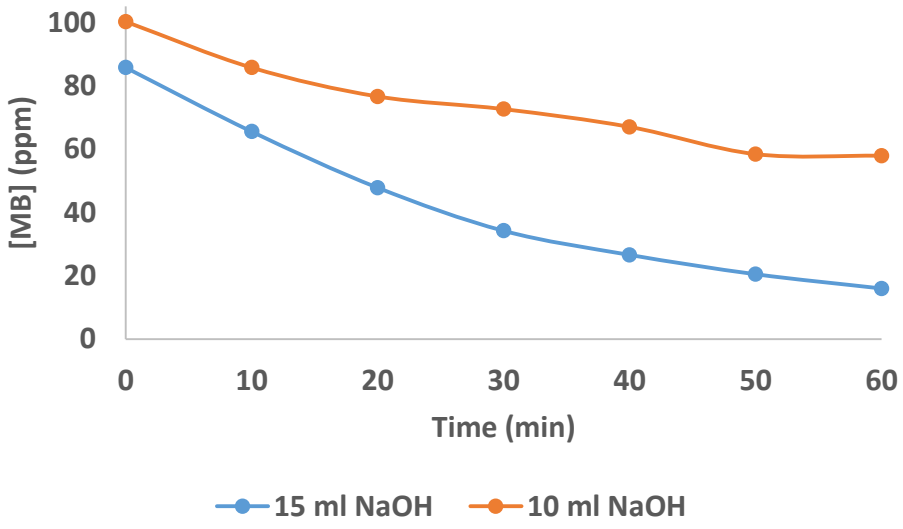

Figure 32: Fenton degradation of MB using 10 mL and 15 mL NaOH copper oxide particles 0.1 mL N_2H_4, 0.852 g $CuCl_2$ and 2.5 mL NH_3 at reaction time of 10 minutes.

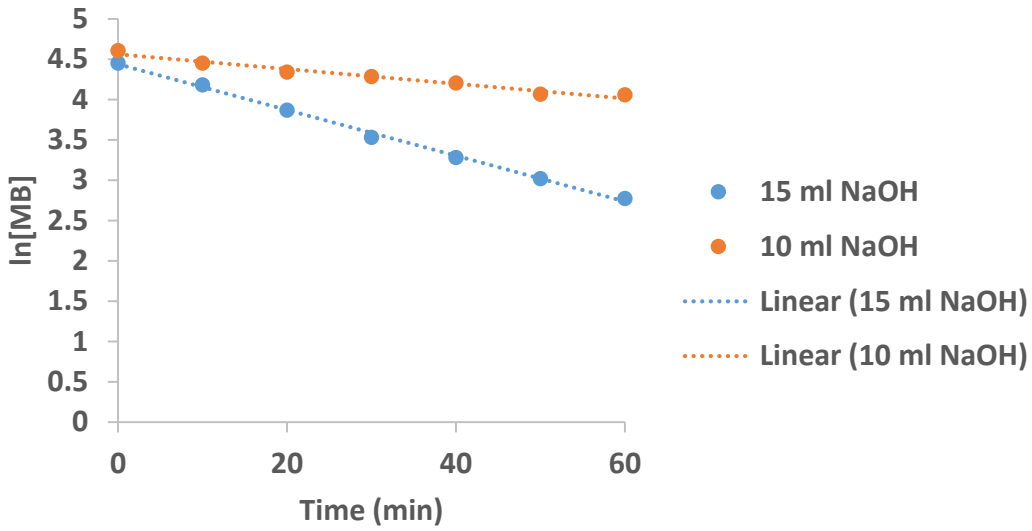

Figure 33: 1st order fits of the degradation of MB using 10 mL and 15 mL NaOH copper oxide particles prepared with 0.1 mL N_2H_4, 0.852 g $CuCl_2$ and 2.5 mL NH_3 at reaction time of 10 minutes.

4.3.6 Photo degradation of methylene blue with copper oxide particles prepared using hydrazine as a reducing agent

The prepared copper oxide particles were used as catalyst for the degradation of methylene blue by photocatalysis and the Fenton reaction. During both reactions, photocatalysis and Fenton, an initial time of 60 minutes was allowed for adsorption before the catalytic reaction was initialized. The catalytic reaction was initialized for the photocatalysis by switching on the light and the Fenton reaction by introducing hydrogen peroxide. The methylene blue concentration decreased due to adsorption. During photocatalysis no further decrease in the methylene blue concentration was observed when the light was switched on.

In a study done by Haung et al., (2009) similar findings of photo corrosion were first observed. It was observed that during photo degradation Cu_2O particles were oxidized after the light was illuminated and this was confirmed by the presence of CuO diffraction peaks which indicated that the rate of photo corrosion of Cu_2O nanoparticles was fast. This was explained as follows: when the catalyst is added to the organic pollutant, the

Cu_2O adsorbed the organic pollutant and there was a decrease in the concentration of the organic pollutant and the photocatalytic degradation of the organic pollutant was very low. Cu_2O was oxidized to CuO which has very little photocatalytic activity which caused the organic pollutant to desorb from the catalyst resulting in an increase in the concentration of the organic pollutant which remained constant throughout the degradation process.

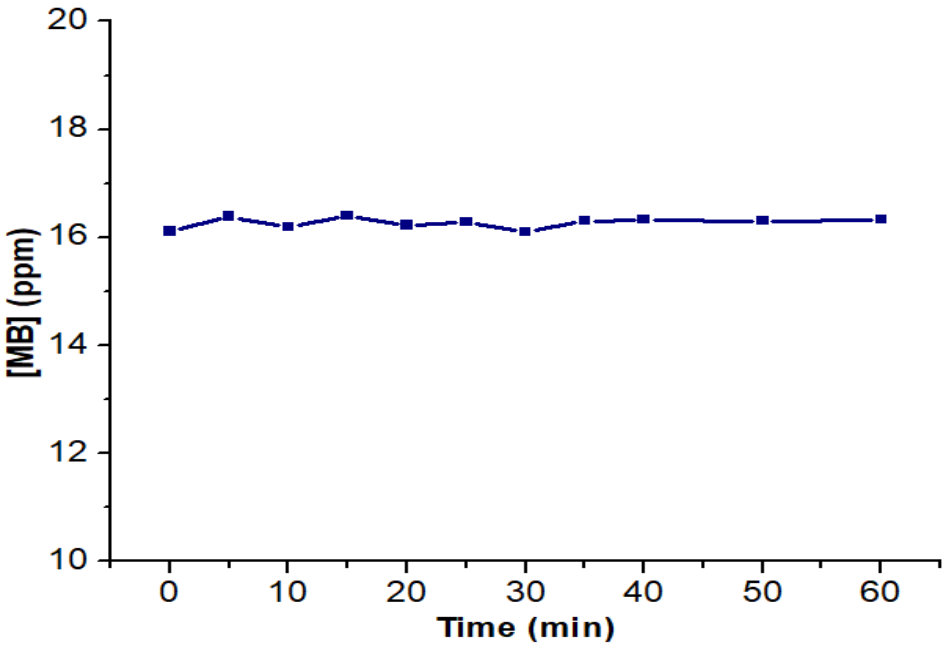

Figure 34: Photo degradation of methylene blue using copper oxide particle prepared by varying 0.1 mL hydrazine, 10 mL NaOH, 2.5 mL NH_3, 0.852 g $CuCl_2$ and reacted at 10 minutes.

4.3.7 Discussion

The sizes appeared larger than the calculated XRD sizes one can argue that the particles consisted of an agglomeration of smaller particles, this might be attributed to the low amount of NaOH used in the preparation of the nanoparticles. An increase in hydroxide ions may result in an increase in the hydroxyl groups on the surface of the Cu_2O nanoparticles leading to an increase in oxolation condensation type of reactions such as shown in reaction 44 resulting in an increase in agglomeration of these nanoparticles forming larger microparticles

particle-Cu-O-H + H-O-Cu-particle $\rightarrow$ particle-Cu-O-Cu-particle + H_2O reaction 44

The particles prepared using N_2H_4 as a reducing agent and varying the amount of NaOH it was observed that when the concentration of NaOH was increased the size of the nanoparticles increased as well and this was observed in both XRD and SEM images. XRD analyses confirmed that higher amounts of hydrazine resulted in an over reduction resulting in the formation of Cu metal which is an inactive phase for photodegradation and Fenton degradation.

XRD analyses showed that particles prepared using N_2H_4 as a reducing agent were not stable in air. Surface oxidation to form CuO may have caused to photocatalytic inactivity since CuO is known to be inactive for photocatalysis (Haung et al., (2009). XRD also confirmed that the particles prepared using hydrazine oxidized after preparation resulting in unstable catalyst, this resulted in an inactive catalyst during photodegradation and it may be hypothesized that the catalyst deactivated due to photocorrosion. The XRD results indicated that Cu_2O, which is an active phase for Fenton degradation, was obtained during the preparation of copper oxide particles prepared using different amounts of hydrazine. This may attribute to the high Fenton reaction rate that was observed. The particle prepared using 0.1 mL was less agglomerated as seen in SEM and smaller in size. Smaller particles are known to have a higher catalytic activity because of their higher surface area and this can be attributed to the catalyst's high Fenton reaction rate.

Particles with smaller size usually have a higher catalytic activity because of their higher surface area, however the particle prepared using 15 mL NaOH were larger in size and cubic in shape as seen in SEM, yet they had higher activity. The higher activity may be attributed to the shape of the particles. Similar findings were obtained in a study by Zhang et al., (2010) where larger cubic particles had a higher catalytic activity compared to smaller particles.

4.4 Preparation of copper oxide catalysts with sodium borohydride ($NaBH_4$) as reducing agent.

4.4.1 Preparation of Cu_2O particles varying $NaBH_4$

Copper oxide particles were prepared using 0.2 mols (0.5 mol L^{-1} 40 mL) NaOH and 0.1 mols (0.5 mol L^{-1}, 20 mL) $CuCl_2$. Different concentrations of the reducing agent were varied (0.1 and 0.5 mol L^{-1} $NaBH_4$).

$$8Cu(OH)_2 + BH^-_4 \rightarrow B(OH)^-_4 + 4Cu_2O + 8H_2O \qquad \text{Equation 36}$$

Based on equation 36, 1 mol of $NaBH_4$ reacts with 8 mol of Cu^{2+}, the stoichiometric amount was calculated to be 0.0125 mols (0.025 mol L^{-1}, 50 mL) $NaBH_4$ reacting with 0.1 moles (0.5 mol L^{-1}, 20 mL) Cu^{2+}.

4.4.1.1 ***XRD analyses***

The prepared copper oxide particles were analyzed with XRD to determine the crystallite size and the phases of the particles prepared. The calculated sizes of the particles are shown in Table 19. At high concentration (0.5 mol L^{-1}) of the reducing agent there was a mixture of phases obtained which were CuO and Cu metal with sizes of 9 and 6nm, respectively. High concentration of $NaBH_4$ caused over reduction of the copper oxide since the predominant phase that was formed was copper metal, small amounts of copper oxide were present in the samples. At concentrations of 0.1 mol L^{-1} $NaBH_4$ Cu metal with size of 14 nm was the main phase obtained with small amounts of CuO with sizes 11 nm. At stoichiometric amounts of $NaBH_4$ (0.025 mol L^{-1}) the phase obtained was CuO with crystallite size of 5 nm. No reduction had taken place indicating that stoichiometric amounts of $NaBH_4$ were unable to reduce copper (I) to copper (II). The difference in the

sizes of the prepared particles may be from the different concentrations of the reducing agents that was used during degradation.

Table 19: properties of copper oxide particles prepared using 0.5, 0.1 and 0.025 mol L^{-1} $NaBH_4$ as a reducing agent with 0.5 mol L^{-1} NaOH.0.5 mol L^{-1} $CuCl_2$.

0.5 mol L^{-1} $NaBH_4$			
phase	**Angle (2θ°)**	**FWHM (2θ°)**	**Size (nm)**
Cu	50.56	0.93	9.4
CuO	38.70	1.44	5.8
0.1 mol L^{-1} $NaBH_4$			
Phase	**Angle (2θ°)**	**FWHM (2θ°)**	**Size (nm)**
Cu	50.44	0.63	13.9
CuO	36.85	0.77	10.8
0.025 mol L^{-1} $NaBH_4$			
Phase	**Angle (2θ°)**	**FWHM (2θ°)**	**Size (nm)**
CuO	35.87	1.55	5.4

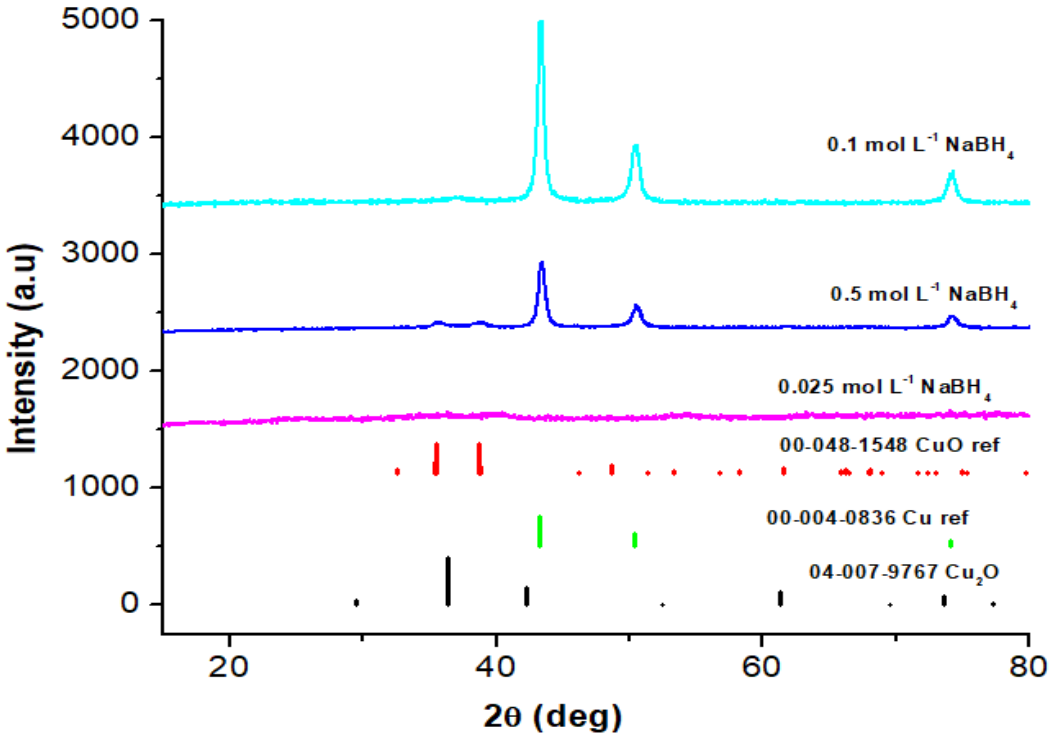

Figure 35: XRD diffraction pattern of copper oxide particles prepared using 0.5,0.1 and 0.025 mol L^{-1} $NaBH_4$, with 0.5 mol L^{-1} NaOH and 0.5 mol L^{-1} $CuCl_2$.

4.4.1.2 ***SEM analyses***

SEM analyses was performed on the prepared copper oxide particles prepared using $NaBH_4$ as the reducing agent and it was observed that at low concentrations (0.1 mol L^{-1}) the particles were small in size, agglomerated and the size could not be estimated. As the concentration was increased to 0.5 mol L^{-1} the particles increased in size and appeared to be spherical in shape. Agglomerated particles with flat sheets were obtained when 0.025 mol $L^{-1}$of $NaBH_4$ was used (Figure 36 C).The difference in the shape of the nanoparticle may be attributed to the different concentrations of $NaBH_4$. The same concentration of NaOH was used in the preparation of all the nanoparticles.

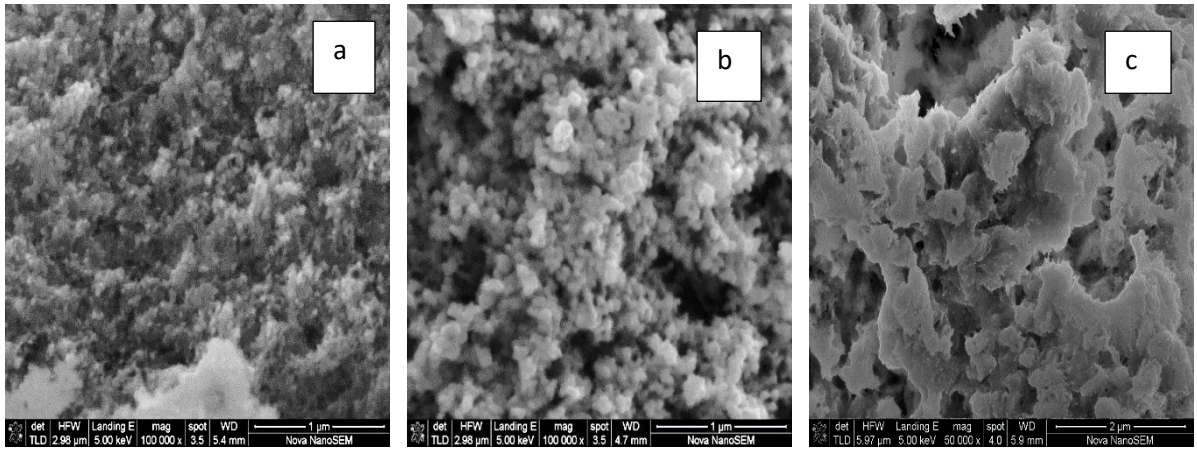

Figure 36: SEM images of copper oxide particles prepared using (a) 0.1 mol L^{-1} (b) 0.5 mol L^{-1} and (c) 0.025 mol L^{-1} $NaBH_4$ as reducing agent with 0.5 mol L^{-1} NaOH.0.5 mol L^{-1} $CuCl_2$.

4.4.1.3 ***FTIR analyses***

The copper oxide particles that were prepared using $NaBH_4$ as reducing agent were characterized using FTIR (Figure 37). $NaBH_4$ has a B-H stretching around 2000-2500 cm^{-1} and also a B-H bending around 1500-1000 cm^{-1}. The functional groups of $NaBH_4$ were expected to be observed on the surface of the catalysts prepared with 0.5 and 0.1 mol L^{-1} $NaBH_4$ however no functional groups were observed. The $NaBH_4$ could have been washed away during the washing step during the preparation of the copper oxide particles. A B-H bending at 1000 cm^{-1}, O-H stretch at 3300 cm^{-1}, C-H stretch at 1260 cm^{-1} and C-C stretch at 1600 cm^{-1} was observed on the surface of the particles prepared using 0.025 mol L^{-1} $NaBH_4$. The observed functional groups are from the $NaBH_4$, methanol, $CuCl_2$ and NaOH during the washing and preparation steps. The particles were not capped by the reducing agent.

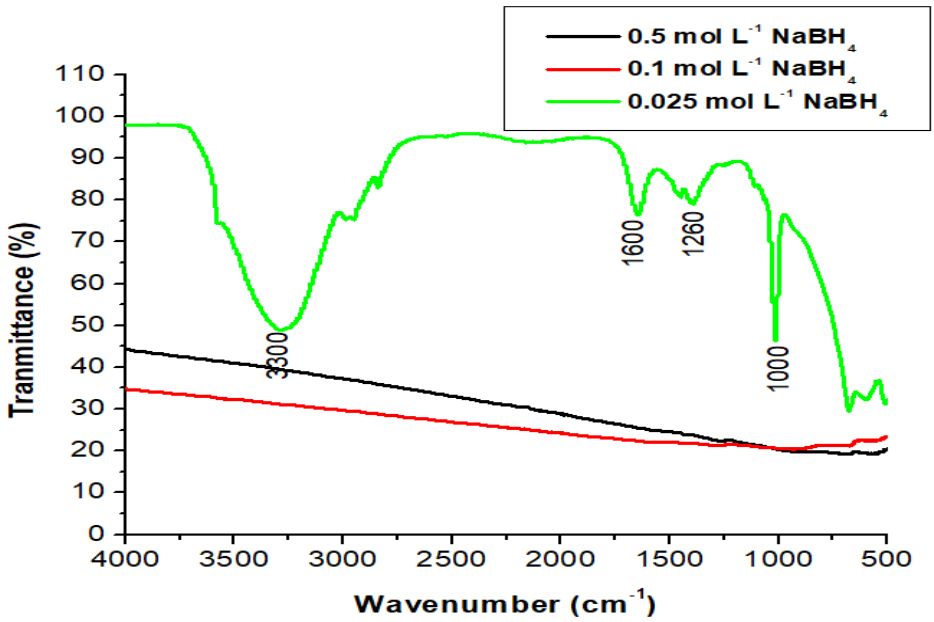

Figure 37: FTIR spectra of copper oxide particles prepared using 0.5,0.1 and 0.025 mol L^{-1} $NaBH_4$ as reducing agent, 0.5 mol L^{-1} of NaOH and 0.5 mol L^{-1} $CuCl_2$.

4.4.2 Degradation of methylene blue using copper oxide particles prepared using $NaBH_4$ as the reducing agent.

4.4.2.1 ***Fenton degradation and Photo-Fenton degradation***

The copper oxide particles prepared using 0.1 and 0.5 mol L^{-1} of $NaBH_4$ were used as catalysts during the Fenton degradation of MB (Figure 38). The rate of reaction of the catalyst prepared using 0.5 mol L^{-1} $NaBH_4$ was higher than the rate of reaction of the catalyst prepared using the catalyst prepared using 0.1 mol L^{-1} $NaBH_4$, however there was no large difference between the two rates of reaction. The particle prepared using 0.025 mol L^{-1} $NaBH_4$ had the lowest reaction rate compared to the other two catalyst. The highest concentration of $NaBH_4$ had an 86% removal of the MB. The catalyst prepared using different concentrations of $NaBH_4$ were used to degrade MB using Photo-Fenton degradation method (Figure 39). There was a difference between the rate of reactions of the catalyst prepared using 0.1 and 0.5 mol L^{-1} $NaBH_4$ during Photo-Fenton degradation however the catalyst prepared using the 0.5 mol L^{-1} $NaBH_4$ had the highest rate of reaction. The catalyst prepared using 0.025 mol L^{-1} $NaBH_4$ had the lowest reaction rate. The reaction fitted the 1^{st} order reaction for both the Fenton and photo-Fenton

degradations which suggest that the degradation of MB was mainly from the Fenton reaction.

When comparing the Fenton and Photo-Fenton degradation for both catalysts it was observed that the Photo-Fenton out-performed the Fenton degradation in both cases. The high reaction rate of photo-Fenton reaction can be attributed to the addition of four pathways for $OH^{\bullet}$ generation during the degradation process (Miao et al., 2018).The Fenton and photo-Fenton rate constants were different (Table 13), which indicates that the catalysts had a high photocatalytic activity.

Table 20: Rate constants of degradation of methylene blue using Fenton and Photo-Fenton degradation.

Fenton degradation					
catalyst (mol L^{-1} $NaBH_4$)	**k-values (1^{st} order) (s^{-1})**	**k-values (2^{nd} order) (M^{-1} s^{-1})**	**R^2 (1^{st} order)**	**R^2 (2^{nd} order)**	**percentage (%) removal (after 60 min of degradation)**
0.1	0.0245	0.0007	0.9888	0.9831	78
0.5	0.0313	0.0012	0.9967	0.9285	86
0.025	0.0105	0.0002	0.9880	0.9852	47
Photo-Fenton degradation					
catalyst (mol L^{-1} $NaBH_4$)	**k-values (1^{st} order) (s^{-1})**	**k-values (2^{nd} order) (m^{-1} s^{-1})**	**R^2 (1^{st} order)**	**R^2 (2^{nd} order)**	**percentage (%) removal (after 60 min of degradation)**
0.1	0.0363	0.0015	0.9989	0.9118	89
0.5	0.0588	0.0082	0.9894	0.8630	98
0.025	0.0110	0.0002	0.9865	0.9690	50

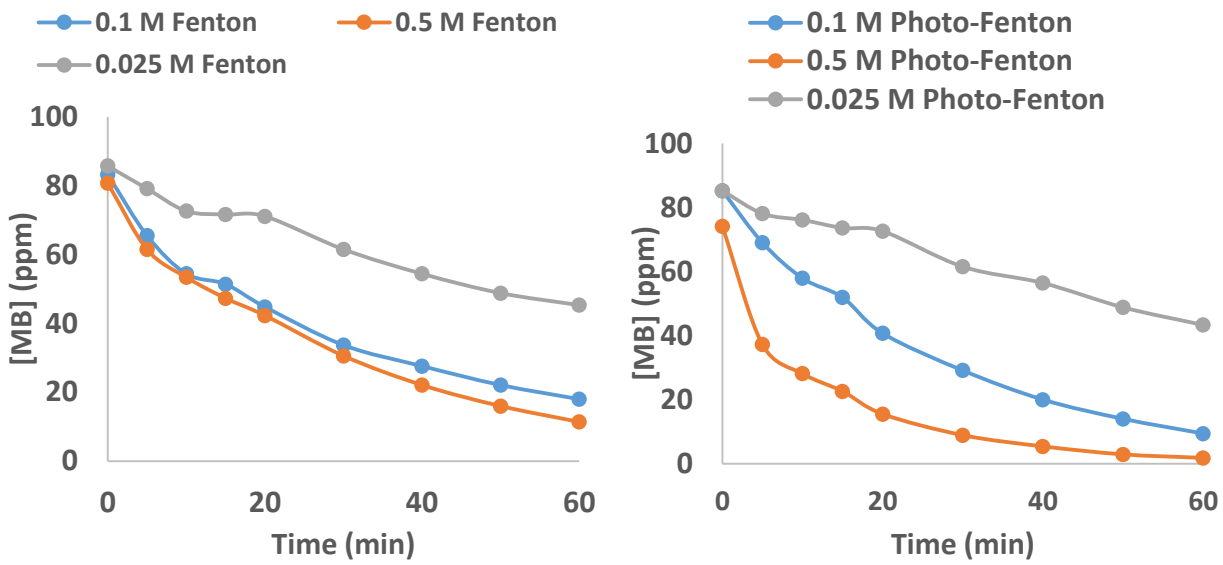

Figure 38: Fenton and Photo-Fenton degradation of MB using copper oxide catalyst prepared using 0.1, 0.5 and 0.025 mol L^{-1} $NaBH_4$, 0.5 mol L^{-1} of NaOH. 0.5 mol L^{-1} $CuCl_2$.

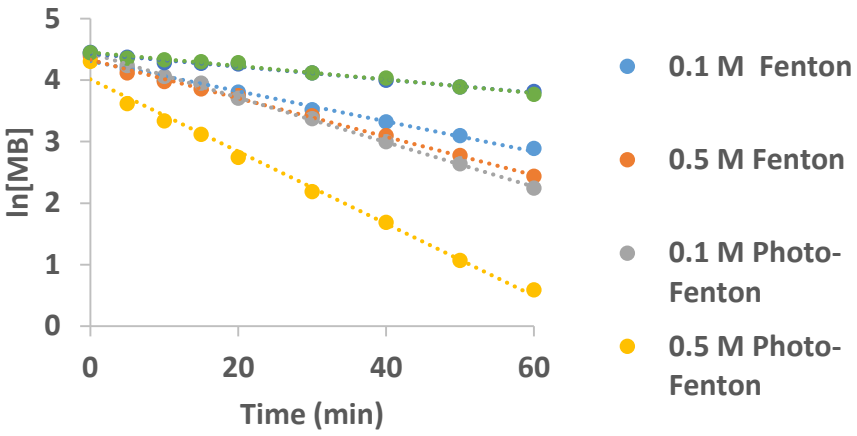

Figure 39: First order plots of the degradation of MB using copper oxide particles prepared with 0.1 mol L^{-1}, 0.5 and 0.025 mol L^{-1} $NaBH_4$ as reducing agent. 0.5 mol L^{-1} of NaOH.0.5 mol L^{-1} $CuCl_2$

4.4.3 Discussion

From the XRD, the stoichiometric amount (0.025 mol L^{-1}) was unable to reduce copper (I) to copper (II). A higher concentration resulted in an over reduction to Cu metal. The catalyst that was over reduced to Cu metal had the highest reaction rate for both Fenton and photo-Fenton reaction however the Photo-Fenton was the most active. The high reaction rate in Photo-Fenton degradation may be attributed to the additional pathways for $OH^{\bullet}$ generation.

4.5 Preparation of copper oxide catalysts with glucose as reducing agent.

A precipitation reduction method was used to prepare the copper oxide crystallites. The preparation method used were based on the method of Zhang et al. (2010) with slight modification, $CuCl_2$ was used as a precursor instead of $CuSO_4$. NaOH was used as the precipitating agent and glucose was used as reducing agent. The amount of glucose was varied to investigate the effect of the size, shape, copper phase of the crystals and catalytic activity.

4.5.1 Preparation of Cu_2O particles varying glucose

Cu_2O particles were prepared using glucose as reducing agent, $CuCl_2$ and NaOH were also used during the preparation. During the preparation method different concentrations of glucose were varied which were 0.4 and 0.1 mol L^{-1}.

$$2Cu(OH)_2 + C_6H_{12}O_6 \rightarrow C_6H_{12}O_7 + 2H_2O + Cu_2O \quad \text{(Reaction 32)}$$

Based on reaction 32, 1 mol of glucose reacts with 2 mols of Cu^{2+}, the stoichiometric amount was calculated to be 0.005 mols (50 mL of 0.1 mol.L^{-1}) glucose reacting 0.01 mol of Cu^{2+}(20 mL of 0.5 mol.L^{-1}) .

4.5.1.1 ***XRD analyses***

The copper oxide particle size was thus smaller when a higher concentration of reducing agent was used as shown in Table 21. The glucose may have functioned as a capping agent as well leading to a decrease in the particle size. Both the XRD patterns of the prepared copper oxide particles corresponded with the reference spectra of CuO (Figure 40). Glucose was used with the aim to reduce Cu (II) to Cu (I) but the major phase formed was CuO and not Cu_2O which indicated that reduction did not take place.

In a study by Sharma and Sharma (2012) copper oxide particles were prepared using glucose as a reducing agent at low temperature of 25°C. The particles did not reduce but as the temperature was increased to 80 °C the particles were reduced to Cu_2O. The reducing ability of glucose was enhanced by increasing the reaction temperature. In this study a low concentration of glucose and a low reaction temperature of 27 °C was used and this may have attributed to reduction not taking place.

Table 21: XRD sizes calculations of copper oxide particles prepared using 0.4 and 0.1 mol L^{-1} glucose.

0.1 mol L^{-1} glucose				**0.4 mol L^{-1} glucose**			
Phase	**Angle (2θ°)**	**FWHM (2θ°)**	**Size (nm)**	**Phase**	**Angle (2θ°)**	**FWHM (2θ°)**	**Size (nm)**
CuO	35.52	0.35	23.7	CuO	35.16	0.56	14.8

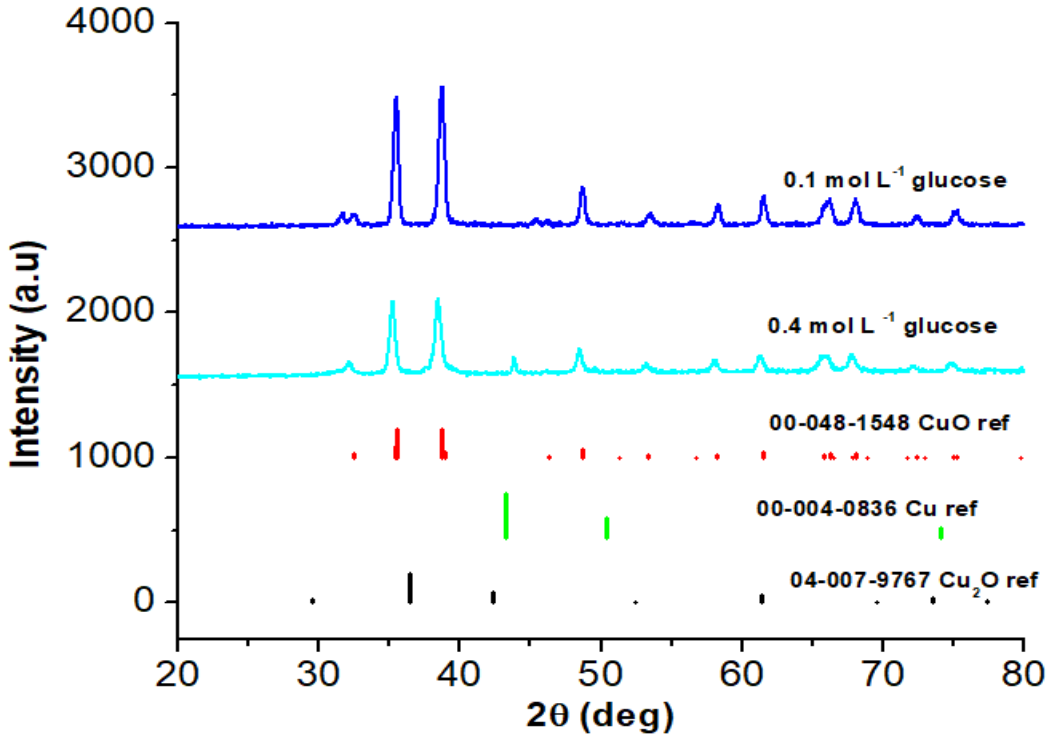

Figure 40: XRD diffraction patterns of copper oxide particles prepared using 0.1 and 0.4 mol L^{-1} glucose as reducing agent, 0.5 mol L^{-1} NaOH and 0.5 mol L^{-1} $CuCl_2$.

4.5.1.2 ***BET analyses***

The specific surface area of the 0.1 mol L^{-1} glucose catalyst was investigated using the adsorption and desorption isotherms. The surface area was 1.5383 m^2/g. The pore size distribution from the BJH pore size distribution was in the range of 200–450 nm indicating that the particles were macro porous structures with a pore size of 100.1 Å.

4.5.1.3 ***SEM analyses***

SEM analyses (Figure 44) show that at a low glucose concentration (0.1 mol L^{-1}) there was a mixture of shapes which were spheres and cubes and the size was 232 nm. At a higher glucose concentration of 0.4 mol L^{-1}, the particles were spherical in shape and the size 100 nm.

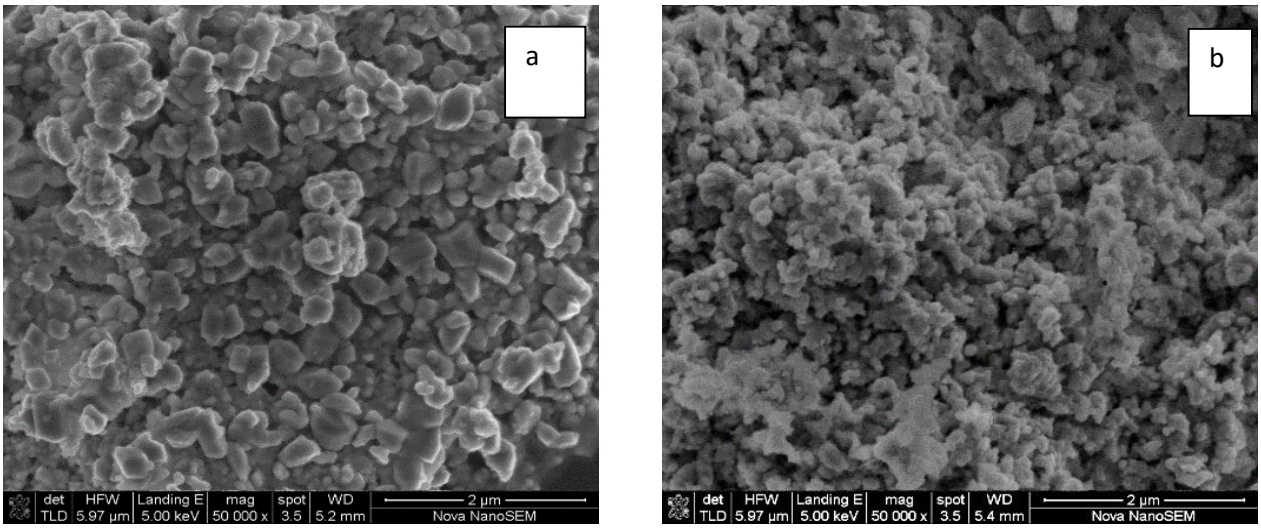

Figure 41: SEM images of copper oxide particles prepared using 0.1 and 0.4 mol L^{-1} glucose as reducing agent. 0.5 mol L^{-1} NaOH. 0.5 mol L^{-1} $CuCl_2$.

4.5.1.4 ***FTIR analyses***

From Figure 42, Glucose has an O-H stretching around 3500-3200 cm^{-1}, a C=O stretching around 2830 - 2695 cm^{-1}, C-H stretch around 3000-2850 cm^{-1} and C-C stretch around 1600-1585 cm^{-1}. These functional groups were present on the surface of the prepared copper oxide particles as shown in Figure 51. The glucose remained on the surface of the particle during the washing step during the preparation of the particles and this resulted in the capping of the copper oxide particles by the reducing agent (glucose).

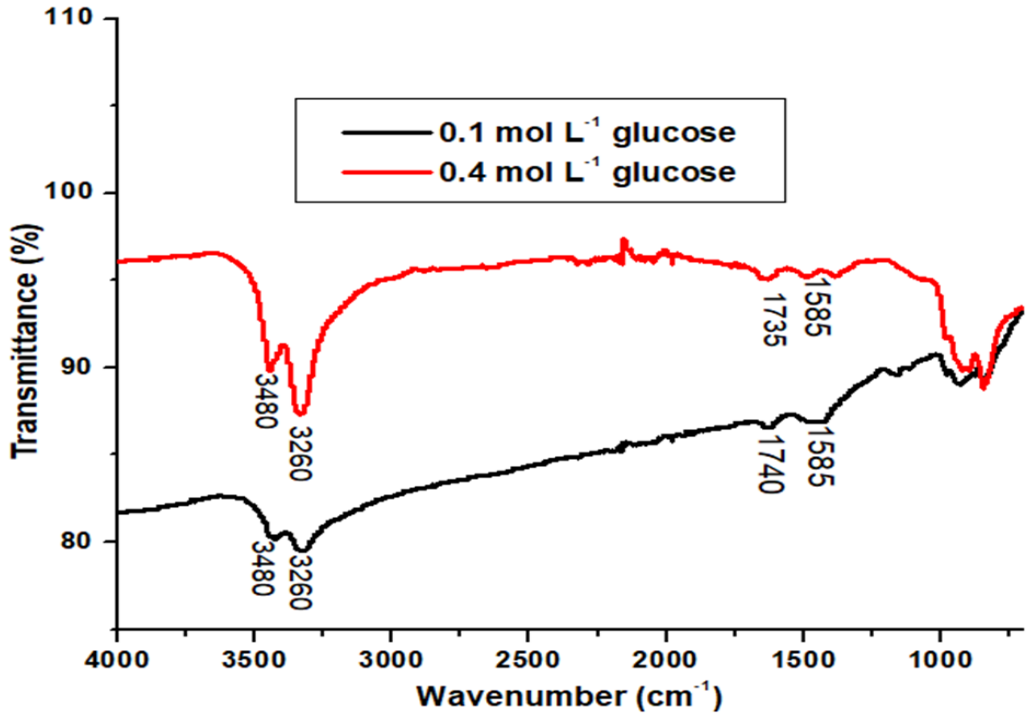

Figure 42: FTIR spectra of copper oxide particles prepared using 0.1 and 0.4 mol L^{-1} glucose as reducing agent, 0.5 mol L^{-1} $CuCl_2$ and 0.5 mol L^{-1} NaOH.

4.5.2 Degradation of methylene blue using copper oxide particles prepared using glucose as the reducing agent.

4.5.2.1 ***Fenton and Photo-Fenton degradation***

The copper oxide particles prepared using 0.1 and 0.4 mol L^{-1} of glucose were used as catalysts during the Fenton degradation and Photo-Fenton degradation of MB (Figure 43). There was no difference in the reaction rate of the catalyst prepared using 0.1 and 0.4 mol L^{-1} glucose during Fenton degradation and Photo-Fenton degradation. Since the percentage degradation are similar for both Fenton and Photo-Fenton it might be that the photo degradation did not work and the degradation was only by Fenton reaction.

Table 22: Rate constants of degradation of methylene blue using Fenton and Photo-Fenton degradation with catalysts prepared using glucose as a reducing agent.

Fenton degradation					
Catalyst (mol L^{-1} glucose)	**k-values (1^{st} order) (s^{-1})**	**k-values (2^{nd} order) (m^{-1} s^{-1})**	**R^2 (1^{st} order)**	**R^2 (2^{nd} order)**	**Percentage (%) removal (after 60 min degradation)**
0.1	0.0120	0.0002	0.9820	0.9538	50
0.4	0.0087	0.0001	0.9879	0.9932	39
Photo-Fenton degradation					
Catalyst (mol L^{-1} glucose)	**k-values (1^{st} order) (s^{-1})**	**k-values (2^{nd} order) (m^{-1} s^{-1})**	**R^2 (1^{st} order)**	**R^2 (2^{nd} order)**	**Percentage removal (%) (after 60 min degradation)**
0.1	0.0130	0.0002	0.9394	0.9954	53
0.4	0.0080	0.0002	0.9974	0.9675	40

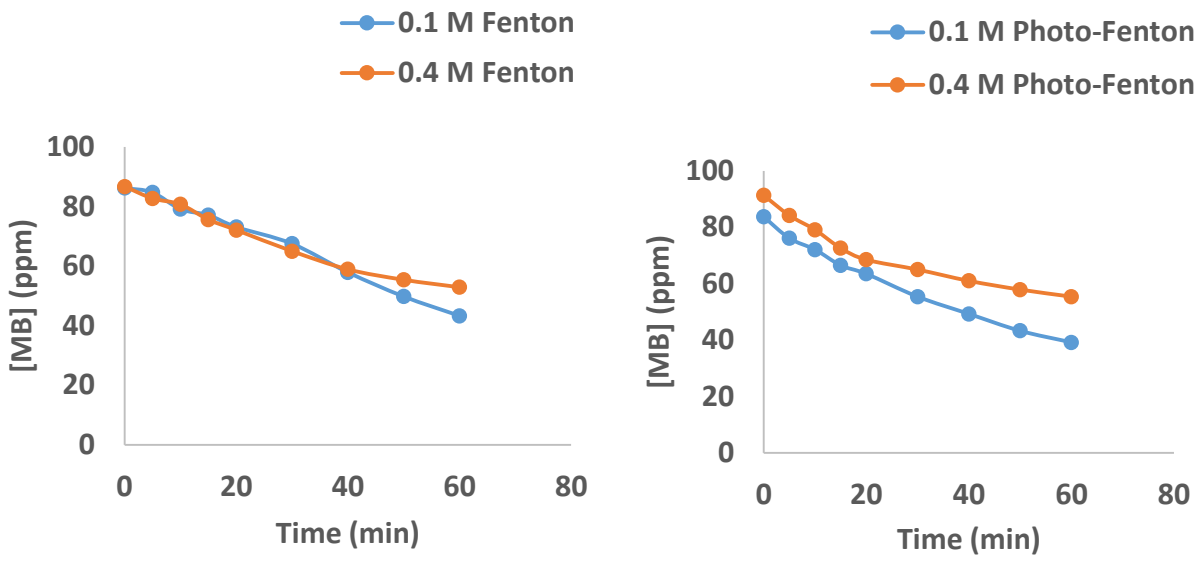

Figure 43: Fenton and Photo-Fenton degradation plots of the degradation of MB using copper oxide particles prepared with 0.1 mol L^{-1} and 0.4 mol L^{-1} glucose as reducing agent, 0.5 mol L^{-1} CuCl and 0.5 mol L^{-1} NaOH.

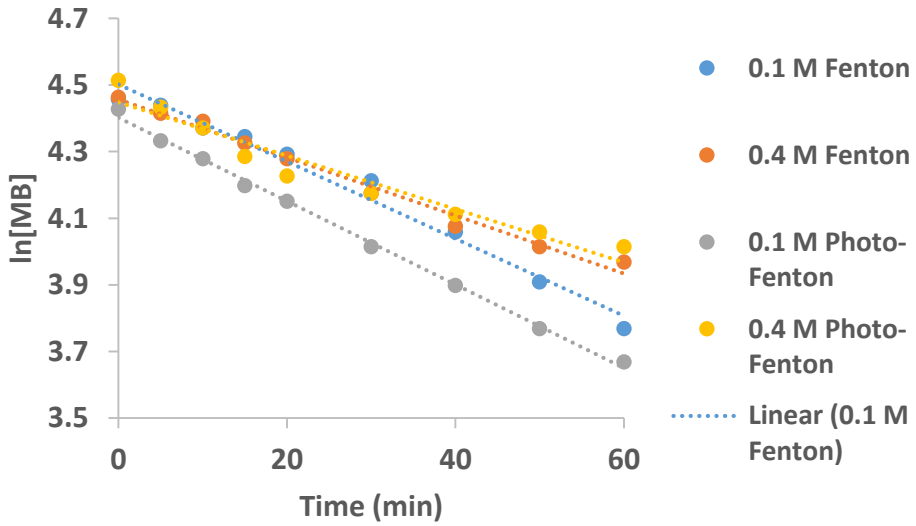

Figure 44: First order plots of the degradation of MB using copper oxide particles prepared with 0.1 mol L^{-1} and 0.4 mol L^{-1} glucose as reducing agent, 0.5 mol L^{-1} CuCl and 0.5 mol L^{-1} NaOH.

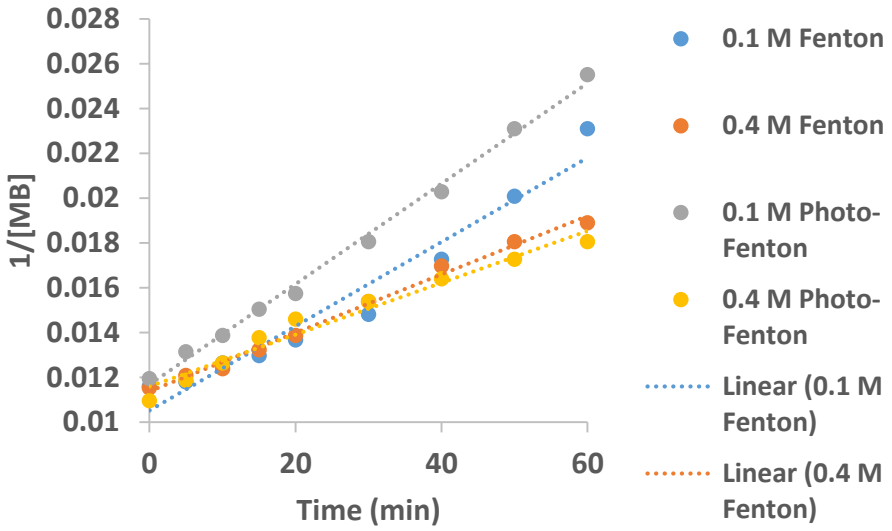

Figure 45: Pseudo second order plots of the degradation of MB using copper oxide particles prepared with 0.1 mol L^{-1} and 0.4 mol L^{-1} glucose as reducing agent.

4.5.3 Effect of Temperature on the preparation of copper oxide particles prepared using glucose as reducing agent

Glucose did not reduce the copper (II) to copper (I) when the copper oxide particles were prepared at room temperature. The preparation temperature was therefore increased. The copper oxide particles were prepared at 85, 90, 95 and 100 °C.

4.5.3.1 ***XRD analyses***

At room temperature CuO particles with a size of 24 nm was formed and at higher temperatures of 85,90,95 and 100 the glucose were able to reduce the copper (II) to copper (I) and the Cu_2O phase formed with sizes of 20,17,20 and 17, respectively (Figure 46). The temperature did not have a significant effect on the size of the copper oxide nanoparticles when the temperature was increased from 85 °C to 100 °C (Table 23).

Table 23: XRD sizes calculations of copper oxide particles prepared by varying different temperatures 27, 85, 90, 95 & 100 °C with 0.1 mol L^{-1} glucose, 0.5 mol L^{-1} NaOH and 0.5 mol L^{-1} $CuCl_2$.

Temperature (°C)	**85**	**90**	**95**	**100**	**27**
Phase	Cu_2O	Cu_2O	Cu_2O	Cu_2O	CuO
Angle (2θ°)	36.22	36.57	36.57	36.64	35.52
FWHM (2θ°)	0.423	0.49	0.42	0.49	0.35
Size (nm)	19.8	17.0	19.8	17.0	23.7

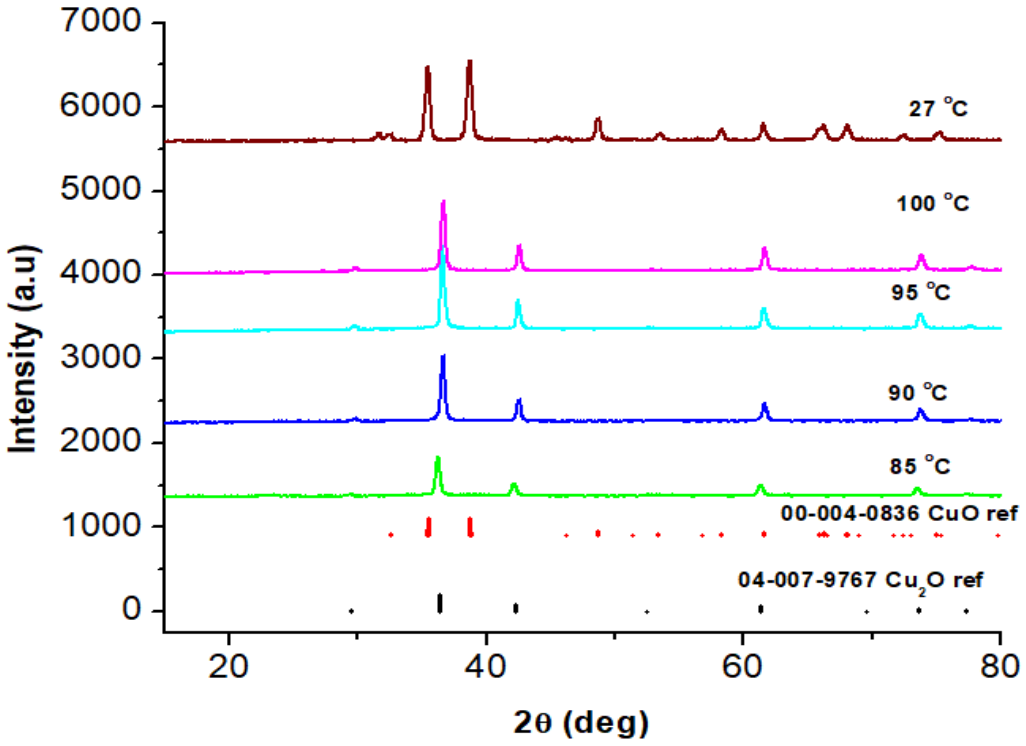

Figure 46: XRD patterns of copper oxide particles prepared using different temperatures 27, 85, 90, 95 , 100 °C, with 0.1 mol L^{-1} glucose, 0.5 mol L^{-1} NaOH and 0.5 mol L^{-1} $CuCl_2$.

4.5.3.2 ***SEM analyses***

SEM analyses (Figure 47) of the prepared copper oxide particles prepared by varying different temperatures. Particles with a size of 232 nm were observed at a temperature of 27 °C with a mixture of morphology but mostly spherical particles were observed. At 85 °C the particles consisted mostly of spheres and the size was 766 nm. At 90 °C the particles had a mixture of spherical and octahedral morphology with a size of 840 nm. Particles prepared at 95 °C consisted of only spherical particles that were less agglomerated with a size of 737 nm. When the temperature was increased to 100 °C a mixture of spheres and large octahedral with an estimated size of 697 nm. The particles prepared at 80°C were the most agglomerated and the particles prepared at 100°C were the least agglomerated.

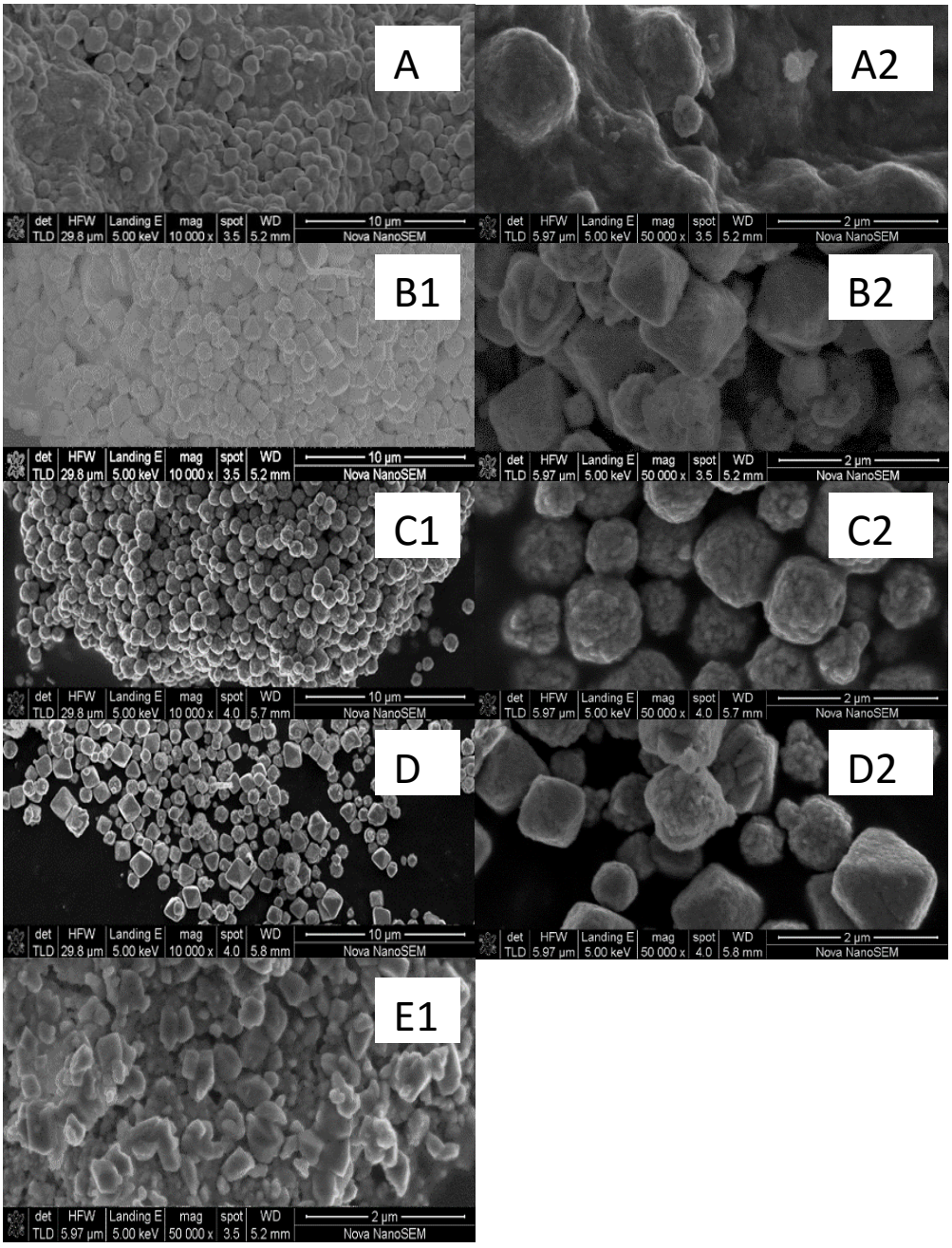

Figure 47: SEM images of copper oxide particles prepared using different temperatures: (A.1&2) 85 °C, (B.1&2) 90 °C , (C.1&2) 95 °C, (D.1&2) 100 °C and (e) 27 °C. 0.1 mol L^{-1} glucose. 0.5 mol L^{-1} NaOH and 0.5 mol L^{-1} $CuCl_2$.

4.5.3.3 ***FTIR analyses***

Figure 48 shows that glucose has functional groups O-H around 3500 cm^{-1} and C=O around 1740 -1720 cm^{-1}, from the prepared copper oxide particles it was observed that the particles had a O-H stretching at 3250 cm^{-1} , an C=O stretching at 1720 cm^{-1}. An C-O alcohol stretching was observed at 1010 cm^{-1} and 1250 cm^{-1}.The FTIR spectra thus indicated that glucose was adsorbed on the surface of the prepared copper oxide particles which meant that glucose was acting as a reducing agent as well as a capping agent.

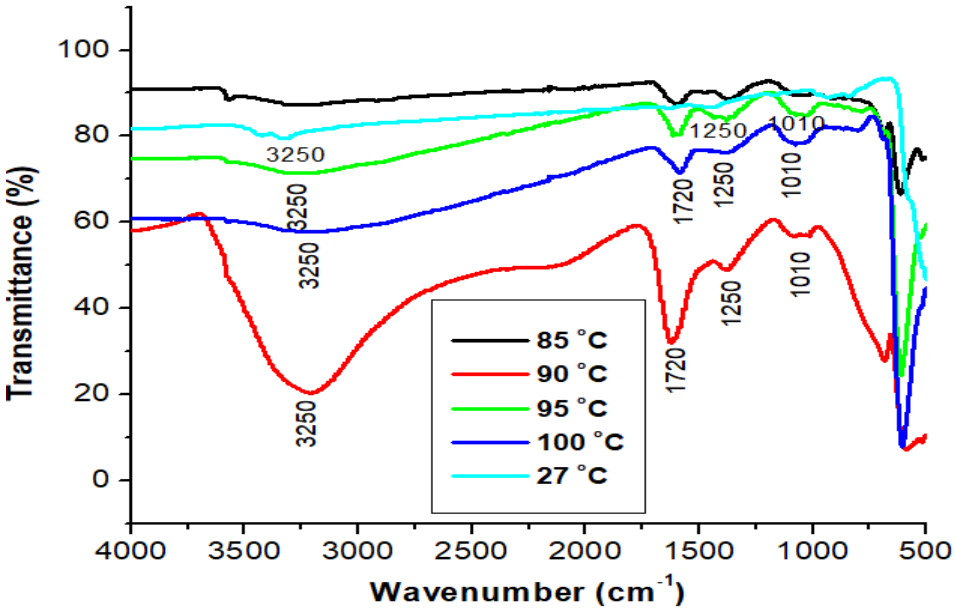

Figure 48: FTIR spectra of copper oxide nanoparticles prepared using different temperatures 85 °C, 90 °C, 95 °C,100 °C and 27 °C. 0.5 mol L^{-1} NaOH, 0.5 mol L^{-1} $CuCl_2$, 0.1 mol L^{-1} glucose.

4.5.4 Degradation of MB using the prepared copper (I) oxide particles prepared with different temperatures.

The prepared copper oxide catalysts were used to degrade MB using Fenton and Photo-Fenton degradation (Figure 49). Both reactions fitted the second order reaction (Table 24). During Fenton degradation the 90 °C catalyst had the highest removal for both Fenton and Photo-Fenton reaction as shown in Figure 49. When comparing the Fenton and Photo-Fenton degradation for the catalyst prepared using 90 °C it was observed that the Fenton reaction was more active. Fenton degradation was more active compared to

the Photo-Fenton in regards to all the catalysts prepared. The low photo-Fenton reaction rate may be attributed to photocorrosion (Photo oxidation, Equation 36) where the catalyst is reduced to CuO by photo induced holes during degradation.

Table 24: Rate constants of degradation of methylene blue using Fenton and Photo-Fenton degradation with catalysts prepared varying different temperatures and glucose as the reducing agent.

Fenton degradation					
Catalyst (°C)	**k-values (1^{st} order) (s^{-1})**	**k-values (2^{nd} order) (m^{-1} s^{-1})**	**R^2 (1^{st} order)**	**R^2 (2^{nd} order)**	**Percentage removal (%) (after 60 min degradation)**
85	0.0158	0.0004	0.8590	0.9579	69
90	0.0267	0.0010	0.9086	0.9579	86
95	0.0228	0.0006	0.9210	0.9697	81
100	0.0048	0.0007	0.8439	0.8717	28
27	0.0120	0.0002	0.9820	0.9538	50
Photo-Fenton degradation					
Catalyst (°C)	**k-values (1^{st} order) (s^{-1})**	**k-values (2^{nd} order) (m^{-1} s^{-1})**	**R^2 (1^{st} order)**	**R^2 (2^{nd} order)**	**Percentage removal (%)(after 60 min degradation)**
85	0.0114	0.0002	0.8481	0.9311	58
90	0.0218	0.0014	0.8603	0.9775	80
95	0.0192	0.0005	0.8784	0.9463	77
100	0.0114	0.0002	0.8793	0.9400	58
27	0.0130	0.0002	0.9394	0.9954	53

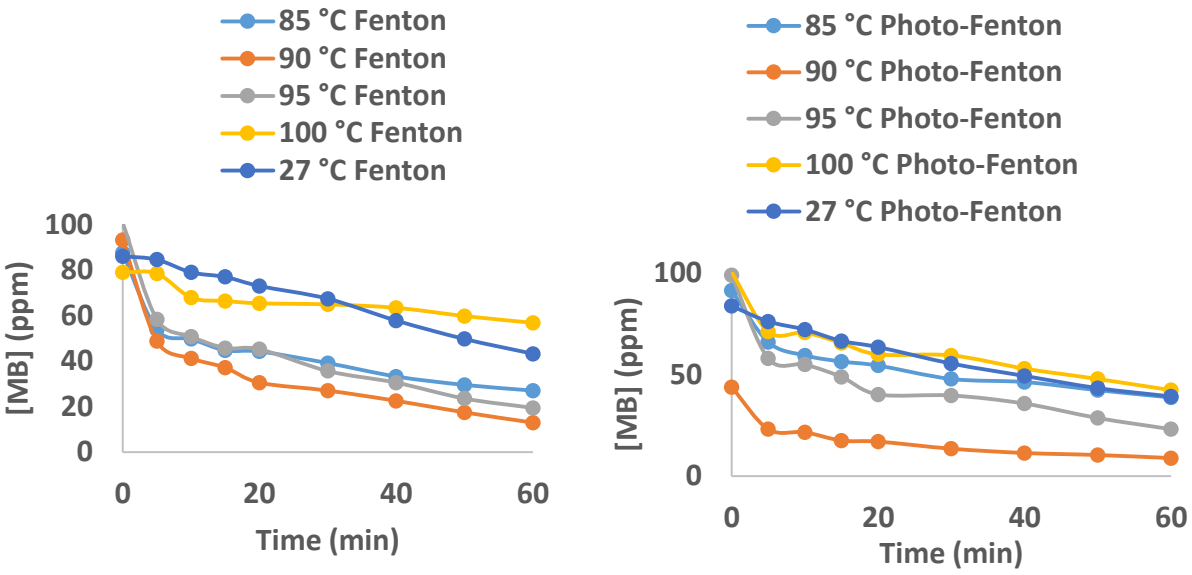

Figure 49: Fenton and Photo-Fenton degradation of MB using catalysts prepared by varying different temperatures, 27, 85, 90, 95 , 100 °C, with 0.1 mol L^{-1} glucose, 0.5 mol L^{-1} NaOH and 0.5 mol L^{-1} $CuCl_2$.

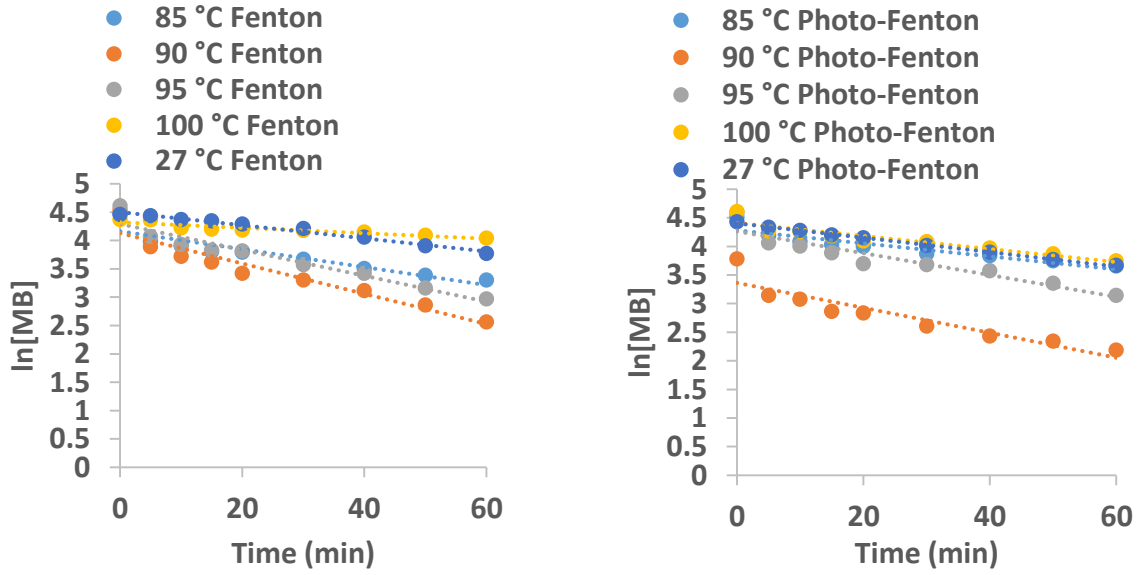

Figure 50: Pseudo Second order plots of the degradation of MB using copper oxide particles prepared with different temperature, 27, 85, 90, 95 , 100 °C, with 0.1 mol L^{-1} glucose, 0.5 mol L^{-1} NaOH and 0.5 mol L^{-1} $CuCl_2$.

4.5.5 Discussion

The XRD and SEM sizes are different and can be explained by that the particles observed by SEM consist of an agglomeration of smaller particles. Both the XRD and SEM indicated that smaller particles formed at a higher glucose concentration. The FTIR spectra showed that the glucose was adsorbed on the copper oxide surface. The glucose may have acted like a capping agent which might explain the smaller particle size when a higher glucose concentration was used.

The particle prepared at 90 °C had the highest reaction rate and from the SEM it was observed that the particles had a mixture of spheres and octahedral shapes. The SEM also revealed that the particles were smaller in size, and smaller particles are known to have a higher activity. Particles with a rough surface are known to have a higher activity because the rough surface increases the surface area of the particles. The surface roughness may have attributed to the high reaction rate of the particle prepared at 90 °C.

The degradation of MB from the two different degradation method was very low for the catalysts prepared using 0.1 and 0.4 mol L^{-1} glucose which may be attributed to the CuO phase which is an inactive phase for both Fenton and Photo-Fenton.

4.6 Comparison of catalysts.

4.6.1 Comparing the stoichiometric amounts of the different reducing agents.

4.6.1.1 ***XRD analyses***

The phases of the particles were determined using XRD (Figure 51) and the crystallite sizes were calculate (Table 25). For the stoichiometric amount of ASC CuO and Cu_2O phases were obtained but the major phase was Cu_2O. Cu and Cu_2O phases were obtained from the stoichiometric amount of hydrazine however Cu_2O was the major phase. Stoichiometric amount of $NaBH_4$ was not enough to reduce Cu (II) to Cu (I) and the major phase that was obtained was CuO indicating that reduction did not take place. The major phase obtained at the stoichiometric amount of glucose at room temperature was CuO indicating that reduction from Cu (II) to Cu (I) did not take place, however an increase in temperature to 90 °C reduced Cu (II) to Cu (I) as the major phase obtained was Cu_2O.

Table 25: XRD sizes and phase of copper oxide particles prepared using stoichiometric amounts of the different reducing agents.

Catalyst	**Phase**	**Angle (2θ°)**	**FWHM (2θ°)**	**Size (nm)**
0.1 mol L^{-1} ASC	CuO	43.33	0.63	13.5
	Cu_2O	36.29	0.42	19.8
0.1 mL N_2H_4	Cu	42.70	0.42	20.2
	Cu_2O	36.78	0.49	17.0
0.025 mol L^{-1} $NaBH_4$	CuO	35.87	1.55	5.4
0.1 mol L^{-1} glucose (27 °C)	CuO	35.52	0.35	23.7
0.1 mol L^{-1} glucose (90 °C)	Cu_2O	36.57	0.49	17.0

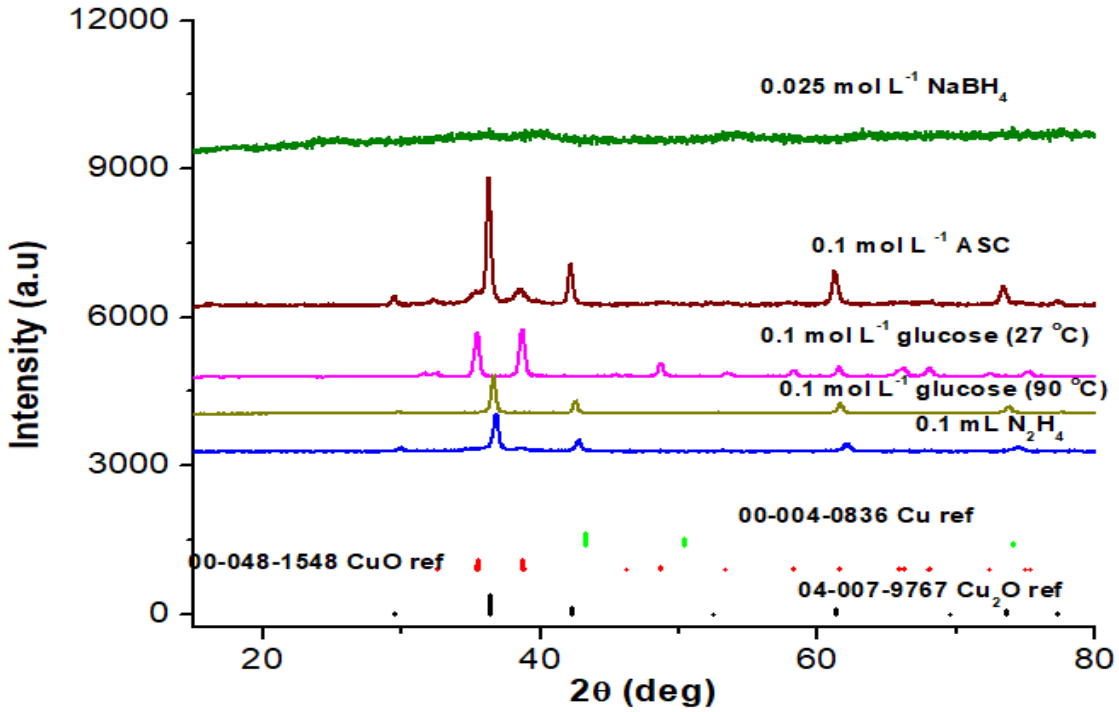

Figure 51: XRD diffraction pattern of copper oxide particles prepared using stoichiometric amounts of different reducing agents (0.1 mol L^{-1} ASC, 0.1 mL N_2H4, 0.025 mol L^{-1} $NaBH_4$, 0.1 mol L^{-1} glucose (27 °C) & 0.1 mol L^{-1} glucose (90 °C))

4.6.1.2 ***SEM analyses***

Stoichiometric amount of ASC had spherical and agglomerated particles with a size of about 119 nm (Figure 52). Particles with a mixture of cubic and spherical particles were obtained when the stoichiometric amount of hydrazine was used. Agglomerated particles with flat sheets were obtained when stoichiometric amounts of $NaBH_4$ was used. Particles with a mixture of morphology but mostly spherical morphology with a size of about 232 nm was obtained when glucose at room temperature was used. An increase in temperature to 90 °C (glucose) gave spherical and octahedral particles with a rough surface and a size of about 452 nm.

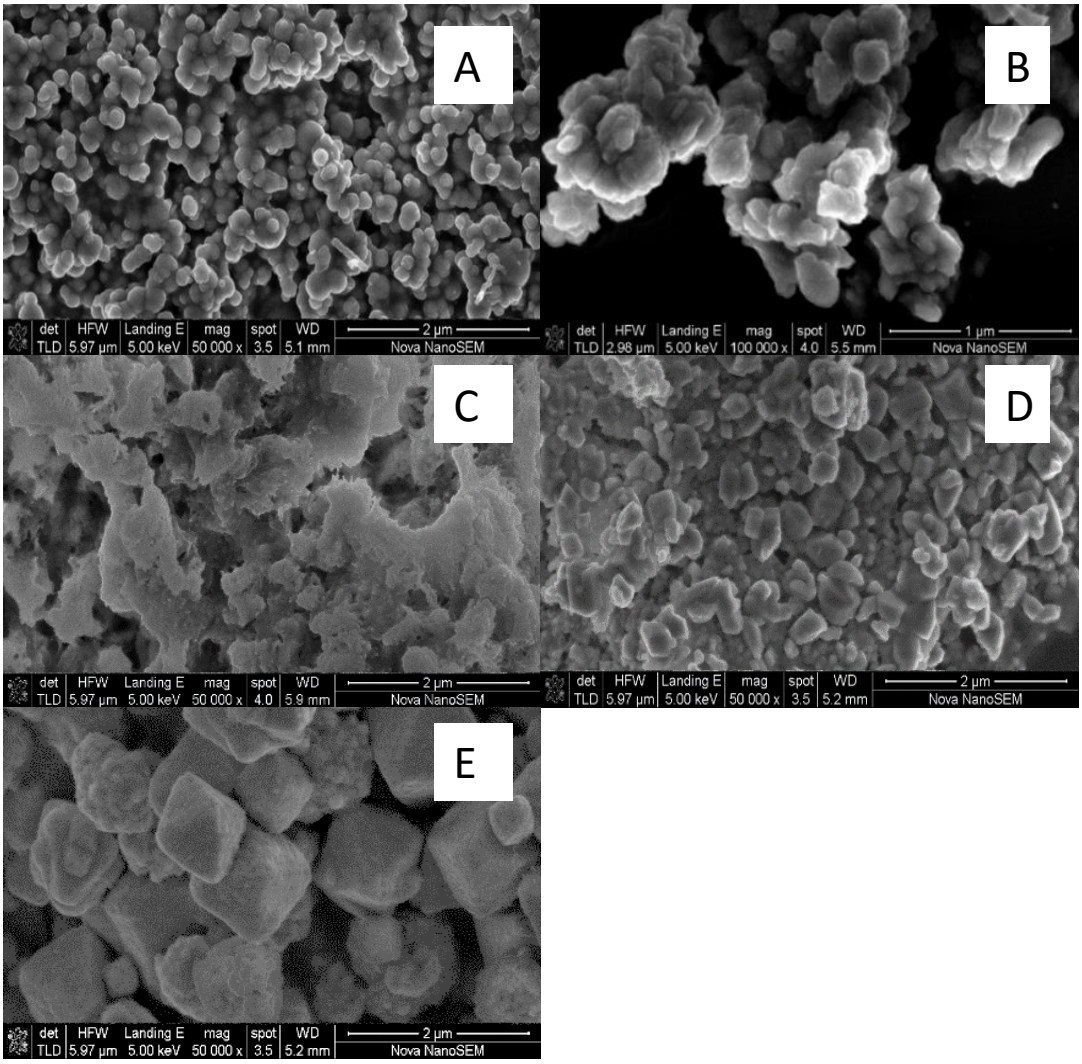

Figure 52: SEM images of copper oxide particle prepared using stoichiometric amounts of the reducing agents (a) 0.1 mol L^{-1} ASC, (b) 0.1 mL N_2H4, (c) 0.025 mol L^{-1} $NaBH_4$, (d) 0.1 mol L^{-1} glucose (27 °C) and (e) 0.1 mol L^{-1} glucose (90 °C).

4.6.1.3 ***Degradation of MB using particle prepared with stoichiometric amounts of the reducing agent.***

The prepared copper oxide particles prepared with stoichiometric amounts of the different reducing agents were used to degrade MB using Fenton degradation method (Figure 53) and their activity was compared (Table 26). It was observed that the catalyst prepared using 0.1 mol L^{-1} glucose (90 °C) had the highest reaction rate and a percentage removal of 86% of the MB. The catalyst prepared using the stoichiometric amount of $NaBH_4$ had the lowest reaction rate and the percentage removal of 47% of the MB. There was not a big difference between the reaction rate of the particles prepared using the stoichiometric amounts of hydrazine and glucose (27 °C).

Table 26: Rate constants of degradation of methylene blue by copper oxide particles prepared using stoichiometric amounts of different reducing agents (0.1 mol L^{-1} ASC, 0.1 mL N_2H_4, 0.025 mol L^{-1} $NaBH_4$, 0.1 mol L^{-1} glucose (27 °C) & 0.1 mol L^{-1} glucose (90 °C))

Catalyst	**k-values 1st order (s^{-1})**	**k-values 2nd order (m^{-1} s^{-1})**	**R^2 (1st order)**	**R^2 (2nd order)**	**Percentage removal (%) (after 60 min degradation)**
0.1 mol L^{-1} ASC	0.0222	0.0011	0.9567	0.9888	77
0.1 mL N_2H_4	0.0091	0.0001	0.9682	0.9781	50
0.025 mol L^{-1} $NaBH_4$	0.0105	0.0002	0.9880	0.9852	47
0.1 mol L^{-1} glucose (27 °C)	0.0120	0.0002	0.9820	0.9538	53
0.1 mol L^{-1} glucose (90°C)	0.0267	0.0010	0.9086	0.9579	86

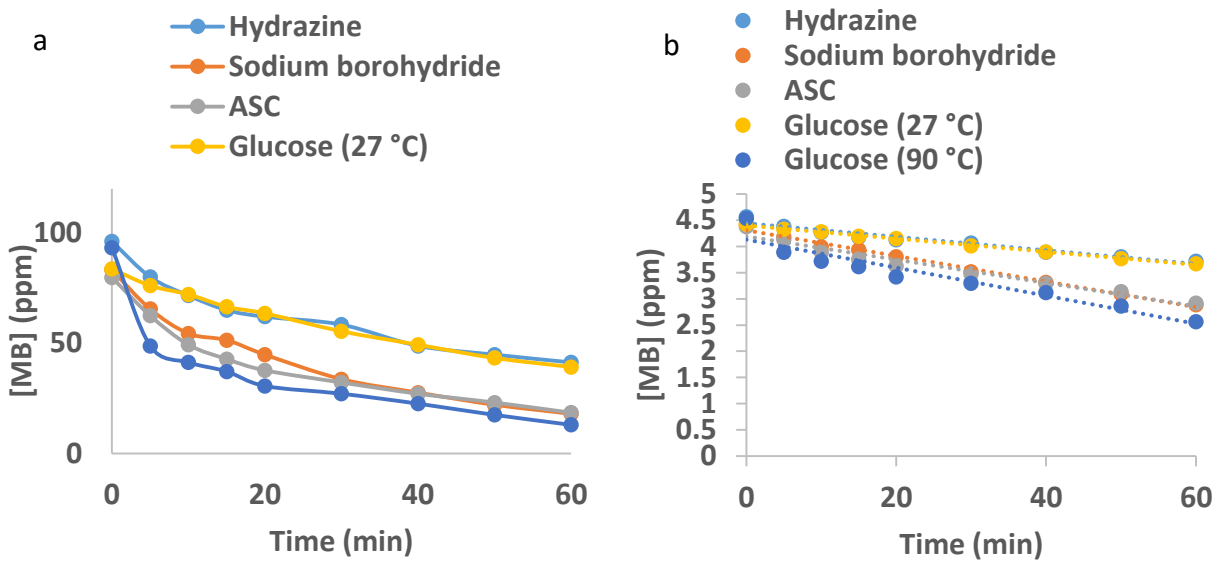

Figure 53: (a) Fenton degradation of MB. (b) 1st order plots of the degradation of MB using copper oxide particle prepared using stoichiometric amounts of the different reducing agents.

4.6.2 Comparison of the most active catalyst prepared using different reducing agents

From the catalyst prepared using different reducing agents, the catalysts that had the highest activity for the Fenton degradation were selected for each reducing agent and compared (Figure 54). It was observed that the catalyst prepared using 0.1 mol L^{-1} ASC (1 mol L^{-1} NaOH) had the highest reaction rate and a percentage removal of 94% of the MB. The catalyst prepared using hydrazine (15 mL NaOH) had the lowest reaction rate with a percentage removal of 81%. The catalyst prepared using $NaBH_4$ (27 °C) and glucose (90 °C) did not have a difference in the reaction rate.

Table 27: Rate constants of degradation of methylene blue by the most active catalysts using Fenton degradation.

Catalyst	**k-values (1^{st} order) (s^{-1})**	**k-values (2^{nd} order) ($m^{-1}.s^{-1}$)**	**R^2 (1^{st} order)**	**R^2 (2^{nd} order)**	**Percentage removal (%) (after 60 min degradation)**
15 mL NaOH) (0.1 mL N_2H4, 2.5 mL NH_3, 0.852 g $CuCl_2$, 27 °C)	0.0290	0.0008	0.9927	0.9639	81
0.1 mol L^{-1} ASC (1 mol L^{-1} NaOH, 0.5 mol L^{-1} $CuCl_2$, 27 °C)	0.0431	0.0025	0.9723	0.9438	94
0.5 mol L^{-1} $NaBH_4$ (0.5 mol L^{-1} NaOH, 0.5 mol L^{-1} $CuCl_2$, 27 °C)	0.0313	0.0012	0.9967	0.9285	86
90 °C glucose (0.1 mol L^{-1} ASC, 0.5 mol L^{-1} NaOH, 0.5 mol L^{-1} $CuCl_2$)	0.0267	0.0010	0.9086	0.9579	86

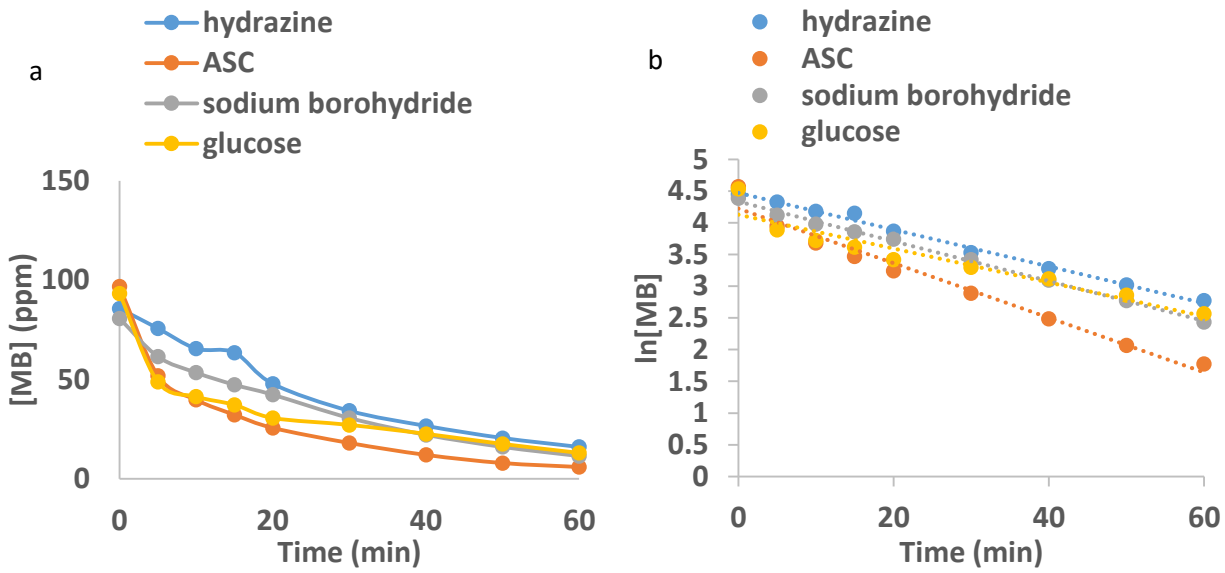

Figure 54: Fenton degradation of MB copper oxide particles that had the highest activity for each reducing agent. (b) Pseudo 1st order plots of the degradation of MB using copper oxide particle that had the highest activity.

4.6.3 Discussion on pore areas

The catalytic activity of metal oxides is influenced by the metal oxide particle size (Wang et al., 2016; Kuo et al., 2007), metal oxide surface area (Kim 2002), shape (Ke et al., 2016; Ouyang et al., 2016) and phase (Nguyen et al., 2015; Haung et al., 2015;Sun et al., 2018; Yang et al., 2015). The activity of the catalyst is expected to increase with an increase in the metal oxide surface area when comparing catalyst with the same shape and phase. Most of the catalysts in this study had a Cu_2O phase and were spherical in shape and these catalysts were thus selected to determine if the catalytic activity correlates with the surface area (Figure 55). It was found that the percentage degradation increased with an increase in the surface area when the surface area increased from 1.5 m^2/g to 10 m^2/g and the percentage degradation decreased with a further increase in the surface area.

The surface area has been determined by the adsorption of nitrogen. The nitrogen molecule is much smaller (4 Å x 3 Å) than the methylene blue molecule (17 x 7.6 x 3.3 Å (Gratten-Bellew, 2001); 12.5 to 16.0 Å long, 5.7 to 8.4 Å wide, 5 Å thick (Gratten-Bellew, 2001)) which means the nitrogen molecule can enter small micro pores and access surface area which may not be possible for the methylene blue molecule. Even if the pores that are large enough for the methylene blue to enter, small pore sizes may still slow down the rate of reaction due to mass transfer limitations (slow diffusion). Therefore, the effect of the pore size on the Fenton reaction were investigated.

Literature on the effect of the pore size on the Fenton catalytic activity has not been found. The effect of the pore size on the catalytic activity of other reactions have been reported on. The dependence of catalytic activity on the pore size of silica was studied by Iwamoto et al. (2003) for the acetalization of cyclohexanone with methanol. The catalytic activity strongly depended on pore diameter of the catalyst and a pore size of 19 Å yielded the most active catalysts. The catalytic activity was lower when silica with smaller and larger pores were used. Ghampson et al. (2015) tested silica supported cobalt catalysts with support pore diameters from 30 Å to 220 Å for the Fischer–Tropsch reaction. The reaction rate and turnover frequency (TOF) increased with an increase in the support pore diameter and was explained by an increase rate of diffusion with an increase in the pore size.

The effect of the pore size on the percentage degradation for this study are shown in Figure 55. The percentage degradation increased linearly with the average pore size till a pore size of 66 Å. The maximum degradation of 94 % was found at an average pore size of 66 Å and this catalyst had a surface area of 9.8 m^2/g. One can hypothesise that the rate of the Fenton reaction increases with an increase in the average pore size because the small pores cause mass transfer limitations and increases with methylene blue accessible surface area in the absence of mass transfer limitations.

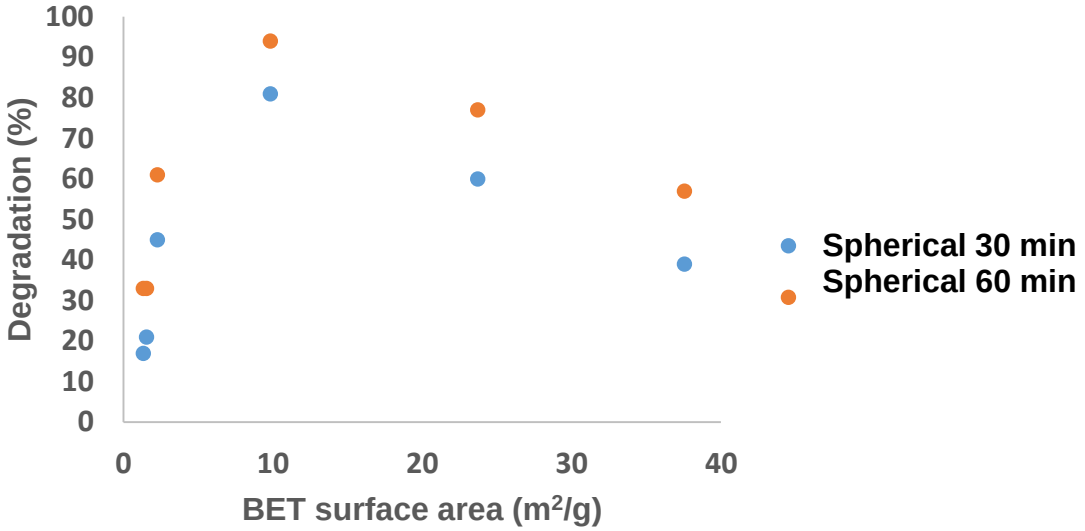

Figure 55: Effect of the surface area on the percentage methylene blue degradation after 30 min and 60 min for Cu_2O catalysts with spherical morphology. Catalyst with different shapes and phases were excluded.

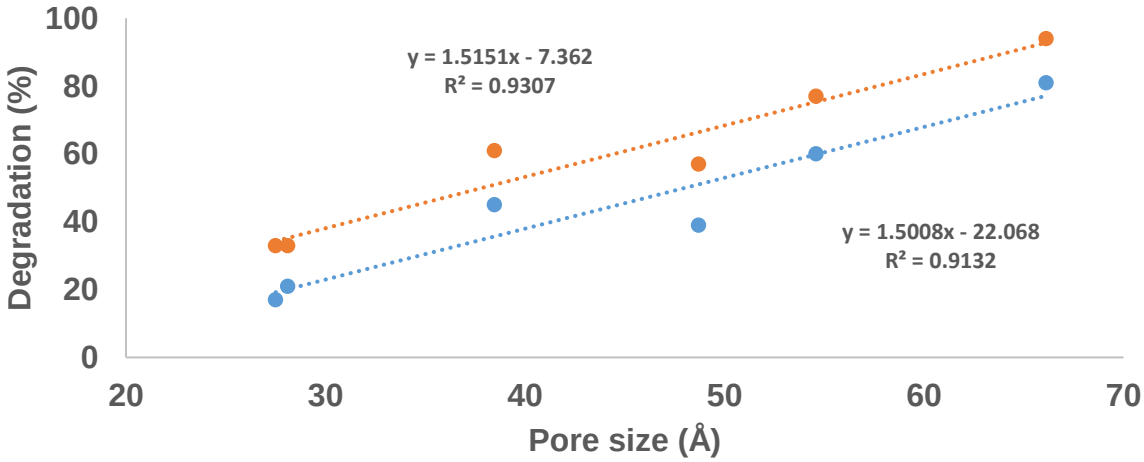

Figure 56: Effect of the average pore size of Cu_2O catalyst with spherical morphology the percentage methylene blue degradation after 30 min and 60 min. Catalyst with different shapes and phases were excluded.

Insufficient catalyst information is available in this study to make firm conclusions on the effect of shape and phase on the catalytic activity. The Cu_2O catalyst with cubic morphology has a pore size of 63.4 Å and a surface area of 12.7 m^2/g which is similar to

the Cu_2O catalyst with spherical morphology with a pore size of 66.1 Å and a surface area of 9.8 m^2/g. The percentage degradation of 81% for the cubic shaped catalyst were lower than the 94 % degradation for the catalyst with spherical particles or 89% predicted from the correlation shown in Figure 56, which may indicate that the cubic shaped particles were less active than spherical particles. The Cu metal catalyst (0.5 mol L^{-1} $NaBH_4$) with spherical morphology had a pore size of 56.6 Å and a surface area of 13.6 m^2/g and a percentage degradation of 86 % were obtained. A degradation percentage of 78 % is expected based on Figure 56, which may indicate that the copper metal is more active than the Cu_2O phase. More data is required to make statistically sound conclusions.

4.7 The addition of carbon material

Carbon material were added to the copper oxide since literature has suggested it to increase the catalytic activity. The addition of carbon to copper oxide catalysts increases the activity of the catalyst by increasing the dispersion of the copper oxide phase (Gau et al., 2012). Concentration of the pollutant on the surface increasing catalytic activity (He et al., 2016; He et al., 2011).

In this study copper (I) oxide catalyst were prepared containing 0%, 1% and 5% graphene and AC. A mass of 0.0066 g and 0.0344 g of graphene and AC were used to prepare the 1% and 5% graphene and AC-copper oxide composite catalysts.

4.7.1 XRD analyses

The addition of graphene and AC to the copper oxide catalyst changed the phase of the copper oxide from Cu_2O to copper (I) chloride. Similar phase was obtained in a study by Chen and Xue (2013) where CuCl was used as a precursor salt to form Cu_2O. However it was reduced to CuCl. The CuCl/ graphene and AC (0.0000 g) catalyst phase of Cu_2O. An amorphous peak around 25 θ° for pure graphene was observed for pure graphene with additional peaks that are in-line with the blank XRD sample holder.

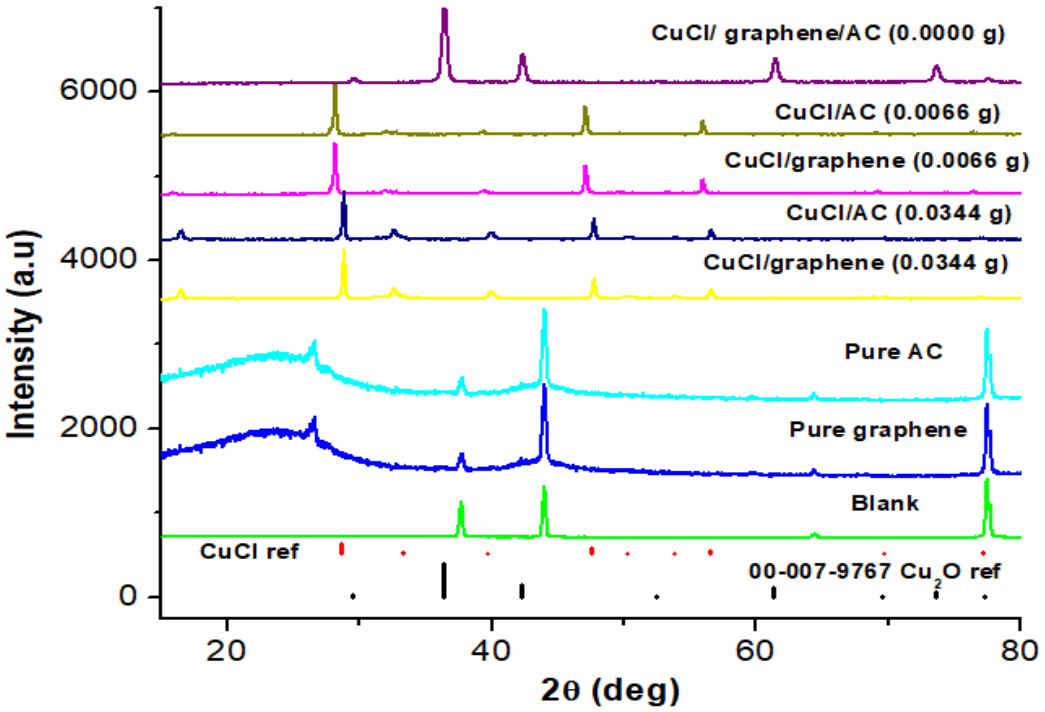

Figure 57: XRD diffraction patterns of copper oxide particles containing 0.0066 g, 0.0344 g graphene/AC, CuCl/graphene and AC (0.0000 g).

4.7.2 SEM analyses

SEM (Figure 58) of the prepared particles showed that the particles containing 1 and 5% graphene consisted of an agglomeration of small particles that had a mixture of morphologies. For the CuCl/graphene particles containing 1% graphene, the size was 181 nm and 150 nm for the CuCl/graphene particles prepared using 5% graphene and 104 nm for the CuCl/graphene (0.0000 g) particles. Figure 58c shows that the particles of pure graphene had a smooth surface. The CuCl/graphene (0.0000 g) particles were spherical in shape and the copper oxide-graphene composites were more cubic in morphology (Figure58).The CuCl/AC (0.0066 g) particles (Figure 58e) had an agglomeration of larger and smaller particles which were spherical with an average size of 200 nm. The CuCl/AC (0.0344 g) particles (Figure 58.f) had an agglomeration of spherical particles and were 140 nm in size. Figure 58.g shows CuCl/AC (0.0000 g) particles were spherical in shape and were about 104 nm.

.

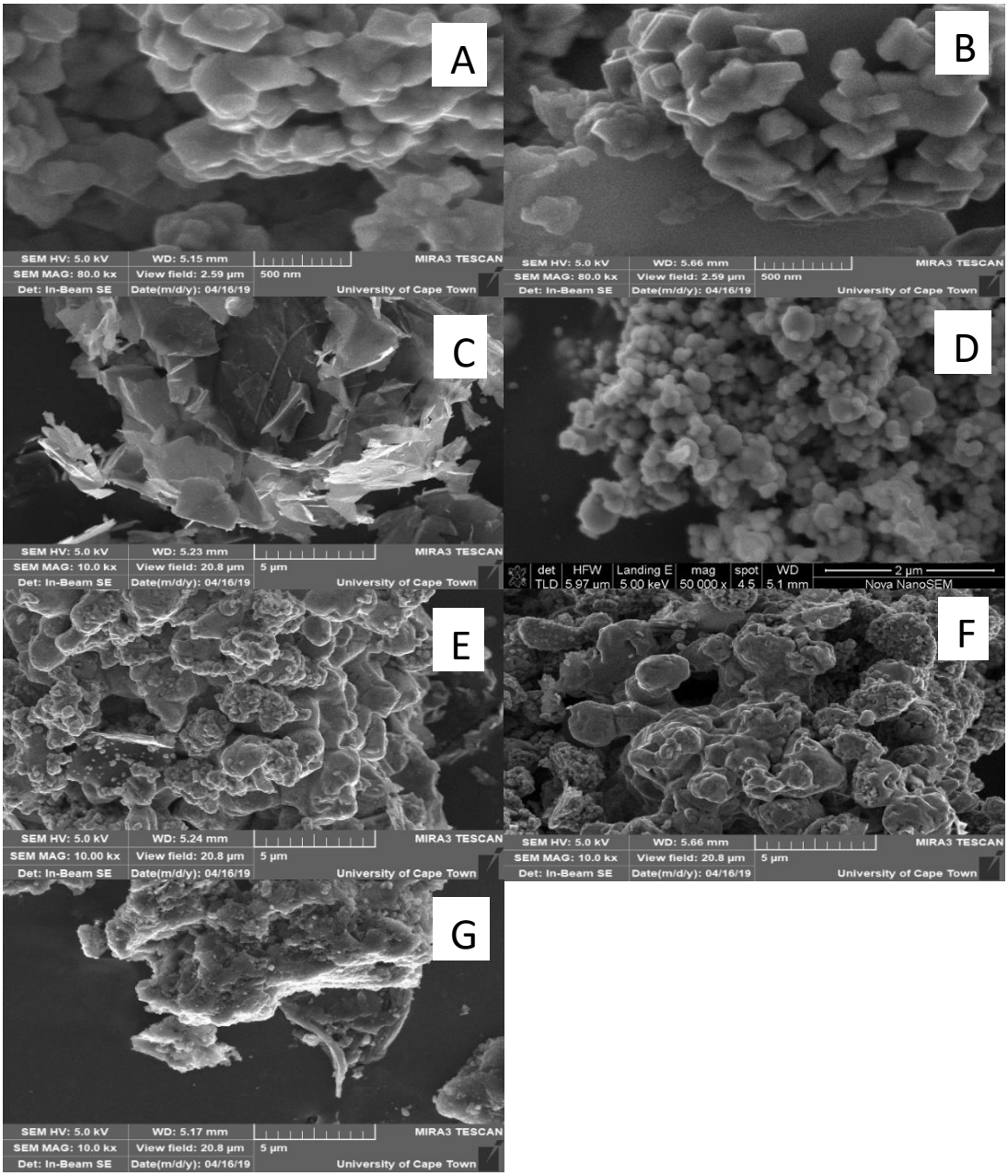

Figure 58: SEM images of copper oxide particles prepared using (a) 0.0066 g , (b) 0.0344 g graphene, (c) pure graphene,(D) no graphene and AC, (e) 0.0066 g AC, (F) 0.0344 g AC and (g) pure AC.

4.7.3 FTIR analyses

Graphene has different C-C functional groups. From the FTIR spectrum as seen in figure 59 it was observed that there was an aromatic C-C stretch (in-ring) around 1500 – 1400 cm^{-1}. An alkene C=C stretch around 1680 – 1640 cm^{-1} was observed for both graphene and AC particles. An O-H stretch around 3500 – 3200 cm^{-1} was observed. In both particles prepared using 0.0066 g and 0.0344 g graphene and AC, respectively, the functional group were observed on the surface of both the particles which indicated that the particles contained graphene. Ascorbic acid consists of O-H stretching at around 3500-3200 cm^{-1}, a carbonyl C=O stretching at around 1760-1665 cm^{-1}, C=C stretching around 1680-1640 cm^{-1} , a =C-H alkene stretching around 3100-3000 cm^{-1} and an alkane C-H stretching around 3000-2850 cm-1 . These peaks characteristic of ascorbic acid were observed on the surface of the catalyst prepared using 0.0000 g graphene/AC.

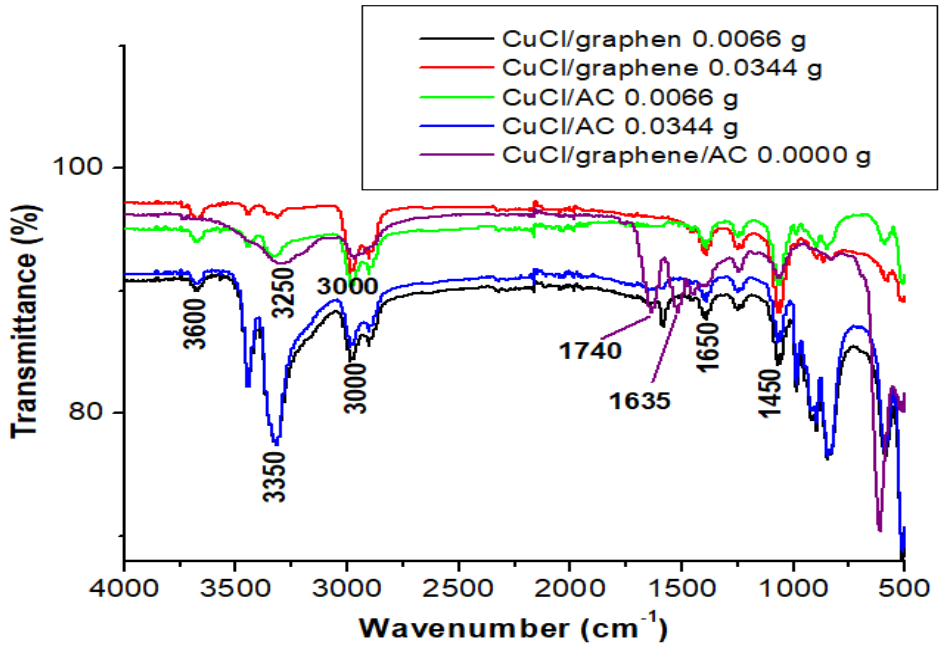

Figure 59: FTIR spectra of CuCl particles containing 0.0066 g graphene, 0.0344 g graphene, 0.0066 g AC, 0.0344 g graphene and no graphene and AC.

4.7.4 Degradation of MB using copper oxide particles containing carbon material.

The prepared CuCl particles containing 0.0066 g and 0.0344 g graphene/AC were used in the degradation of MB using Fenton degradation and it was observed that about 75%

of the MB was adsorbed during the 1 hour of equilibration and once the H_2O_2 was added and the UV-lamp switched on the reaction was inactive and no degradation was taking place. The CuCl/graphene/AC (0.0000 g) particles had about 78% removal of the MB during Fenton degradation. MB was degraded using a physical mixture of graphene/AC and Cu_2O, indicating that when the graphene and Cu_2O are added separately into the reaction they are more active.

In a study by Rey et al. (2008) it was observed that the surface of the activated carbon promotes H_2O_2 decomposition to non-reactive O_2 instead of to $OH^{\bullet}$. A study by Khalil et al. (2001) carbon nanotubes and activated carbon can catalyse the decomposition of H_2O_2 to O_2 and water decreasing the H_2O_2 concentration.

In a study by Xing et al. (2014) where different graphene covered grids were placed in different concentrations of H_2O_2, the H_2O_2 was observed to attack and destroy the carbon-carbon bonds on the grid. A study by Zubir et al. (2015) showed that graphene oxide oxidises thus consuming free radicals that were supposed to degrade the pollutant.

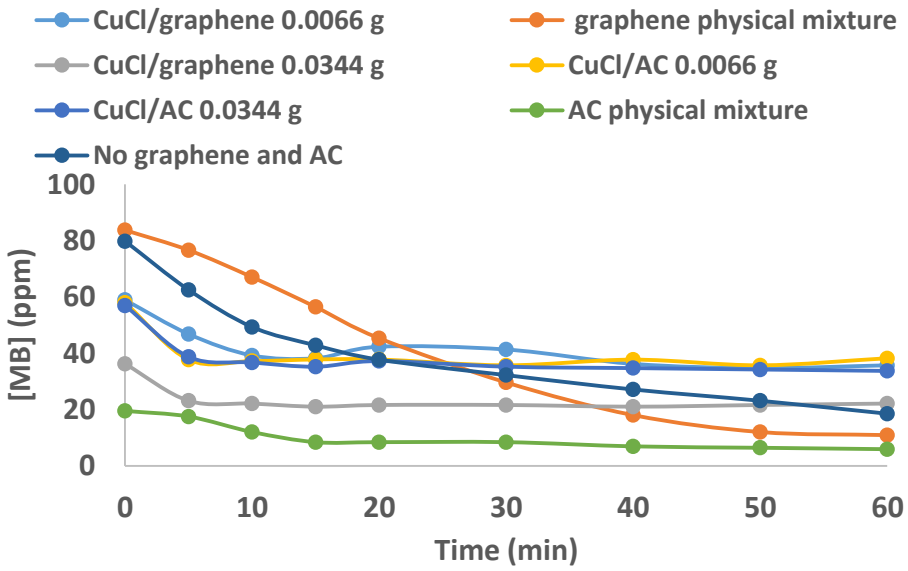

Figure 60: Fenton degradation of MB using copper-oxide particles containing 0.0066 g graphene, 0.0344 g of graphene,0.0066 g AC, 0.0344 g AC, physical mixture graphene/AC and no graphene and AC.

4.7.5 Mass loss (decomposition of H_2O_2) analyses

H_2O_2 easily decomposes when it is exposed to impurities or catalysts like metallic surfaces (Pedziwiatr et al., 2018). The resulting decomposition produces dissolved oxygen and water as shown in reaction 33.

$H_2O_2 \rightarrow 2H_2O + O_2$ (Fungene et al., 2018). Reaction 33

The effect of mass loss was studied using a catalyst that contained 0.0344 g of graphene 0.0344 g of AC, 0.0000 g graphene/AC and H_2O_2. The study was done to see which catalyst catalyzed the decomposition of H_2O_2 faster. Without the presence of a catalyst the decomposition reaction rate is slow however the addition of a catalyst can increase the reaction rate (Pedziwatr et al 2018). From this study the catalyst that contained no graphene and AC had the highest percentage loss than the catalyst containing 0.0344 g graphene and 0.0344 g AC (Figure 61). This suggested that the catalyst containing no graphene and AC catalyzed the decomposition of H_2O_2 more. The percentage loss of the catalyst containing 0.0344 g graphene and 0.0344 g AC was lesser.

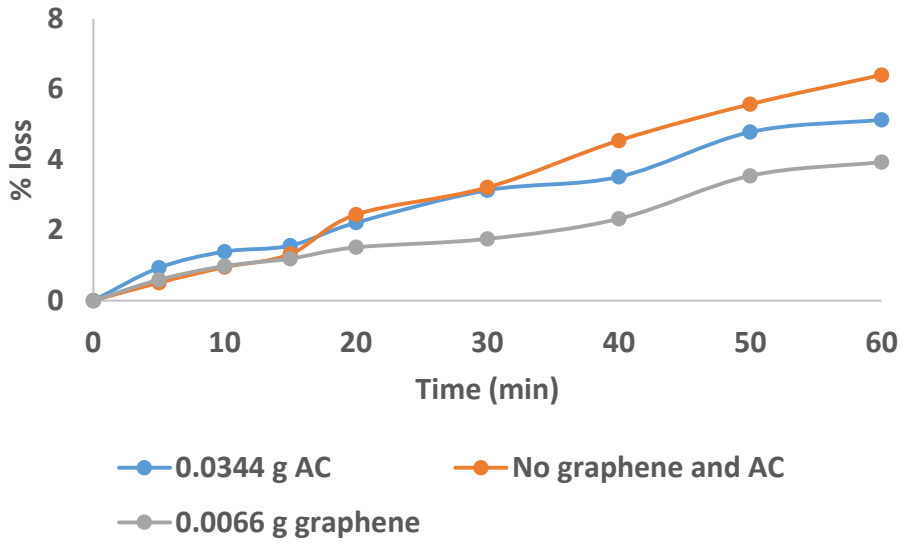

Figure 61: Effect of mass loss of catalysts containing 0.0000 g graphene/AC, 0.0344 g of graphene and 0.0344 g of AC.

4.8 Discussion

XRD indicated that the particles prepared with graphene and AC resulted in the formation of CuCl and the particles prepared without graphene and AC resulted in the formation of copper(I) oxide. When the copper oxide-graphene/AC composites were used in the degradation of MB, the composites were inactive and this resulted in no degradation taking place. The inactiveness of the catalyst may be attributed to AC/graphene consuming radicals that were supposed to degrade the pollutant (MB).

Chapter 5

5.1 CONCLUSIONS

The different catalyst preparation parameters influenced the size, shape, surface area and catalytic activity of the catalysts. The desired Cu_2O phase could be prepared using any of the reducing agents, ascorbic acid (ASC), hydrazine, sodium borohydride and glucose. However, different preparation conditions were required for the various reducing agents to get the Cu_2O phase. ASC, N_2H_4 and $NaBH_4$, but not glucose, were able to reduce copper (II) to copper (I) at room temperate. Glucose could reduce the copper at an elevated reduction temperature of 85°C. Stoichiometric amounts of the reducing agents ASC, N_2H_4 and glucose and double the stoichiometric amount of $NaBH_4$ yielded Cu_2O. A further increase in the amounts of $NaBH_4$ and N_2H_4 resulted in the formation of copper metal (Cu (0)). Higher amounts of glucose at room temperature did not reduce the copper (II) to copper (I). High amounts of ASC did not over-reduce the copper (II) to copper metal. The addition of graphene and activated carbon to the copper-based catalysts resulted in the formation of different product from Cu_2O to CuCl.

ASC functioned as a capping molecule since the FTIR analyses showed the presence of ASC on the surface of the copper oxide particles. The Cu_2O particles prepared using ASC were stable in the presence of air at room temperature whereas the Cu_2O prepared with hydrazine, oxidized to CuO. The ASC acted as anti-oxidant preventing the oxidation of the Cu_2O to CuO.

The SEM results showed that an increase in the amount of the precipitating agent, NaOH, resulted in doubling the particle sizes when the copper particles were prepared using ASC and hydrazine as reducing agents. The particle shape changed from spherical to cubic when a high amount of NaOH was used with hydrazine but the shape remained spherical when ASC was used. The copper precursor was found to influence the size of the particles. The copper precursor, $CuCl_2$ yielded Cu_2O particles with an average size of 300 nm. The sizes increased to 659 and 910 nm when $Cu(NO_3)_2$ and $CuSO_4$ were used, respectively. The size of the copper oxide was 240 nm when prepared with glucose as

reducing agent at room temperature and became significantly larger (737-840 nm) when the preparation temperature was 85 °C and higher. Octahedral shaped particles were observed when the copper oxides were prepared at 100°C. The shapes were mostly spherical when lower preparation temperatures were used.

The sizes determined by TEM and XRD analyses were smaller than 30 nm and the sizes based on SEM analyses were larger than 100 nm. The TEM analyses showed that the micro-particles seen in SEM analyses are made up of nano-particles. The catalysts were not active for photocatalysis which may be explained by the oxidation of the nano-particles to form the photocatalytic inactive CuO. The catalysts were shown to be active for Fenton and photo-Fenton degradation.

The photo-Fenton reaction removed more methylene blue than the Fenton reaction for some catalyst. The highest methylene blue removal achieved was 98 % in one hour by the photo-Fenton reaction for the catalyst made with 0.5 mol L^{-1} $NaBH_4$. This catalyst had a lower methylene blue removal of 86 % in one hour by the Fenton reaction. The best catalyst for the Fenton reaction was the catalyst prepared using copper chloride, 1.0 M NaOH and 0.1 M ASC. A methylene blue removal of 94 % in one hour was observed. However, this catalyst only removed 66% when the photo-Fenton reaction was used.

The addition of graphene and activated carbon to the copper-based catalysts increased the amount of methylene blue adsorbed but were detrimental to the catalytic activity.

The catalysts with the same shape (spherical) and phase (Cu_2O) were compared. There was no correlation between the particle size and the BET surface area since the surface roughness and the amount of agglomeration also influences the surface area besides the particle size. The percentage degradation of methylene blue by the Fenton reaction increased with an increase in the BET surface area from 1.5 m^2/g to 10 m^2/g and a further increase in the surface area resulted in a decrease in the percentage degradation. A direct correlation between the Fenton catalytic activity and the pore size were found which indicate that the reaction was mass transfer limited.

5.2 RECOMMENDATIONS

An increase in the amounts of NaOH using hydrazine as reducing agent should be investigated to see the effect of NaOH at higher amounts. BET analysis should be conducted on all nanoparticles to properly compare the surface area of the nanoparticles. The particles should be characterized with TEM in order to calculate accurate particle size. Degradation pathway of MB should be studied to find out what the degradation by products are and application should be done in real water samples.

Chapter 6

6.1 REFERENCES

ABDELRAHMAN, E. A.HEGAZEY, R.M., KOTP, Y.H. & ALHARBI, A. 2019. Facile synthesis of Fe_2O_3 nanoparticles from Egyptian insecticide cans for efficient photocatalytic degradation of methylene blue and crystal violet dyes. *Spectrochemica Acta part A: Molecular and Biomolecular.*222.p.1-11.

AGUILAR, M.S. & ROSAS, G. 2019. A new synthesis of Cu_2O spherical particles for the degradation of methylene blue dye. *Environmental Nanotechnology, Monitoring and Management.*11.p.1-7.

ANDAL, V. & BUVANESWARI, G. 2017. Effect of reducing agents in the conversion of Cu_2O nano-colloid to Cu nano-colloid. *Engineering Science and Technology, an International Journal.*20.p.340-344.

ATKINS, P. & JONES, L. Chemical principles: the quest for insight.5th edition .chapter 14.p.561.

BANNE, V.S., PATIL, M.S., KULKARNI, R.M. & PATIL, S .J. 2016. Synthesis and characterization of silver nanoparticles for EDM applications. *Materials today Proceedings* .4.p. 12054-12060.

BENZAOUAK,A.,ELLOUZI,I.,OUANJI,F.,TOUACHI,N.,KACIMI,M.,ZIYAD,M.,EL MAHI,M.& LOFTI,M.2018. Photocatalytic degradation of methylene blue (MB) dye in an aqueous solution by ferroelectric $Li_{1-x}W_xO_3$ materials. *Colloids and Surfaces A*.553.p.586-592.

CHEN, K. & XUE, D. 2013. Chemoaffinity-mediated crystallization of Cu_2O: a reaction effect on crystal growth and anode property. *Royal Society of Chemistry*.15.p.1739-1746.

CHEN,Q.,LIU,G.,CHEN,G.,MI,T.&TAI,J.2017.Green synthesis of silver nanoparticles with glucose for conductivity enhancement of conductive ink. *Bioresources*.12.p.608-621.

CHUNFA, D., XIANGLIN, Z., HAO, C. & CHUANLIANG,C. 2016.Sodium alginate mediated route for the synthesis of monodisperse silver nanoparticles using glucose as reducing agents. *Rare Metal Materials and Engineering*.45.p.0261-0266.

DANG,T.M.,LE,T.T.,FRIBOURGE-BLANC,E.&DANG,M.C.2011.Synthesis and optical properties of copper nanoparticles prepared by a chemical reduction method. *Advances in Natural Sciences: Nanoscience and Nanotechnology*.2.p.1-6.

DENG, X., WANG, C., SHAO, M., XU, X., & HUANG, J. 2017.Low-temperature solution of CuO/Cu_2O nanostructure for enhanced photocatalytic activity with added H_2O_2 : synthesis effect and mechanism insight. *RSC Advances*.7.p4331-4335.

DU, J., CULLEN, J.J. & BUERRNER, G.R. 2012. Ascorbic acid: chemistry, biology and the treatment of cancer. *Biochimica et Biophysica Acta (BBA)-Reviews on Cancer*.1826.p.443-457.

DUTTA, K., MUKHOPADHYAY, S., BHATTACHARJIEE, S., &CHAUDHURI, B. 2001. Chemical oxidation of methylene blue using a Fenton-like reaction. *Journal of Hazardous Materials B*. 84.p. 58-59.

EJAZ, A. & JEON, S. 2019. Electro oxidation of N_2H_4 through CuCuO electronic oscillation on a nitrogen doped GO surface. *Sensors and Actuators B: Chemical*.284.p.494-504.

FANG,M., ZHENG,R., WU,Y., YUE, D., QIAN,X., ZHAO, Y., & BIAN,Z. 2019. CuO nanosheets as a recyclable Fenton-like catalyst prepared from simulated Cu(II) waste effluents by alkaline H_2O_2 reaction. *Environmental cience Nano*

FUJISHIMA, A., RAO, T.N. & TRYK, D.A. 2000. Titanium dioxide photocatalysis. Journal of Photochemistry and Photobiology C: *Photochemistry Reviews.* 1. p. 1-21.

FUNGENE, T., GROOT, D.R., MAHLANGU, T. & SOLE, K.C. 2018.Decomposition of hydrogen peroxide in alkaline cyanide solutions. *The Journal of the South African Institute of Mining and Metallurgy*.118.p.1259-1264.

GAO, Z., LIU, J., XU, F., WU, Z., & JIANG, K. 2012. One-pot synthesis of graphene-cuprous oxide composite with enhanced photocatalytic activity. *Solid State Sciences*.14.p276-280.

GAWANDE, B.M., GOSWAMI, A., FELPIN, F.X., ASEFA, T., HUANG, X., SILVA, R., ZOU,X., ZBORIL,R. & VARMA,R.S. 2016. Cu and Cu-based nanoparticles synthesis and applications in catalysis. *Chemical Reviews*. 116 p3723-3730.

GEORGI, A. & KOPINKE, F.D. 2005. Interaction of adsorption and catalytic reactions in water decontamination process Part I. oxidation of organic contaminants with hydrogen peroxide catalyzed by activated carbon. *Applied catalysis B: environmental*. 58. p.9-18.

GHAMPSON,I.T.,NEWMAN,C.,KONG,L.,PIER,E.,HURLEY,K.D.,POLLOCK,R.A.,WALSH,B.R.,GOUNDIE.B.,WRIGHT,J.,WHEELER,M.C.,MEULENBURG,R.W.,DESISTO,W.J., FREDERICK,B.G.&AUSTIN,R.N.2015. Effects of pore diameter on particle size, phase, and turnover frequency in mesoporous silica supported cobalt Fischer-Tropsch catalysts. *Applied Catalysis A: General*.388.p.57-67.

GRATTEN-BELLEW, P.E. 2001.2-Petrographic and technical methods for evaluation of concrete aggregates. *Hand book of analytical techniques in concrete science and technology*.p.63-104.

HAN,X.,LIAO,F.,ZHANG,Y.,YUAN,Z.,CHEN,H. & XU,C.2018. Rapid and template-free synthesis of Cu_2O truncated octahedral using glucose as green reducing agent. *Materials Letter*.210.p.31-34.

HOUAS, A., LACHHEB, H., KSIBI, M., ELALOUI, E., GUILLARD, C., & HERRMANN, J.M. 2001. Photocatalytic degradation pathway of methylene blue in water. *Applied Catalysis B: Environmental 31*. p 145.

HUANG,L.,PENG,F.,YU,H.&WANG,H.2009.Preparation of cuprous oxides with different sizes and their behaviours of adsorption, visible-light driven photocatalysis and photocorrosion .*Solid State Sciences*. 11. p.129-138.

IBHADON, A.O. & FITZPATRICK, P. 2013. Heterogeneous photocatalysis: recent advances and applications. *Open Access Catalysts*. 3. p. 190-192.

ISHCHENKO, O.M., ROGE, V., LAMBLIN, G. & LENOBLE, D., 2016. TiO_2 and ZnO based materials for photocatalysis: material properties, device architecture and emerging

concepts. Intech: Semiconductor Photocatalysis-Materials, Mechanisms and Application.3-10. Chapter 1. Prof. Wenbin Cao (Ed.), InTech, DOI: 10.5772/62774. Available from: https://www.intechopen.com/books/semiconductor-photocatalysis-materials-mechanisms-and-applications/tio2-and-zno-based-materials-for-photocatalysis-material-properties-device-architecture-and-emerging (last accessed 2 May 2017).

JAIN, S., JAIN, A., KACHHAWAH,P.&DEVRA,V.2015. Synthesis and size control of copper nanoparticles and their catalytic application. *Transactions of Nonferrous Metals Society of China*.25.p.3995-4000.

JOUALI,A.,SALHI,A.,AGUEDACHA,A.,AARFANE,A.,GHAZZAF,H.,LHADI,E.K.,EL KRATI,M.&TAHIRI,S.2019. Photocatalytic degradation of methylene blue and reactive blue 21 dyes in dynamic mode using Ti_2O particles immobilized on cellulosic fibers. *Journal of Photochemistry & Photobiology A: Chemistry* .383.p.1-8.

KANG,L.,ZHOU,M.,ZHOU,H.,ZHANG,F.,ZHONG,Z.&XING,W.2019. Controlled synthesis of Cu_2O microcrystals in membrane dispersion reactor and comparative activity in heterogeneous Fenton application. *Powder Technology*.343.p.847-854.

KAREKAR, E.S. & PINJARI, D.V. 2017. Sonochemical synthesis and characterization of molybdenium sulphide nanoparticles: effect of calcination temperatures. *Chemical Engineering & Processing: Process Intensification*.120.p.268-275.

KE, W.H., HSIA, C.F., CHEN, Y.J., & HAUNG, M.H. 2016. Synthesis of ultra-small Cu_2O nano-cubes and octahedra with tunable sizes for facet-dependent optical property examination. *Small.* 12(26) p. 3530-3534.

KHALIL, L. B., GIRGIS, B.S., &TAWFIK, T.A. 2001. Decomposition of H_2O_2 on activated carbon obtained from olive stones. *Chemical Technology and Biotechnology.*76.p.1132-1140.

KIM, S C .2002. The catalytic oxidation of aromatic hydrocarbons over supported metal oxide. *Journal of Hazardous Materials B*.91.p.285-299.

KOSHY, J. & GEORGE, K.C. 2015. Annealing effects on crystallite size and band gap of CuO nanoparticles. *International Journal of Nanoscience and Nanotechnology*.6.p.1-8.

KUMAR, M., DAS, R.R., SAMAL, M.& YUN,K.2016. Highly stable functionalized cuprous oxide nanoparticles for photocatalytic degradation of methylene blue. *Materials Chemistry and Physics*.218.p.272-278.

KUO, C.H., CHEN, C.H. & HAUNG, M.H. 2007. Deed-mediated synthesis of monodispersed Cu_2O nanocubes with five different size ranges from 40 to 420 nm. *Advanced Functional Material*. 17. p. 3773-3780.

LEE, K.M., LAI, C.W., NGAI, K. S. & JUAN, J.C. 2016. Recent developments of zinc oxide based photocatalyst in water treatment technology: A review. *Water Research*.88.p 429-435.

LI, Y., ZHAO, M., ZHANG, N., LI, R. &CHEN, J. 2015. Synthesis and photocatalytic activity of carbon spheres loaded Cu_2O/Cu composites. *Journal of Alloys and Compounds.* 643. p. 106-110.

LIU,Q.M.,ZHOU,D.,YAMAMOTO,Y.,ICHINO,R.& OKIDO,M.2012. Preparation of Cu nanoparticles with $NaBH_4$ by aqueous reduction method. *Transactions of Nonferrous Metals Society of China.*22.p.117-123.

LWAMATO, M., T ANAKA, Y., S AWAMURA, N. & NAMBA, S. 2003. Remarkable effect of pore size on the catalytic activity of mesoporous silica for the acetalization of cyclohexanone with methanol. *American Chemistry Society*.125.p.13032-13033.

MA, Y. , LI, X., YANG, Z., XU, S., ZHANG, W., SU, Y., HU, N., LU, W., FENG, J. & ZHANG, Y. 2016. Morphology control and photocatalysis enhancement by in situ hybridization of cuprous oxide with nitrogen-doped carbon quantum dots. *Langmuir.* 32. p. 9418-9427.

MAVANI, K. & SHAN, M. 2013. Synthesis of silver nanoparticles by using sodium borohydride as a reducing agent. *International Journal of Engineering Research & Technology.*2.p.1-5.

MCMURRAY, J.E., FAY,R. G.&ROBINSON,J.K.Chemistry.6thedition.Pearson.Chapter13.p.491.

MENEGAZZO, F., SIGNORETTO, M., GHEDINI, E. & STRUKUL, G. 2019. Looking for the dream catalyst for hydrogen peroxide production from hydrogen and oxygen. *Catalysts*.9.p.1-32.

MIAO, X., DAI, H., CHEN, J. & ZHU, J. 2018. Enhanced method of hydroxyl radical generation in the heterogeneous UV-Fenton system with α-FeOOH as catalyst. *Separation and Purification Technology.* 200. p.36-43.

NGUYEN, C.H., FU C.C., & JUANG, R.S. 2012 .Degradation of methylene blue and methyl orange by palladium doped TiO_2 photocatalysis for water reuse: efficiency and degradation pathways*. Journal of Cleaner Production*.202.p.413-427.

NIE,J.,LI,G.,JIN,Z.,HU,W.,WANG,W.,HAUNG,J.,&WANG,Y.2019. Fabrication of MCC/Cu2O /GO composites foam with high photo-catalytic ability toward methylene blue. *Carbohydrate Polymers*.223.p.1-11.

OUYANG, J., YANG, H. & TANG, A. 2016. Shape controlled synthesis and optical properties of Cu_2O micro-spheres and octahedrons. *Materials and Design*. 92. p. 261-267.

PABISCH,S.,WAYERMAIER,W.,ZANDER,T.,LI,C.&FRATZL,P.2013.Imaging the nanostructure of bone and dentin through small-and wide-angle x-ray scattering. *Methods in Enzymology*.532.p.391-413.

PEDZIWIATR,P.,MIKOLAJCZYK,F.,ZAWADZKL,D.,MIKOLAJCZYK,K.& OKTAN,A.B.2018. Decomposition of hydrogen peroxide kinetics and review of chosen catalysts. *Acta Innovations*.26.p.45-52.

PIGNNATELLO, J.J., OLIVEROSE,.E., & MACKAY, A. 2006. Advanced oxidation processes for organic contamination destruction based on the Fenton reaction and related chemistry. Environmental science and technology. *Critical Reviews in Environmental Science and Technology*. 36. p. 1-84.

QUING-MING, L., Y ASUNAMI, T., KURUDA, K. &OKIDO, M. 2012. Preparation of Cu nanoparticles with ascorbic acid by aqueous solution reduction method. *Transactions of Nonferrous Metals Society of China*.22.p.2198-2203.

RAHMATOLAHZADEH, R., ALIABADI, M. & MOTEVALLI, K. 2017. Cu and CuO nanostructures: facile hydrothermal synthesis, characterization and photocatalytic activity using new starting reagents. *Journal of Material Sciences: Mater electrons*.28.p.148-156.

RAMOS,A.R.,TAPIA,A.K.G.,PINOL,C.M.N.,LANTICAN,N.B.,DELMUNDO,L.F.,MANALO, R.D&HERRERA,M.U.2018. Effects of reaction temperatures and reactant concentrations on the antimicrobial characteristics of copper precipitates synthesized using L-ascorbic acid as reducing agent. *Journal of Science: Advanced matarials Materials and Devices*.4.p.66-71.

RASHED, M.N. 2013. Adsorption technique for the removal of organic pollutants from water and wastewater. Intech: organic pollutants-monitoring, risk and treatment. Chapter 7. Prof. M. Nageeb Rashed (Ed.) DOI: 10.5772/54048. Available from: https://www.intechopen.com/books/organic-pollutants-monitoring-risk-and-treatment/adsorption-technique-for-the-removal-of-organic-pollutants-from-water-and-wastewater. (last accessed 2 May 2017).

RASTABI, S,A., MOGHADDAM, J., & ESKANDARIAN, M,R. 2015. Synthesis, characterization and stability of Cu_2O nanoparticles produced via supersaturation method considering operational parameters effect. *Journal of Industrial and Engineering Chemistry.* 22.p.34-40.

REY, A., FARALDOS,M.&BAHAMONDE,A.2008. Role of the activated carbon surface on catalytic wet peroxide oxidation. *Industrial & Engineering Chemistry Research*.47, p.8166-8174.

SABBAGHAN, M., BEHESHTIAN, J. &LIARJDAME, R.N. 2015. Preparation of Cu_2O nanostructures by changing reducing agent and their optical properties. *Materials Letters.*153.p.1-4.

SAEED,M., MUNEER., AKRAM,N., HAQ,A., AFZAL,N.& HAMAYUN,M. 2019. Synthesis and characterization of silver loaded alumina and evaluation of its photocatalytic activity on photodegradation of methylene blue dye. *Chemical Engineering Research and Design*.148.p.218-226.

SCUDERI,V.,AMIARD,G.,BONINELLI,S.,SCALESE,S.,MIRITELLO,M.,SBERNA,P.M.,IMPELLIZZERI,G.&PRIVITERA,V.2016. Photocatalytic activity of CuO AND Cu2O nanowires. *Materials Science in Semiconducting Processing*.42. p 90.

SHAHRZAD, A.R., JAVAD, M. & MOHAMMAD, R.E. 2014. Synthesis, characterization and stability of Cu_2O nanoparticles produced via supersaturation method considering operational parameters effect. *Journal of Industrial and Engineering chemistry*.22.p.34-40.

SHARMA, P. &SHARMA, S.K. 2013. Microscopic investigations of Cu_2O nanostructures. *Journal of Alloys and Compounds*.557.p.152-159.

SHIKHA, J., JAIN, A., KACHHAWAH, P. & DEVRA, V., 2015. Synthesis and size control of copper nanoparticles and their catalytic application. *Transactions of Nonferrous Metals Society of China.*25.p.3995-4000.

SILVA JUNIOR,O.J., MONTERERO,A.F.F., OLIVEIRA,J.B.L., ARAUJO,A.M.U., SILVA,D.G., KULESZA,J.& BARROS,B.S. 2019. Coordination polymer-derived CuO catalysts for oxidative degradation of methylene blue. *Materials Chemistry and Physics*.235.p.1-8.

SIRAJUDHEEN, P. & MEENAKSHI, S. 2019. Facile synthesis of chitosan La^{3+} -graphite composites and its influence in photocatalytic degradation of methylene blue. *International Journal of Biological Macromolecules*.133.p.253-261.

SONG, K.C., LEE, S. M., PARK, T.S. & LEE,B.S. 2008. Preparation of colloidal silver nanoparticles by chemical reduction method. *Korean J.Chem.Eng.*26.p.153-155.

SUN, B., LI, H.,LI X.,ZHANG,C.&XU,H.2018. Degradation of organic dyes over Fenton-like Cu_2O-Cu/C catalyst. *Industrial & Engineering Chemistry Research*. 57. p. 14011-14021.

TOE, C.Y., SCOTT,J.,AMAL,R.& HAUNG,Y.2018. Recent advances in suppressing the photocorrosion of cuprous oxide for photocatalytic and photochemical energy conversion. *Journal of Photochemistry and Photobiology C Photochemistry Reviews*.300.p.1-21.

UMAR, M. & AZIZ, H.A. 2013. Photocatalytic degradation of organic pollutants in water. Intech organic pollutants monitoring, risk and treatment.195-203. Intech: Monitoring, Risk and Treatment, Chapter 8. Prof. M.Nageeb Rashed (Ed.), DOI: 10.5772/53699. Available from: https://www.intechopen.com/books/organic-pollutants-monitoring-risk-and-treatment/photocatalytic-degradation-of-organic-pollutants-in-water (last accessed 2 May 2017).

UMER,A.,NAVEED,S.,RAMZAN,N.,RAFIQUE,M.S.&IMRAN,M.2014. A green method for the synthesis of copper nanoparticles using L-ascorbic acid. *Revistamateria*.19.p.197-203.

VOITKO,K.,TOTH,A.,DEMIANENKO,E.,DOBOS,G.,BERKE,B.,BAKALINSKA,O.2015. Catalytic performance of Carbon nanotubes in H_20_2 decomposition: experimental and quantum chemical study. *Colloid and Interface Science*.437.p.283-290.

WANG, G.,VAN DEN BERG, R.,DE MELIO DONEGA, C., DE JONG, K.P. & DE JONGH, P.E. 2016. Silica-supported Cu_2O nanoparticles with tunable size for sustainable hydrogen generation. *Applied Catalysis B: Environmental*. 192. p. 199-207.

WANG,H.,TIAN,F.,LI,X.,LIU,F.& SHEN,Q.2010. Preparation and shape evolution of cuprous oxide in the solution phases of copper (ll) dodecyl sulfate. *Powder Technology*.197.p.298-302.

WANG,Y.,HUANG,D.,ZHU,X.,MA,Y.,GENG,H.,WANG,Y.,YING,G.,HE,D.,YANG,Z.,& HU,N. 2014. Surfactant-free synthesis of Cu_2O hallow spheres and their wavelength-dependent visible photocatalytic activity using LED lamps as cold light sources. *Nanoscale Research Letters*. 9 (624) p. 1-8.

WU, S. 2007. Preparation of fine copper powder using ascorbic acid as reducing agent and its application in MLCC. *Materials and Letters*. 61.p.1125-1129.

XAVEIR, S.G., GANDHIMATHI, R., NIDHEESH, P.V. & RAMESH, S.T. 2016. Comparative removal of magenta MB from aqueous solution by homogeneous and heterogeneous photo Fenton processes*. Desalination and Water Treatment.* 57(27) p. 12832-12841.

XING, W., LALWANI, G., RUSAKOVA, I. & SITHARAMAN, B. 2014. Degradation of graphene by hydrogen peroxide*. Particle and Particle System Ccharacterization*.31.p.745-750.

XIONG, Y., CHE, L., FU, Z. &MA, P. 2018.Preparation of Cu_xO/C composite derived from Cu-MOFs as Fenton-like catalyst by two step calcination strategy. *Advanced Powder echnology.*29.p.1331-1338.

XU, H., WANG, W. & ZHU, W. 2006. Shape evolution and size-controllable synthesis of Cu_2O octahedra and their morphology-dependent photocatalytic properties. *Journal of Physics and Chemistry B.* 110. p. 13829-13834.

YANG, L., CHU, D., WANG, L., WU, X. & LUO, J. 2016. Synthesis and photocatalytic activity of chrysanthemum-like Cu_2O/carbon nanotubes nanocomposites. *Ceramics International.* 42. p. 2502-2509.

YANG,M.,BJORKBACKA,A.,GASPARRINI,C.,LEYGRAF,C.&JANSSON,M.2013. Kinetics and mechanisms of reactions between H_2O_2 and copper oxides. *Royal Society of Chemistry*.p.1-8.

YANG,Y.,HE,M.Q.,LI,M.X.,HUANG,Y.,CHI,T. & WANG,Z.X.2018. Ferrimagnetic copper-carboxyphosphate compounds for catalytic degradation of methylene blue. *Inorganic Chemistry Communications*.94.p.5-9.

YURDERI, M., BULUT, A., ERTAS , I.E.,ZAHMAKIRAN, M.& KAYA, M. 2015. Supported copper-copper oxide nanoparticles as active, stable and low cost catalysts in the methanolysis of ammonia- borane for chemical hydrogen storage. *Applied Catalysis B: Environmental*. 165. p. 169-175.

ZHANG, W., LI, X., YANG, Z., TANG, X., MA, Y., LI, M., HU, N., WEI, H., & ZHANG, Y. 2016. In-situ preparation of cubic Cu_2O-RGO nanocomposites for enhanced visible-light degradation of methyl orange. *Nanotechnology.* 27(26). Art. No. 265703.

ZHANG, X., SONG, J., JIAO, J. &MEI, X. 2010. Preparation and photocatalytic activity of cuprous oxides. *Solid State Sciences*.12.p.1215-1219.

ZHOU, Y., HU, W. &YU, JIAO F. 2013. Effective photocatalytic degradation of methylene blue by Cu_2O/MgAl layered double hydroxides. *Reaction Kinetics Mechanisms and Catalysis.*115.p.581-596.

ZUBIR,A.,YACOU,C.,MOTUZAS,J.,ZHANG,X.,ZHAO,X.S.&JOAO,C.2015. The sacrificial role of graphene oxide in stabilizing a Fenton like catalyst GO-Fe_3O_4. *Royal Society of Chemistry*.P.1-3.

Appendix A

Calculation of the crystalline size from XRD (Pabisch et al., 2013).

The Scherrer equation can be written as:

$$\mathrm{T} = \frac{k\lambda}{B\cos\theta}$$

Where:

- T is the mean size of the ordered (crystalline) domains, which may be smaller or equal to the grain size.
- K is a dimensionless shape factor, with value close to unity, the shape factor has a typical value of about 0.9 but varies with actual shape.
- λ is the X-ray wavelength nm
- Bis the line broadening at half maximum intensity (FWHM which stands for full width at half maximum) after subtracting the instrumental line broadening in radians. This quantity is also sometimes denoted as Δ (2θ).
- θ is the bragg angle (2θ°).

For example the crystallite size of the phase CuO of the particle prepared using 0.5 mol L^{-1} $NaBH_4$ was calculated as follows:

Center = 38.7041 (2θ°)

FWHM = 1.444 (2θ°)

The center and FWHM were determined using Fityk and converted to radians

$$\frac{k\lambda}{B\cos\theta}$$

$$= \frac{0.9 * 1.5418\, nm}{\cos\left(\frac{0.67551\ °}{2}\right) * 0.02520\ °}$$

= 6 nm

Appendix B

The repeatability study was done as follows

A mass of 0.1000 g of the catalyst (1.5 mol L^{-1} NaOH using ascorbic acid as a reducing agent) was used in the degradation of MB using Fenton degradation at 27 °C. The experiment was carried out 5 times at the same reaction conditions, using new catalysts each time.

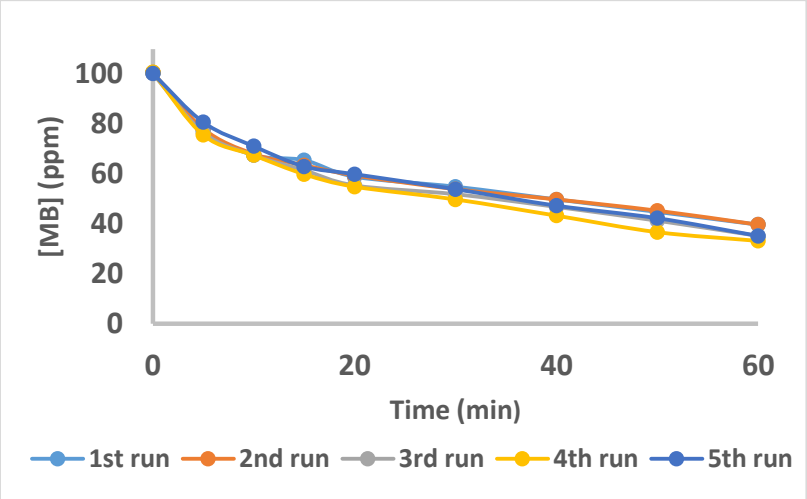

Figure 62:Degradation of MB using 1.5 mol L^{-1} NaOH catalyst.

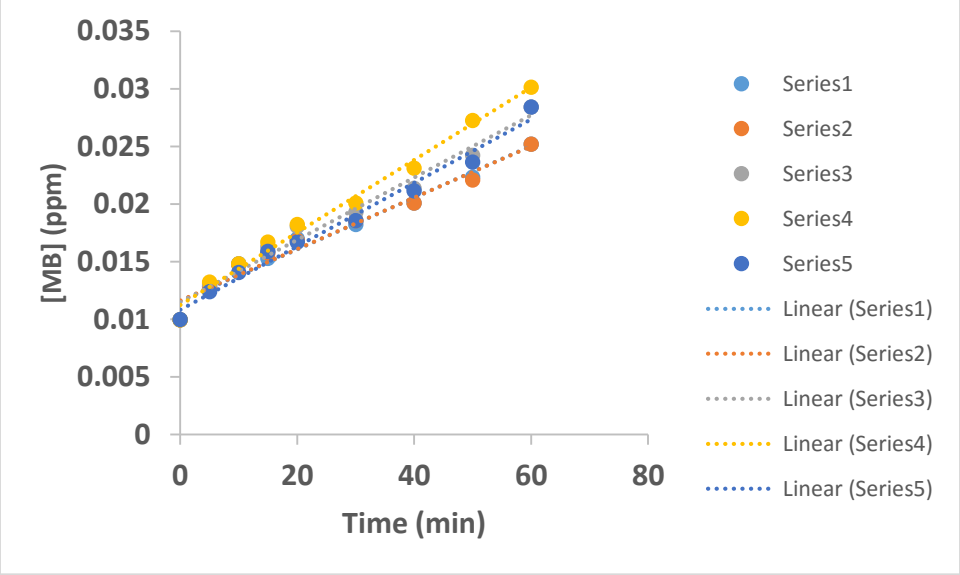

Figure 63: Pseudo 2nd order plot of the degradation of MB using 1.5 mol L^{-1} NaOH catalyst.

The repeatability study best fitted the pseudo 2nd order and the k values of each run were used to calculate the mean, standard deviation and the 2σ.

Mean:

$$\bar{x} = \frac{\sum xi}{n}$$

$$= \frac{0.0013\ (in\ ppm)}{5}$$

= 0.00026 (in ppm)

Standard deviation

$$s^2 = \frac{\sum(xi - \bar{x})^2}{n - 1}$$

$$= \frac{\sum(0.0013 - 0.00026)^2}{5 - 1}$$

$= 2.7 \times 10^{-7}$

$s = 5.2 \times 10^{-4}$ (in ppm)

2σ:

Standard deviation x 2

$= 5.2 \times 10^{-4} * 2$

= 0.00104 (in ppm)

- If the difference between the k values of catalysts is larger/same than the 2σ of the repeatability study it indicates that the activity of the catalysts were different.
- If the difference between the k values of the catalysts is smaller than the 2σ of the repeatability study it indicates that there is no difference in the catalytic activity of the catalysts.

Degradation percentage removal

The percentage of the methylene blue that was removed during degradation was calculated as follows:

The results used are of the degradation of MB using a catalyst prepared using 0.1 mol L-1 ASC.

C_i = initial degradation concentration

C_f = final degradation concentration

$$\%Removal = \frac{Ci-Cf}{Ci} * 100$$

$$= \frac{0.798-0.185}{0.798} * 100$$

= 77%

Appendix C

Determination of rate law (Atkins and Jones; McMurry and Fay)

One of the primary goals of chemical kinetics experiments is to measure the rate law for chemical reaction. The pattern in a reaction rate data can often be identified by examining the initial concentration of reaction, the instantaneous rate of change in concentration of a species at the instant the reaction begins. The advantage of examining the initial rate is that the products present later in the reaction may affect the rate and the interpretation of the rate is the quite complicated.

A first order reaction is one whose rate depends on the concentration of a single reactant raised to the first power. For the general reaction, A→ products, the rate law is:

Rate of consumption of A $= -\frac{\Delta[A]}{\Delta t} = k[A]$

A second order reaction is one whose rate depends either on the concentration of a single reactant raised to the second power or on the concentration of two different reactants, each raised to the first power. For the simpler type, A → products the rate law is

Rate of consumption of A $= -\frac{\Delta[A]}{\Delta t} = k[A]^2$

The pseudo 1st order reaction is a reaction in which one of the reactant is a solvent which is present in excess and its concentration does not change. Suppose we have a reaction:

A + B → C +D where B is an excess solvent, the rate law can be written as

r = k'[A] (pseudo 1st order reaction) where k' = [B]. This turns the actual second order reaction into a pseudo first order reaction, a reaction that is effectively first order. The rate law for a pseudo first order reaction is much easier to analyze than the true rate law because its rate depends on the concentration of only one substance.

First order integrated rate law is one of the simplest integrated rate laws for first order reactions, the aim is to find an expression for the concentration of a reactant A at a time t, given that the initial molar concentration of A is [A]. for example:

To find the concentration of a reactant A in a first order reaction at any time after it has begun, the rate law for the consumption of A in the reaction A→ products can be written in the form:

$$\frac{-d[A]}{dt} = k[A]$$

The integration of this first order reaction is

$$ln\frac{[A]t}{[A]o} = -kt$$

The integrated first order rate law can be used to confirm that a reaction is first order and to measure its rate constant. It can be re-written as

$\ln[A]_t = \ln[A]_o - kt$

This equation has the form of a straight line and it can be used to plot $\ln[A]_t$ as a function of t to get a straight line with slope –k and an intercept ln[A]. Second order integrated rate law can be derived from the second order reactions with the rate law:

Rate of disappearance of A = $k[A]^2$

To get the integrated rate law for a second order reaction it is recognized that the rate law is a differential equation written as

$$-\frac{d[A]}{dt} = k\,[A]^2$$

To get the final equation $\frac{1}{[A]t} - \frac{1}{[A]o} = kt$ which can be re-written as: $\frac{1}{[A]t} = kt + \frac{1}{[A]o}$

To determine whether a reaction is a second order in a reactant, plot the inverse of the concentration as a function of time to see whether a straight line results. The slope of the line is equal to k.